2020

THE DEVELOPMENT OF TEMPERATURE AND PH RESPONSIVE HYDROGELS AND MEMBRANES FOR SELECTIVE SORPTION OF PERFLUOROORGANICS AND NANOPARTICLE INTEGRATED CATALYTIC DEGRADATION OF PCB

Anthony Saad

University of Kentucky, anthony.saad@uky.edu
Digital Object Identifier: https://doi.org/10.13023/etd.2020.331

Right click to open a feedback form in a new tab to let us know how this document benefits you.

STUDENT AGREEMENT:

I represent that my thesis or dissertation and abstract are my original work. Proper attribution has been given to all outside sources. I understand that I am solely responsible for obtaining any needed copyright permissions. I have obtained needed written permission statement(s) from the owner(s) of each third-party copyrighted matter to be included in my work, allowing electronic distribution (if such use is not permitted by the fair use doctrine) which will be submitted to UKnowledge as Additional File.

I hereby grant to The University of Kentucky and its agents the irrevocable, non-exclusive, and royalty-free license to archive and make accessible my work in whole or in part in all forms of media, now or hereafter known. I agree that the document mentioned above may be made available immediately for worldwide access unless an embargo applies.

I retain all other ownership rights to the copyright of my work. I also retain the right to use in future works (such as articles or books) all or part of my work. I understand that I am free to register the copyright to my work.

REVIEW, APPROVAL AND ACCEPTANCE

The document mentioned above has been reviewed and accepted by the student's advisor, on behalf of the advisory committee, and by the Director of Graduate Studies (DGS), on behalf of the program; we verify that this is the final, approved version of the student's thesis including all changes required by the advisory committee. The undersigned agree to abide by the statements above.

<div align="right">

Anthony Saad, Student

Dr. Dibakar Bhattacharyya, Major Professor

Dr. Stephen Rankin, Director of Graduate Studies

</div>

THE DEVELOPMENT OF TEMPERATURE AND PH RESPONSIVE HYDROGELS
AND MEMBRANES FOR SELECTIVE SORPTION OF PERFLUOROORGANICS
AND NANOPARTICLE INTEGRATED CATALYTIC DEGRADATION OF PCB

_____

DISSERTATION

_____

A dissertation submitted in partial fulfillment of the
requirements for the degree of Doctor of Philosophy in the
College of Engineering
at the University of Kentucky

By
Anthony Saad

Lexington, Kentucky

Director: Dr. Dibakar Bhattacharyya, Professor of Chemical and Materials Engineering

Lexington, Kentucky

2020

ABSTRACT OF DISSERTATION

THE DEVELOPMENT OF TEMPERATURE AND PH RESPONSIVE HYDROGELS
AND MEMBRANES FOR SELECTIVE SORPTION OF PERFLUOROORGANICS
AND NANOPARTICLE INTEGRATED CATALYTIC DEGRADATION OF PCB

The functionalization and use of responsive and catalytic polymeric membranes and materials were explored for contaminant capture and degradation. While membranes have a wide variety of uses across multiple industries, the inclusion of materials that are temperature and pH responsive in the membrane pore domain yields a wide range of applications and possibilities for water treatment. Temperature and pH responsive polymers, as well as controlled nanostructured materials, were synthesized in membrane pores for advanced adsorption-desorption and catalytic treatment of emerging organic contaminants in water. In this study, supported by the NIEHS, poly-N-isopropylacrylamide (PNIPAm) was used as a model thermo-responsive polymer, while perfluorochemicals (PFCs) and polychlorinated biphenyls (PCBs) are used as model emerging water contaminants. A stimuli-responsive membrane-based adsorptive-desorptive system was developed by incorporating PNIPAm and poly-methyl methacrylate (PMMA) into a PVDF membrane structure and quantified through in-situ characterizations. Furthermore, a novel membrane system was developed for enhanced degradation of emerging halo-organics that is both stimuli-responsive and catalytic due to the incorporation of Fe-Pd nanoparticles into the polymeric membrane matrix.

By incorporating a thermo-responsive polymer into a membrane platform, temperature was used to control permeability, hydrophilicity, and pollutant partitioning. Solubility parameters of the model contaminants and of the thermo-responsive polymer in its different conformational states were determined. This was used to develop a fundamental understanding of the interaction between the polymer domain and halo-pollutant domain in order to conduct reversible temperature swing adsorption through manipulation of external stimuli. In doing so, PNIPAm's temperature-responsive behavior and hydrophilic/hydrophobic transition was leveraged for reversible adsorption and desorption of perfluoro-organics from water. Adsorption of perfluorooctanoic acid (PFOA) onto PNIPAm hydrogels yielded adsorption capacities lower than commercially used adsorbents. However, the initial rates of 28 mg/g/h and 41 mg/g/h for adsorption and desorption, respectively, and the ability to reversibly desorb with ease through external temperature manipulation make the use of stimuli-responsive polymeric membranes an

exciting avenue for the development of advanced adsorbents that can be easily regenerated. Temperature swing adsorption-desorption of pollutants using the thermo-responsive membrane was demonstrated and quantified.

The incorporation of stimuli-responsive polymers as well as reactive bimetallic nanoparticles into membrane pores enabled the development of an advanced stimuli-responsive catalytic membrane for enhanced halo-organic degradation. Iron nanoparticles were used due to iron's ability to react with water and form hydrogen species, unlike other reactive metal-based nanoparticles that would require a hydrogen source, with Palladium as a reaction catalyst. By adding stimuli-responsive polymers into the catalytic membrane matrix, temperature variations were used to selectively control adsorption and diffusion of model halo-organic contaminants into the membrane's catalytic domain. Chloro-organic degradation in batch and convective flow mode was achieved via the reductive pathway and modeled using advanced material characterization. The effect of temperature on the reaction process was evaluated as a means of increasing contaminant degradation efficiency by using the conformational change of the thermo-responsive polymer. Convective flow degradation of PCB-1 using the PNIPAm-PMMA-functionalized membranes with immobilized Fe-Pd nanoparticles yielded first-order k_{SA} values of 0.13 $L/m^2/g$, 0.28 $L/m^2/g$, 0.72 $L/m^2/g$, and 1.36 $L/m^2/g$ at 15 ºC, 25 ºC, 35 ºC, and 45 ºC, respectively, with an activation energy of 60 kJ/mol. Batch degradation of PCB-1 resulted in first-order k_{SA} values of 0.12 $L/m^2/h$ and 0.35 $L/m^2/h$ at 25 °C and 35 °C, respectively. Stimuli-responsive, functionalized polymeric membranes for reversible contaminant adsorption with high initial rates provide a very exciting technology for the removal of toxic organic contaminants from water.

KEYWORDS: Responsive Membrane, Reactive Membrane, Reversible Adsorption, Chloro-organics Removal, Water Treatment

<div align="right">

_____Anthony Saad_____

_____06/2020_____
Date

</div>

THE DEVELOPMENT OF TEMPERATURE AND PH RESPONSIVE HYDROGELS
AND MEMBRANES FOR SELECTIVE SORPTION OF PERFLUOROORGANICS
AND NANOPARTICLE INTEGRATED CATALYTIC DEGRADATION OF PCB

By

Anthony Saad

<div align="right">

Dr. Dibakar Bhattacharyya
Director of Dissertation

Dr. Steve Rankin
Director of Graduate Studies

06/2020
Date

</div>

ACKNOWLEDGMENTS

I first and foremost would like to thank my advisor, Professor Dibakar Bhattacharyya. Our time together began when I was completing my undergraduate degree at MIT and decided to spend one of my breaks doing innovative research. My father, who also received his PhD under Professor Bhattacharyya, introduced us and I spent the next few months conducting research at the University of Kentucky in Professor Bhattacharyya's lab. It was not only the innovative research in the field of water treatment membranes that Professor Bhattacharyya's group was conducting that convinced me to do my PhD at UK, but also the care and attention that Professor Bhattacharyya displayed towards his students and their long-term success. Over the past 6 years, you have been a constant source of ingenuity, motivation, and support. I was exposed to your vast network of people who have made significant advancement in this field. Most importantly, you and Gale have been like family to me, and I will always cherish these years in Lexington.

I would also like to thank Professor Lindell Ormsbee, Professor John Balk, and Professor Isabel Escobar for serving on my defense committee. From my PhD qualifying exam to all the national and international conferences I attended, I always had support and suggestions that made me look at things through different lenses and be a better student. With Professor Ormsbee's knowledge of treatment methods at hazardous sites, Professor Balk's material characterization expertise, and Professor Escobar's knowledge of membranes, separations, and familiarity with temperature responsive membranes, I was set up for success. I would also like to thank Dr. Dali Qian, Dr. Nicolas Briot, and Dr. Azin Akbari at the UK EMC center, as well as John May, Tricia Coakley, and Megan

there to advise me, support me, motivate me, and care for me, and I could not ask for a better team and hope to do the same for you. I have also had the luxury of having friends who have been like family to me throughout, so I would like to give a special thank you to Faaris Naqvi, Max Dunn, David Arakal, Sachin Manghnani, Ramzi El-Rifai, Wyle Al-Harbi, Jad El Khoury, Bara Badwan, Marc Kaloustian, Luis Fernandez, Ericka Embry, and Stephanie Abou-Jaoude.

TABLE OF CONTENTS

LIST OF TABLES

LIST OF FIGURES

CHAPTER 1: INTRODUCTION

1.1 Overview

While membrane processes provide a highly flexible separation process, the continued development of both sustainable and efficient membrane separation techniques for selective solute separation and water recycling and reuse remains of utmost importance. The development of stimuli responsive membranes is an exciting avenue for novel water treatment membranes [1]. The incorporation of responsive polymeric materials into membrane pores enables added functionality, such as adsorptive, catalytic, and renewable properties. Incorporating pH and temperature responsive polymers like poly-methyl methacrylate (PMMA) and poly-N-isopropylacrylamide (PNIPAm), an LCST polymer commonly used in biomedical applications, into membrane processes can add functionality that can enhance adsorptive and catalytic processes. While a common issue with commercial adsorbents is their regeneration capabilities, stimuli-responsive polymeric membranes could provide an alternative by leveraging their stimuli-responsive conformational changes to perform reversible adsorption. PH-responsive materials like PMMA can be used to immobilize reactive nanoparticles via ion exchange methods. Additional responsive polymers can be added to provide additional functionality to reactive membrane systems. By taking advantage of conformational changes due to external stimuli, catalytic membrane processes, such as the dechlorination of halo-organics, can be enhanced by increasing reactant adsorption and diffusion.

1.2 Background:

1.2.1 Stimuli-responsive water treatment membranes:

Membrane processes, such as Reverse Osmosis, Nanofiltration, Ultrafiltration, and Microfiltration, have generated many successful applications for recovering material from water streams and producing high quality water. The incorporation of responsive polymers, materials, or nanoparticles in macro-porous membranes provides an avenue for increased value in the area of water treatment [1, 2]. Providing access to safe drinking water has been identified as one, and possibly the most important, of the grand challenges facing scientists in the 21st century [3]. Increasing water reuse would tremendously impact the supply of water to a variety of industries, even in geographies where cyclical droughts make current supplies unreliable [4]. Non-conventional water treatment methods exist, including coagulation and flocculation, depth filtration, activated carbon filtration, biological treatment, ion exchange deionization, distillation, chemical treatment, UV treatment, and chlorination [5]. New membrane technologies are proving to be effective in meeting the need for higher quality water through selective separation of small molecules, enhanced durability, simultaneous separation and reaction processes, and selectively removing components from difficult mixtures [4], while challenges still exist with achieving low energy consumption, zero waste, and increased recovery and reusability [6].

Polymeric membranes have gained significant interest for water treatment applications because of their high flexibility, broad range of pore sizes and structure, simple manufacturing processes and low associated costs [7-10]. Advances to membrane technology, specifically the creation of nanocomposite and responsive membranes have

2

led to advancements in emerging applications, such as antifouling/selectivity [11, 12], flux enhancement [13], nanoparticle synthesis [11, 14], responsive nanomaterials [15], advanced reduction/oxidation [16], metal capturing [17], and adsorption [18]. Technological advancement goals for these membranes include obtaining high selectivity and high permeability at low costs and combining reactions within the pore structures to avoid further downstream unit operations, avoiding membrane fouling, and increasing membrane physical durability [9, 19]. These polymeric membranes are fabricated using improved or novel materials mixed with nanomaterials. Responsive and/or nanoscale materials can be added or in-situ synthesized onto the porous surface of commercial membranes to obtain functionalized, responsive, and reactive membranes [20-22]. Figure 1.1 shows a process of functionalizing a membrane pore with a responsive polymer. Responsive polymers can be affected by a variety of external stimuli and react with different mechanisms according to the polymer structure. Table 1.1 details several stimuli, including temperature, pH, magnetic field, ionic strength, electrical signal, and light, as well as examples of polymers that respond to the aforementioned stimuli, as well as the mechanism of said response [23].

1.2.2 Temperature responsive membranes and surfaces:

Some polymers exhibit a physical response to temperature variations, which can be used to create polymeric membranes that have attractive thermo-responsive properties for water treatment applications. Polymers that react to temperature have shown substantial differences in observed physical properties, mostly having to do with solubility. Thermo-responsive polymers are polymers that have been known to display a miscibility gap in their temperature-composition diagrams. These polymers are typically

known as LCST or UCST (upper critical solution temperature) polymers depending on whether this gap exists above a certain temperature (LCST polymers) or below a certain temperature (UCST polymers) [24-28]. Because of their environmental and biological relevance (specifically if the polymer's transition temperature is in the physiological range), much research has focused on the thermo-responsive nature of polymers in aqueous solutions in contrast to organic mixtures.

1.2.2.1 LCST/UCST Polymer Membranes for Selective Permeation/Separation

The most common temperature responsive polymer/hydrogel is poly(N-isopropylacrylamide), or PNIPAm, because of the phase transition it experiences from its hydrophilic state to hydrophobic state at its LCST of around 32 °C. This transition occurs due to alterations in the hydrogen bonding interactions of the amide group [26] – this makes it applicable to physiological processes [29]. By increasing temperature, the polymer side chains undergo property changes that hinder the hydrogen bonds that enabled favorable interaction with water molecules. PNIPAm's isopropyl groups will dehydrate first upon raising temperature above its LCST, causing the polymer chains or hydrogel network to collapse in an aqueous environment. Therefore, manipulating the side chains and their properties can effectively alter the LCST of a polymer. The polymer's LCST value can be influenced by manipulating the hydrophobic/hydrophilic balance in the polymer, adding hydrophobic branches, or controlling the length of the hydrophobic side chains [27].

The ability to control the hydrophobicity of a polymer through slight temperature changes is important for water treatment applications. Firstly, it enables selective control over water permeability through the membrane [30]. Water flux through a PNIPAm-

functionalized membrane can be significantly augmented by raising temperature above its

LCST, or hindered by lowering the temperature below its LCST of 32 °C [31]. Xiao et al.

and Zhao et al. demonstrate this phenomenon by conducting water permeation

experiments at various temperatures, which can be seen in Figure 1.2 [20, 31]. The LCST

can be varied through several means such as introducing salts that interact with the amide

group in the PNIPAm side chain to reduce the LCST [32, 33] and using ionic liquid to

weaken the hydrogen bonds formed between PNIPAm's amide group and surrounding

water molecules [34]. Hydrophilic and hydrophobic monomers can also be added to the

PNIPAm network to manipulate its response temperature [35]. By varying temperature

around the response, membrane fouling caused by pore size oscillations can be reduced.

Furthermore, by using temperature to control pore diameter through polymer swelling

within the pores, hydrophobicity and permeation of nanoparticles of different sizes can be

selectively controlled. One can take advantage of sharp property changes to create

thermo-responsive gating membranes that are only permeable to certain compounds at

temperatures above its LCST, with important potential applications in smart separations

[35].

1.2.2.2 Controlling Pore Size for Selective Particle Fractionation

Frost and Ulbricht demonstrated that temperature can be used to control pore size

in membranes functionalized with a temperature responsive polymer, in order to

selectively reject nanoparticles of various sizes. They used poly(ethylene terephthalate)

ultrafiltration membranes functionalized with PNIPAm to reject silica nanoparticles of

different sizes based on external temperature [36]. Raising the temperature increases the

effective pore size because of the collapse of PNIPAm chains in the membrane matrix.

By measuring water permeation through the membrane and applying Hagen-Poiseuille law, shown in Eq. (1-1), hydrodynamic pore diameters can be estimated at various temperatures [36]:

$$J = \frac{N\pi\Delta P}{A8\eta L}\left(\frac{D}{2}\right)^4$$

(1-1)

Here, J is the transmembrane flux, N represents the number of pores, A represents the area of permeation, η represents viscosity, L represents the membrane thickness, ΔP represents the pressure drop, and D represents the pore diameter. The water flux is corrected for viscosity changes due to temperature, so the changes in diameter are solely due to the thermo-responsive collapse of the polymer chains. It was shown that by changing the operating temperature from 23 °C to 45 °C, effective pore size was increased from 21 nm to 69 nm, allowing larger particles to pass through the membrane, and simultaneously increasing the transmembrane flux. Using 21 nm silica NPs as a model solute, particle rejection decreased from 99 % to 35 % because of the larger effective diameter caused by the temperature change. This confirms that PNIPAm-functionalized thermo-responsive membranes can be used for size-selective NP fractionation [31, 36]. Using PNIPAm to control pore size has also been used to control drug release kinetics due to its biocompatibility [37]. Liu et al created thermo-responsive hydrogel composite graphene oxide membranes with tunable microchannels, with potential applications in smart gating and separation systems [38]. These results confirm that increasing feed temperature for a PNIPAm-functionalized membrane causes increased flux and reduced rejection; increasing pore size enables transport of more molecules and larger molecules at higher temperatures.

1.2.2.3 The effect of Polymerization Time and Chain Length/Density on Membrane Separations

Other means exist to control PNIPAm chains within membrane pores. PNIPAm chain length grafted within the membrane pores can be controlled by the polymerization time, enabling switchable size-selective particle fractionation [36]. Figure 1.3 demonstrates that hydrodynamic membrane pore diameter can be reduced by increasing polymer chain length by simply increasing polymerization time [36]. Wandera et al. have varied polymerization time of PNIPAm-*co*-poly(poly(ethylene glycol) monomethacrylate, PPEGMA) block copolymer nanolayers to functionalize thermo-responsive, low molecular weight cellulose ultrafiltration membranes to study its effect on transmembrane flux, membrane fouling, and oil-water separations [39]. In order to do so, surface-initiated atom transfer radical polymerization (ATRP) was used to grow polymer nanolayers on the membrane surface, and polymer chain density was varied through polymerization time manipulation in order to optimize produced water treatment performance [39]. Higher polymer chain density and longer polymerization times lead to the synthesis of membranes with more stable flux, whereas lower chain density and shorter polymerization times lead to higher instantaneous flux, but do not completely eliminate fouling-related flux decline. Figure 1.4 demonstrates that higher chain density leads to lower, more stable trans-membrane water permeability. The membrane surface can be modified to optimize both permeate flux and flux decline due to fouling for separation of oil emulsion from produced water by varying the structural properties of polymer coating [39]. While PNIPAm can be used to control pore size via control over external temperature due to its thermo-responsive conformational change, other stimuli

responsive materials can also be used for gating membranes in order control substance concentration in reactors, control drug release, perform size-based separations, affinity-based separations, and enhance self-cleaning of membrane surfaces [40].

1.2.2.4 Temperature Responsive behavior for catalysis and metal sorption:

Reactive nanoparticles have been incorporated into temperature responsive hydrogels and also into membranes functionalized with temperature responsive polymers to enhance reactivity [31]. Zero-valent metals, such as iron NPs, have received significant attention for their use in the remediation of chlorinated compounds in contaminated groundwater [41]. Fe and Fe/Pd NPs have been immobilized in poly(acrylic acid)-*co*-PNIPAm (PAA-*co*-PNIPAm)-functionalized membranes for the remediation of trichloroethylene (TCE) in water [31, 42]. Slight variations in temperature affect not only NP reactivity by affecting the reaction rate constant, but can also affect adsorption of hydrophobic/hydrophilic species; as temperature is increased above the polymer's LCST, transition to the hydrophobic state caused increased TCE adsorption onto the membrane surface because of the hydrophobic nature of this solute [43]. Figure 1.5 demonstrates the increase in TCE adsorption percentage onto a P(NIPAAm-AA) hydrogel from 30% to 65% as temperature is increased above the LCST because of enhanced hydrophobicity [43]. Water can also oxidize the Fe NPs and decrease reactivity. By controlling the hydrophilicity of the polymeric membrane, water content within the membrane pores can be controlled, thereby allowing for selective tuning of the reduction reaction [43]. Varying temperature affects NP reactivity because as we know, reaction kinetics are a function of temperature, and also affects diffusivity through the membrane as shown in the Wilke-Chang equation [44]. By incorporating a thermo-responsive polymer into the

8

membrane matrix, transmembrane flux can also be controlled, thereby allowing the

optimization of polychlorinated biphenyl (PCB) degradation by bimetallic Fe/Pd

nanoparticles through regulation of temperature [43]. Xiao et al. studied TCE

dechlorination using Fe/Pd nanoparticles (1.5 wt% Pd relative to Fe) in a P(NIPAAm-

AA) hydrogel matrix above and below the LCST to verify the effect of temperature on

reaction rate constant. The normalized reaction rate for the dechlorination reaction (k_{SA})

increased by a factor of three, from 0.0156 to 0.0411 L/(m^2·h), due to a temperature

increase of only a few degrees above the LCST [43]. Figure 1.6 shows how TCE

concentration versus time changes during the dechlorination reaction by Fe/Pd NPs in a

P(NIPAAm-AA) hydrogel at 30 °C and 34 °C [43].

Thermo-responsive polymers have been used in membranes to improve chelation

of copper ions from wastewater [45, 46]. It was reported that large metal-polymer

complexes can cause significant concentration polarization on the membrane active layer

in polymer-enhanced ultrafiltration [47]. By using PNIPAm in the polymer-metal

complex, copper retention could be increased at low temperatures due to increased

binding sites on the polymer in the swollen state, while fouling could be dramatically

reduced at higher temperatures because the polymer aggregates and unblocks membrane

pores in the hydrophobic state, thereby reducing the formation of the cake layer [45, 48].

1.2.3 pH Responsive Properties

Membranes and surfaces can also be functionalized with polymers that display pH

responsiveness, also called hydrogels. By having ionizable functional groups that have

the ability to gain or lose protons based on the surrounding pH, such polymer chains can

be collapsed or extended based on fluctuation of hydrophobic volume (swelling) caused

9

by generated electrostatic repulsions [49]. Functional groups such as amino and amine groups in polymer chains with pKa values around 5 will lose their protons in basic pH conditions and are responsible for the responsive behavior [50]. While some pH-responsive polymers, like polyacrylic acid, expand at higher pH due to deprotonation, some pH-responsive polymers swell due to electrostatic repulsions at lower pH and deprotonation at higher pH neutralizes the repulsions to collapse the polymer chains. Figure 1.7 demonstrates the physical response of a pH responsive polymer when subjected to pH values above and below its pKa [50].

The swelling behavior of a hydrogel can be predicted by first-order or second-order kinetics [51], as shown in Eq. (2)-(3). This behavior has an increment in the mesh size of the polymer, showed in Eq. (4), which is a parameter of cross-linking density by calculating the average distance of neighbor polymer chains between two cross-linked points [52-55]:

$$\frac{dW}{dt} = K(W_{eq} - W) \tag{1-2}$$

$$\frac{dW}{dt} = K(W_{eq} - W)^2 \tag{1-3}$$

$$\xi = l(v_{2eq})^{-1/3} \cdot \sqrt{\frac{C_n}{X}} \tag{1-4}$$

Here, $W = (m - m_0)/m$ with m_0 and m are the weights of the dry polymer (xerogel) and the swollen hydrogel, respectively and K is the swelling constant. W approaches the value of one when it reaches the highest water uptake possible in equilibrium, W_{eq}. In Eq. (4), ξ is the mesh size, l is the bond length along the backbone chain (1.54×10^{-10} m for carbon-carbon bonds), v_{2eq} is the swollen polymer volume fraction for isotropic swelling

(xerogel/hydrogel), C_n is the Flory characteristic ratio (for PAA, $C_n = 6.7$) and X is the degree of cross-linking (mol % with respect to monomer concentration) [54].

The fabrication of pH responsive polymers that display high hydrophilicity at low pH values is important for water treatment applications. In the past little research was done on wettability of surfaces based on pH responsive membranes that display such characteristics. A pH responsive surface was created by a poly(N-N'-dimethylaminoethyl methacrylate) (PDMAEMA) thin film on silicon substrates. This homopolymer can be prepared via surface-initiated atom transfer radical polymerization. The polymer is deprotonated at high pH and protonated at low pH, thereby allowing it to interact with anionic substances through electrostatic attraction [50]. More recently, hydrophilic and pH-responsive characteristics were incorporated into a polysulfone membrane by blending polyethylene glycol methyl ether and humic acid for recovery of H_2SO_4 from water [56].

Since membrane fouling properties and solute rejection are correlated with membrane surface charge, coating membranes with a polymer that can be selectively deprotonated are able to significantly enhance anti-fouling properties while maintaining high solute rejection [57]. Lowering the surface free energy of the membrane, which lowers the interfacial interactions with foulant molecules, can also significantly reduce membrane fouling [58]. Grafting perfluoroalkyl groups onto NF membrane surface has been shown to reduce fouling by reducing adsorptive interactions and enhancing repulsive interactions between the membrane and foulants [58].

Bhattacharyya's group have reported the functionalization of PVDF with PAA and PMMA to create pH responsive membranes onto which iron and iron oxide NPs can

be immobilized for water remediation [42, 55, 59-62]. PAA and PMMA can be transformed into the ionized state at environmental pH values above their pKa of about 4.5. Membrane functionalization with PAA enables selective pore size tunability and therefore control over water permeability through the membrane. Figure 1.8 shows the effect of environmental pH on water flux and permeation through a PVDF-PAA membrane [59]. Hernández, Papp and Bhattacharyya reported this effect with an approximated 50% decrease in pore size by shifting the pH from 3.0 to 9.0, with a simultaneous increase in the polymer mesh size [55]. The PAA functionalization is made by free radical polymerization using strong oxidants (e. g. persulfate) at 70 – 90 °C depending on the cross-linker used (ethylene glycol (EG); N,N′- methylenebis (acrylamide) (NMBA), etc.), or starting at room temperature using metallic salts as accelerants (redox reactions) and antioxidants, such as ascorbic acid, to control the reaction process [55, 60].

Full-scale PVDF-PAA flat sheet membranes (1×91 m and 70 μm of PVDF thickness, 45-55% porosity and backing fabric for stability) and membrane modules (0.465 m^2 of surface area) were developed by joint work with the industry, see Figure 1.9. The polymerization in solution process at industrial scale is similar to the reported bench-scale studies using EG as cross-linker with a lower amount of acrylic acid to reduce the viscosity of the solution and shorter polymerization times [60, 63, 64]. Pure water permeabilities of these full-scale membranes can vary from 1355 to 383 L/ (m^2·h·bar), when the pH increased from acidic to neutral (3.0-7.3), and have a constant flux at different temperatures with constant pH (see insert in Figure 1.10), whereas the modules can go from around 320 to 230 L/ (m^2·h·bar) when the pH goes from 4.0 to 9.0

[31, 59, 62]. These full-scale membranes and modules have also been post-functionalized with iron and iron oxide NPs for degradation and metal capture studies and with PNIPAm to get both temperature and pH responsive behaviors, see Figure 1.11 [31, 59, 62].

Other studies have reported the fabrication of smart fiber membranes for gravity-driven oil-water separations by depositing poly(methyl methacrylate)-block-poly(4-vinylpyridine) (PMMA-*b*-P4VP) pH responsive copolymer fibers on stainless steel mesh [65]. The pH responsiveness allows for switchable wetting states of the membrane from a superhydrophobic/superoleophilic to superhydrophilic/underwater superoleophobic state. A pH-responsive sponge has been developed to do the same [66]. By wetting the membrane with acidic water, the smart fiber membrane switches from allowing oil to selectively pass through the membrane with high separation efficiency, to allowing water to selectively pass through the membrane with similar high efficiency [65]. High flux, gravity driven flow with switchable wettability for many cycles makes the smart fiber-pH responsive membrane cost-effective and appropriate for large-scale oil recovery and water purification applications [65].

1.2.3.1 Other responsive properties

Electromagnetic responsiveness can also be achieved by incorporating photo-sensitive molecules that rearrange based on ionization upon exposure to electromagnetic irradiation; photo-induced polymer chains can expand/shrink because of the reversible exchange of electrostatic repulsion between ionic states [49]. Molecular structures of photo-responsive monomers have the ability to isomerizes, dimerize, and ionize given a certain irradiation, either inducing a change in charge or conformation. Structures of some photo-responsive monomers are shown in Figure 1.12 at various wavelengths [49].

Much like membranes functionalized with temperature and pH responsive polymers which can be varied to control effective pore diameter and therefore control both transmembrane flux and size-selective exclusion of particles, the use of superparamagnetic NPs can also be used to achieve the same phenomena due to their instantaneous response to an electric field [67, 68]. Himstedt et al. grafted poly(2-hydrocyethyl methacrylate) (polyHEMA) onto polyethyleneterephthalate membranes and attached superparamagnetic Fe_3O_4 NPs to the end of the grafted polymer chains in order to control effective membrane pore diameter through external stimuli. By varying the magnetic field orientation, the NPs cause the polyHEMA chains to extend, thereby reducing water flux through the membrane [69]. Increasing the magnetic field and therefore decreasing pore diameter and reducing permeation of larger particles can enable a nano-valve character. Yang et al. also grafted polyHEMA onto thin film composite polyamide nanofiltration membranes and attached superparamagnetic Fe_3O_4 NPs to obtain magneto-responsive membranes for salt rejection with antifouling properties [67]. Membrane rejection of $CaCl_2$ and $MgSO_4$ was measured in dead-end filtration mode both in the absence and presence of an oscillating magnetic field [67]. Both permeate flux and salt rejection was greater in the presence of the magnetic field, and was also greater with increased magnetic NP density [67]. However, permeate flow decreases with increased grafting and NP density, thereby implying that the trade-off between permeate flow and membrane performance can be optimized for the desired application [67].

Schacher et al. have reported the use of block copolymers displaying responsiveness to more than one stimuli to create functionalized membranes and surfaces that are controllable by multiple environmental factors [70]. They demonstrated that for

PDMAEMA, both pH and temperature can be independently varied with significant

resulting effects on the transmembrane water flux [70]. Incorporating stimuli responsive

materials into membrane processes opens the door to an array of functionalities that can

enhance current techniques and for the treatment of prevalent, hazardous water

contaminants such as perfluorinated compounds and halo-organics.

1.2.4 Perfluorinated compounds

Perfluorinated compounds (PFCs) such as Perfluorooctanoic acid (PFOA) have

gained much attention as emerging pollutants due to their environmentally persistent

nature and toxicity concerns that threaten water safety [71, 72]. Due to their thermal

stability, these highly hydrophobic compounds have been used since the 1960s for a

variety of purposes including: protective coatings, lubricants, surfactants, additives, and

repellants. Methods to remove them from contaminated wastewater, groundwater, and

drinking water continue to gain importance due to their continued production and toxicity

[73-75]. PFC concentrations in contaminated wastewater and groundwater samples range

from below 0.1ng/L to over 1000 mg/L values [75-77].

1.2.4.1 Treatment of Perfluorinated compounds in water

To date, various methods have been explored for the removal of PFCs from

aqueous media, such as reverse osmosis [78], incineration [79], anaerobic defluorination

[80], photochemical defluorination [81], oxidation [82, 83], reduction [84], electrostatic

exclusion by nanofiltration [85], and adsorption [86-89]. The current advised US EPA

level for PFCs is 70 ng/L. Adsorption has proven to be an effective method of removing

PFCs from contaminated water, and Yao et al. have shown the efficiency of PFOA

removal using a variety of commercially available adsorbents, including granulated and

powdered activated carbon, anion-exchange resin (AER), alumina, silica, and non-ion exchange polymers. AER has a very high adsorption constant of 200 $mg^{(1-n)}$ L^n g^{-1} compared to a value of 63 $mg^{(1-n)}$ L^n g^{-1} for granular activated carbon (GAC) [75]. Due to their hollow nanostructures that create high surface areas, carbon nanotubes have been effectively used as a PFC adsorbent, yet their practical application in PFC treatment is limited by available recycling technology [90]. Li et al. used multi-walled carbon nanotubes (MWCNs) to remove PFCs using electrochemical assistance by varying polarization potentials, and demonstrated some regeneration capabilities [90]. Polymeric membranes have also been used to reject PFOA from water using size exclusion and electrostatic forces. Boo et al. used negatively charged nanofiltration membranes in order to achieve approximately 90% PFOA rejection [85]. Patterson et al. used reverse osmosis (RO) membranes to reject PFOA and perfluorooctane sulfonate (PFOS) from drinking water [91].

1.2.4.2 PNIPAm-functionalized PVDF membranes:

The use of responsive polymeric materials provides an alternative opportunity to increase the efficiency of treating perfluorinated contaminant (PFC) contaminated water. Not only could they remove PFCs from water through adsorption mechanisms, but they could also controllably and reversibly desorb the PFCs by changing the environmental conditions. While the adsorption capacity of responsive polymeric materials may be lower than commonly used adsorbents such as activated carbon, the ease of recycling at low cost provides a benefit that makes them attractive pollutant adsorbents for the treatment of contaminated water. Poly-N-isopropylacrylamide (PNIPAm) has been widely studied as a lower critical solution temperature (LCST) polymer that exhibits a

phase transition from a hydrophilic hydrated state to a dehydrated state at its LCST of 32 °C. By increasing the temperature, property changes in the polymer chains affect the hydrogen bonding of water molecules as the chains collapse in an aqueous environment [26]. PNIPAm exhibits one of the largest known volume phase transitions (VPTs) in response to environmental stimuli due to motion of the mobile water phase within the cross-linked polymer network [92]. Studies have shown that the hydrophobicity of PNIPAm can be controlled using slight temperature variations of a few degrees, thereby affecting adsorption of organic compounds [43]. Understanding of the mechanism behind PNIPAm's VPT has been limited and inconsistent until recently, with some asserting that the amide groups dehydrate first, while others state that the isopropyl groups dehydrate first and cause the chain to collapse [92-96]. Wu et al., used non-resonance Raman temperature-jump spectrometry in order to determine that the hydrophobic isopropyl and methylene groups dehydrate much faster than the amide groups, and are thus responsible for initiating PNIPAm's VPT [92]. Furthermore, the partitioning of nonpolar and polar solutes in both collapsed and swollen PNIPAm chains has been studied, with findings that nonpolar solutes tend to reside in the dryer regions of the polymer [97]. The dehydration and rehydration of isopropyl groups on PNIPAm can therefore be leveraged for reversible adsorption of hydrophobic contaminants. Figure 1.13 demonstrates the expected behavior of PNIPAm hydrogels as well as PNIPAm-functionalized membranes when the temperature is increased above its LCST of 32 °C. In an aqueous environment, PNIPAm hydrogels shrink at higher temperature. When functionalized within membrane pores, PNIPAm collapses at higher temperatures, increasing the apparent membrane pore size. The NIPAm concentration and PNIPAm degree of functionalization also have an

17

impact. Increasing the NIPAm content in the polymerization mixture increases the polymer density when functionalized in membrane pores, thereby reducing permeance [31, 98].

Polyvinylidene fluoride (PVDF) membranes have been used as a base membrane for microfiltration and ultrafiltration processes due to their chemical resistance and mechanical stability [16, 99-102]. Functionalizing PVDF membranes with responsive polymers gives the membrane new properties for advanced water separation. PVDF membranes have also been functionalized with PNIPAm to create temperature-responsive surfaces and pores [31, 98, 103]. When PNIPAm is formed inside PVDF membrane pores, controlling its hydrophobicity enables control over effective pore size, and therefore over water flux through the membrane. PNIPAm has been used to increase the adsorption of chlorinated organic compounds such as trichloroethylene (TCE) by raising the temperature just 3 degrees above the LCST [43].

1.2.5 Chlorinated Organic Compounds:

The degradation of chlorinated organic compounds (COCs) has gained interest due to their environmental prevalence and toxicity. Poly chlorinated biphenyls (PCBs) are a group of prevalent, toxic COCs that have been released by poorly maintained hazardous waste sites, contaminating soil and groundwater, thereby causing a serious threat to the environment along with drastic health effects [104]. The development of low-cost methods to treat wastewater containing PCBs continues to carry significance because of the potential impact such technologies could have on human health.

1.2.5.1 Treatment of chlorinated organic compounds with reactive membranes:

The use of reactive polymeric membranes has been studied for the degradation of PCBs [99-102, 105]. Specifically, polyvinylidene fluoride (PVDF) membranes have been used as a base membrane for microfiltration and ultrafiltration processes due to their chemical resistance and mechanical stability. They have been used in various water treatment methods through surface modification, such as dip coating [106], surface grafting [107], layer-by-layer assembly [108], and nanoparticle immobilization [109, 110]. Functionalizing PVDF membranes with responsive polymers gives the membrane new properties for advanced water separation [31, 111-114]. Poly methyl methacrylate (PMMA) and Poly acrylic acid (PAA) have been used to functionalize membranes and create responsive surfaces because of its ability to deionize at high pH. Due to its ionizable functional carboxylic group, it can gain or lose protons, generating electrostatic repulsions that can collapse or expand polymer chains [49, 50, 54, 99]. Furthermore, the carboxylic groups in the PAA chain and the $COOCH_3$ group in PMMA can be deprotonated at high pH and through ion exchange methods, and metal nanoparticles can be immobilized in the polymer domain [102, 115, 116].

1.2.5.1.1 Integrating Fe-Pd nanoparticles:

Reactive metal nanoparticles have been integrated into the polymeric domain of functionalized membranes in order to render them reactive [98, 117]. They have been used in solution and has been immobilized in membranes through ion exchange methods with the PAA domain for the degradation of COCs [98, 99, 101, 117-119]. Zero-valent iron (ZVI) and iron-based bimetallic nanoparticles have gained considerable attention because of their ability to reduce chlorinated organic compounds in water by electron

19

transfer reactions [120-123]. Zero-valent iron and other metal NPs have also been studied

and implemented for chlorinated organic compounds through reductive pathways as

shown in Eq. (1-5) [124-132]:

$$mFe^0 + RCl_m + mH^+ \rightarrow mFe^{2+} + RH_m + mCl^- \qquad (1\text{-}5)$$
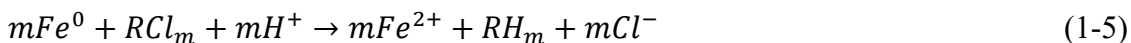
Here, RCl_m is a chlorinated organic compound. For a more rapid and complete reductive

dechlorination, a second metal is often added, resulting in creation of bimetallic NPs. ZVI

has been synthesized through reduction of ferrous iron using reducing agents, such as

sodium borohydride (NaBH4), in aqueous solutions [42, 100, 102, 123, 131]. ZVI

nanoparticles have large surface area, making them appealing for reaction, yet also

vulnerable to oxidation by water and dissolved oxygen, which causes aggregation and

iron oxide formation, reducing reactivity [133-137]. The introduction of a noble metal

can result in enhanced reactivity [138, 139]. Palladium (Pd) has been widely used as a

hydro-dechlorination catalyst. Numerous bimetallic systems that are designed to

dechlorinate toxic chlorinated organic compounds have been reported in literature [140],

including: Fe/Cu [141, 142], Fe/Ni [122, 143] or Fe/Pd [144-149]. Among these, the

Fe/Pd bimetallic system has emerged as the most efficient and most commonly used

system for dechlorination of various chloro-organics due to its low activation barrier

[144]. The Fe acts as an electron source, which reacts with water to generate hydrogen

gas, which is made reactive by the Pd catalyst by producing reactive hydrogen radical

species for de-chlorination [99, 101, 150-154]. This redox reaction is hindered by oxygen

dissolved in water, because it causes oxidation of the ZVI, rendering it unreactive.

Bhattacharyya's group has immobilized Fe/Pd bimetallic nanoparticles in functionalized

membranes for the de-chlorination of PCBs such as chlorobiphenyl, dichlorobiphenyl, 3-3'-4-4'-5-pentachlorobiphenyl, etc. [99, 110].

1.2.5.2 Incorporation of PNIPAm for PCB degradation:

PVDF membranes have also been functionalized with poly-N-isopropylacrylamide (PNIPAm) to create temperature-responsive surfaces and pores [31, 98, 103]. PNIPAm is a lower critical solution temperature (LCST) polymer that exhibits a phase transition from a hydrophilic state to a hydrophobic state at its LCST of 32 °C. By increasing temperature, property changes in the polymer chains affect hydrogen bonding with water molecules, causing the chains to transition and collapse in an water [26, 155]. PNIPAm's hydrophobicity can therefore be controlled using temperature variations, thereby enabling control over adsorption of organic compounds [43]. When PNIPAm is formed inside PVDF membrane pores, controlling its hydrophobicity enables control over effective pore size, and therefore over transmembrane permeance. Furthermore, the environment surrounding immobilized nanoparticles can be controlled. Upon raising the temperature above PNIPAm's LCST, dehydration initially occurs around the hydrophobic isopropyl groups of PNIPAm, initiating the backbone to change structure [92-96]. This transformation reduces the water content and oxidation of immobilized ZVI particles, and further exposing them to the hydrophobic PCB contaminants.

Immobilizing the reactive nanoparticles in membranes gives them a platform that enables their reuse and reduces particle aggregation [110]. Our group has reported the immobilization of Fe/Pd bimetallic nanoparticles in PAA-PVDF membranes for the successful degradation of PCBs. PNIPAm, however, has never been incorporated into the reactive membrane matrix to enhance reaction conditions for PCB degradation. Other

21

than yielding control over effective pore size for particle fractionation, integrating

PNIPAm into membrane pores can affect catalysis and PCB adsorption. Varying

temperature affects the adsorption of hydrophobic and hydrophilic species into the

PNIPAm domain, as well as the intrinsic reaction rate constant of the degradation

reaction. PNIPAm has been used to increase the adsorption of trichloroethylene (TCE),

another COC by raising the temperature a few degrees above the LCST [43]. It has also

been incorporated into a PVDF membrane for temperature swing adsorption of

perfluorooctanoic acid, showing reversible adsorption over several cycles by varying

temperature around its LCST [155]. Since water can oxidize the ZVI nanoparticles and

reduce reactivity, and water content within the membrane pores can be controlled using

temperature in the presence of PNIPAm, selective modification of the reduction reaction

is possible.

1.2.6 Challenges:

While commercial adsorbents exist for the removal of PFCs from water through

adsorption, the regeneration and reuse of these adsorbent tends to be difficult and

expensive. The longevity of adsorbents has been of interest; Du et al. used Fe_3O_4-loaded

fluorinated vermiculite nanoparticles to selectively adsorb PFOS and regenerated the

adsorbent using methanol for five cycles [156]. Despite such options, the regeneration

ability of PFC adsorbent materials is limited. For example, activated carbon must

undergo thermal regeneration in order to be reused. Therefore, it is important to explore

adsorptive materials that are easier and cheaper to regenerate and reuse.

Practical concerns arise with the long-term use of Fe-Pd nanoparticles for the

degradation of PCB through the reductive pathway. The presence of oxygen causes

nanoparticle oxidation, thereby reducing its reactivity over time. Studies have shown that particles can be regenerated and reused through reductive treatment with sodium borohydride [157]. Limiting the amount of water contacting the nanoparticles effectively enhances particle longevity. In order to further limit the oxidation of particles, materials that can attract more hydrophobic contaminants while limiting the presence of water in the reactive domain can be incorporated.

Separation and degradation using membrane-based systems can be pressure-intensive processes where a certain operating pressure is required to achieve given residence times. In order to reduce system pressure requirements while maintaining transmembrane permeance, stimuli responsive polymers can be incorporated that change conformation based on external stimuli. A cost trade-off arises when incorporating such materials between the pressurization cost and the cost of the external stimulus required to instigate the stimuli responsive material's response.

Table 1.1: Environmental stimuli that trigger polymers with conformational transitions. (Reprinted with permission from [23]. Copyright (2019) Elsevier).

Response Stimulus	Mechanisms	Examples of Polymers
Temperature	Balancing between hydrophobic and hydrophilic (hydrogen bonding) states for temperature below or higher than LCST/UCST values[a]	– Poly(N-isopropylacrylamide) (PNIPAAm) – Poly(N,N'-diethylacrylamide) (PDEAAm) – Hydroxyethyl cellulose (HEC) – Poly(methyl vinyl ether) (PMVE) – Poly(N-vinyl caprolactam) (PVC) – N-vinylcaprolactam (NVCI) – Poly(N-ethyl oxazoline) (PEtOx)
Ionic strength	Changes in charge density shift the gel network to a swollen configuration	– Polyacrylamide-acrylic acid copolymers (PAAm-co-PAA) – Poly(acrylic acid) (PAA) – Poly(styrene sulfonate) (PSS) – Polyzwitterion (PZ) – Poly(methacrylic acid) (PMAA)
pH	pH induces ionization of polymer chain, causing increase in osmotic pressure and hydration of the responsive materials	– pH-responsive dendrimers – Crosslinked chitosan hydrogel – Cellulose-based hydrogels – PAA – PMAA – Poly(2-(diethylamino) ethyl methacrylate) (PDEAEMA)
Electrical signal	Electric potential causes swelling and deswelling of polymer network	– Poly(2-acrylamido-2-methyl-1-propanesulfonic acid) (PAMPS) – Polythiophene (PTP) – Poly(2-hydroxyethyl methacrylate) (PHEMA)
Magnetic field	Applied magnetic field causes actuation of magnetic particles and movement of polymer	– Poly(ethylene-co-vinyl acetate) (PE-co-VA) – PNIPAAm containing ferromagnetic material – PNIPAAm-co-AAm – PHEMA with superparamagnetic nanoparticles to the chain ends
Light	Photo-chromic groups incorporated into membrane allow light-induced variations in polymer structure	– Polymers containing photo-chromic units – PHEMA with carboxylic acid functionalized spirobenzopyran – Methacrylic and acrylic spiropyrans and spirooxazines
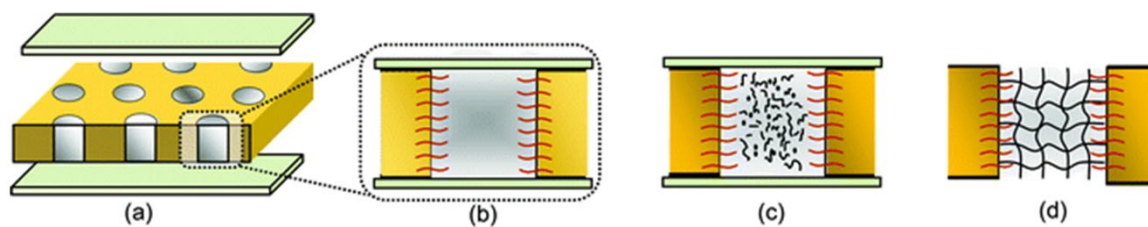
Figure 1.1: Membrane pore functionalization with responsive polymer; (a and b) membrane filled with reaction mixture, and equilibration, (c) in-situ polymerization is initiated by UV (d) hydrogen created within the membrane pore. (Reprinted with permission from [29]. Copyright (2012) Royal Society of Chemistry).
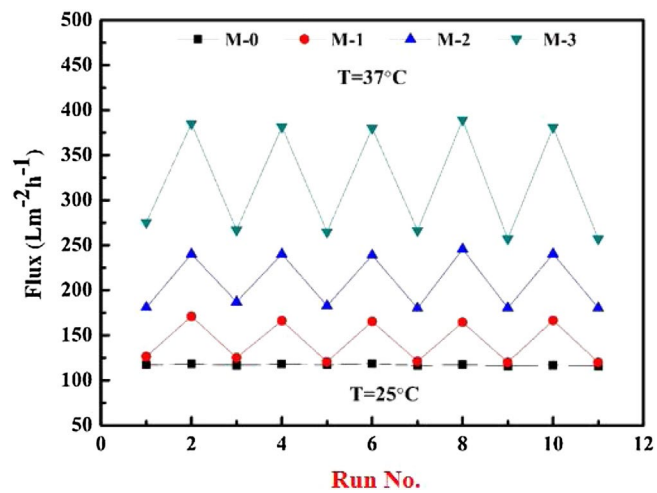
Figure 1.2: Reversible water flux response to temperature variations above and below the LCST through a multiple different PVDF-SiO$_2$-PNIPAm membranes for multiple cycles. (Reprinted from [20]. Copyright (2020) Elsevier).
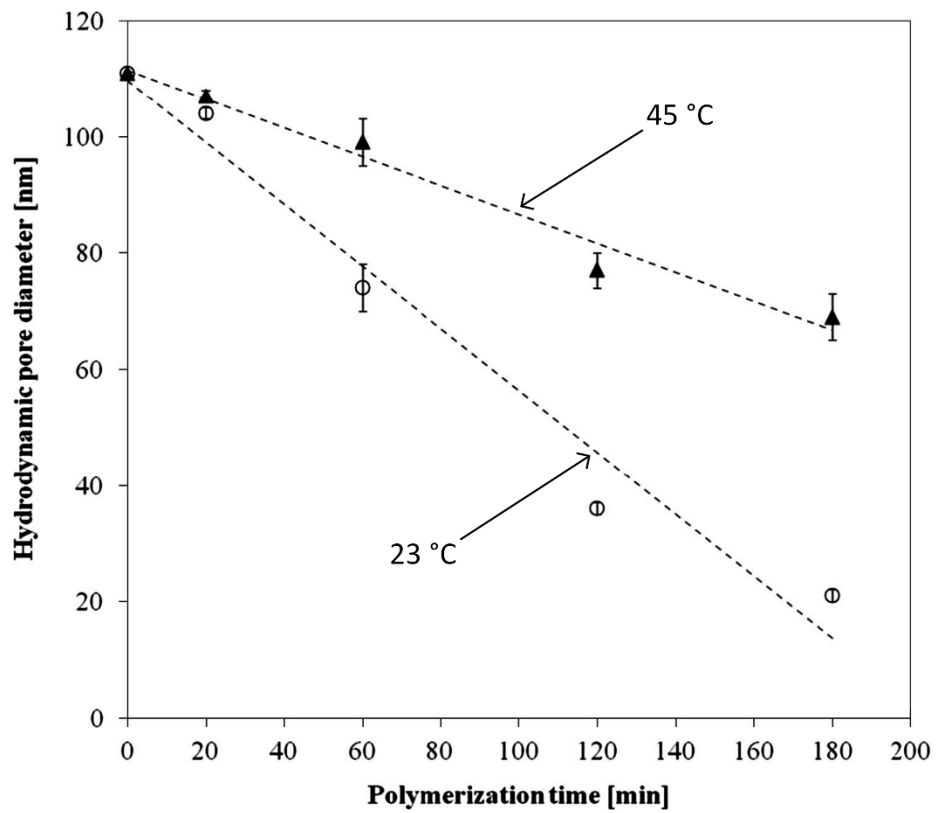
Figure 1.3: Effect of polymerization time on hydrodynamic pore diameters based on Hagen-Poiseuille law for PNIPAm-functionalized poly(ethylene terephthalate) ultrafiltration membranes. (Reprinted with permission from [36]. Copyright (2013) Elsevier).
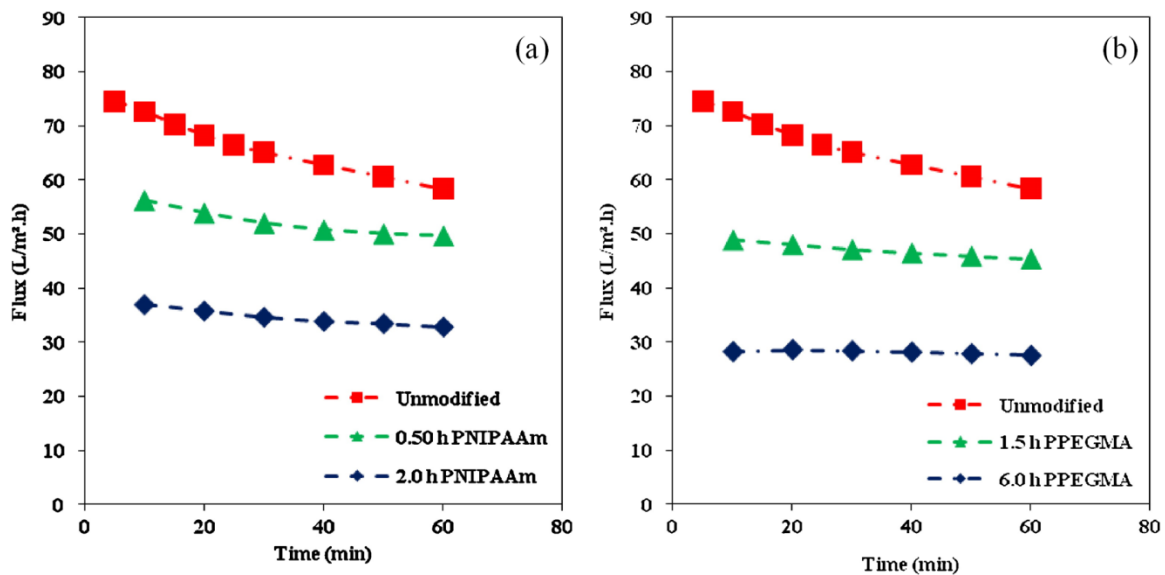
Figure 1.4: (a) Produced water flux of an unmodified membrane (5 kDa Hydrosart membrane), membrane modified by PNIPAAm for 0.5 h and PPEGMA for 3 h, and membrane modified by PNIPAAm for 2 h and PPEGMA for 3 h. (b) Produced water flux of an unmodified membrane (5 kDa Hydrosart membrane), membrane modified by PPEGMA for 1.5 h and PNIPAAm for 1 h, and membrane modified by PPEGMA for 6 h and PNIPAAm for 1 h. All experiments conducted at 210 kPa and 45 °C (Reprinted with permission from [39]. Copyright (2012) Elsevier).
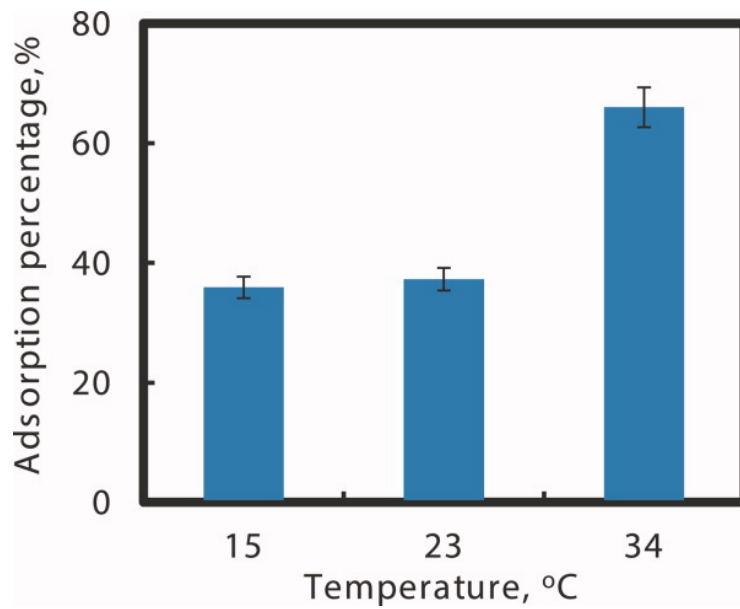
Figure 1.5: Normalized TCE (trichloroethylene) adsorption through temperature responsive P(NIPAAm-AA) hydrogel below LCST (15 and 23°C) and above LCST (34°C), feed concentration: 0.2 mM TCE in water, 20 mL, pH = 6.8. (Reprinted from [43]. Copyright (2012) Elsevier).
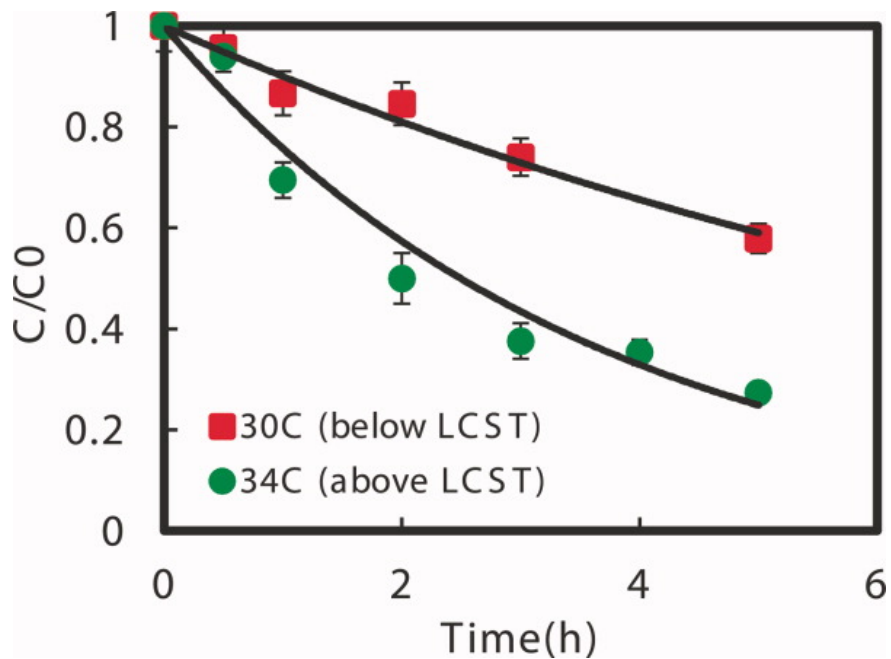
Figure 1.6: Batch dechlorination of TCE with 70 nm Fe/Pd NPs (Pd = 1.5 wt. %) immobilized in P(NIPAAm-AA) hydrogel at 30°C (below LCST) and 34°C (above LCST). Vol. = 43 mL, pH = 6.8; initial TCE concentration: 30 mg/L, iron loading amount: 0.3 g/L. (Reprinted from [43]. Copyright (2012) Elsevier).
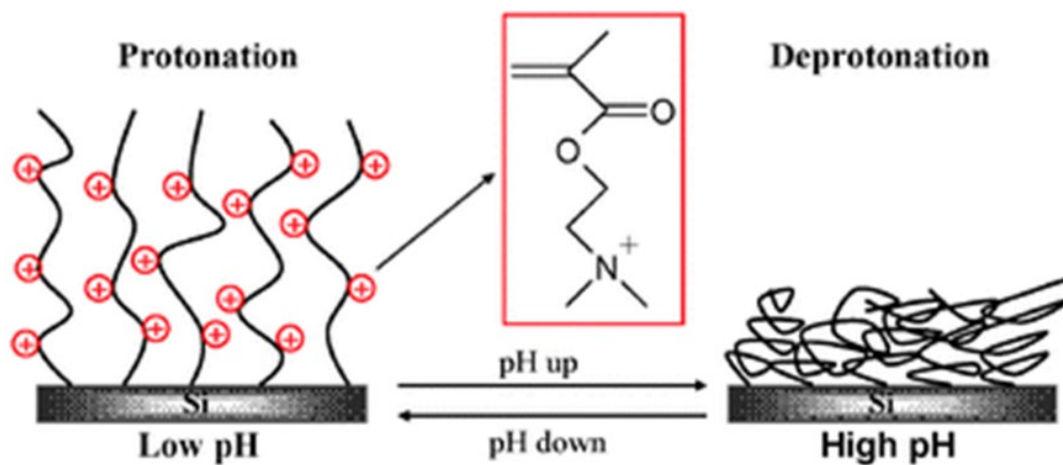
Figure 1.7: Amine functionalized membranes: pH responsive behavior of PDMAEMA above and below pKa, characterized by deprotonation of the amine group at high pH, thereby reducing repulsion between chains and allowing for higher water permeability. (Reprinted with permission from [50]. Copyright (2008) Royal Society of Chemistry).
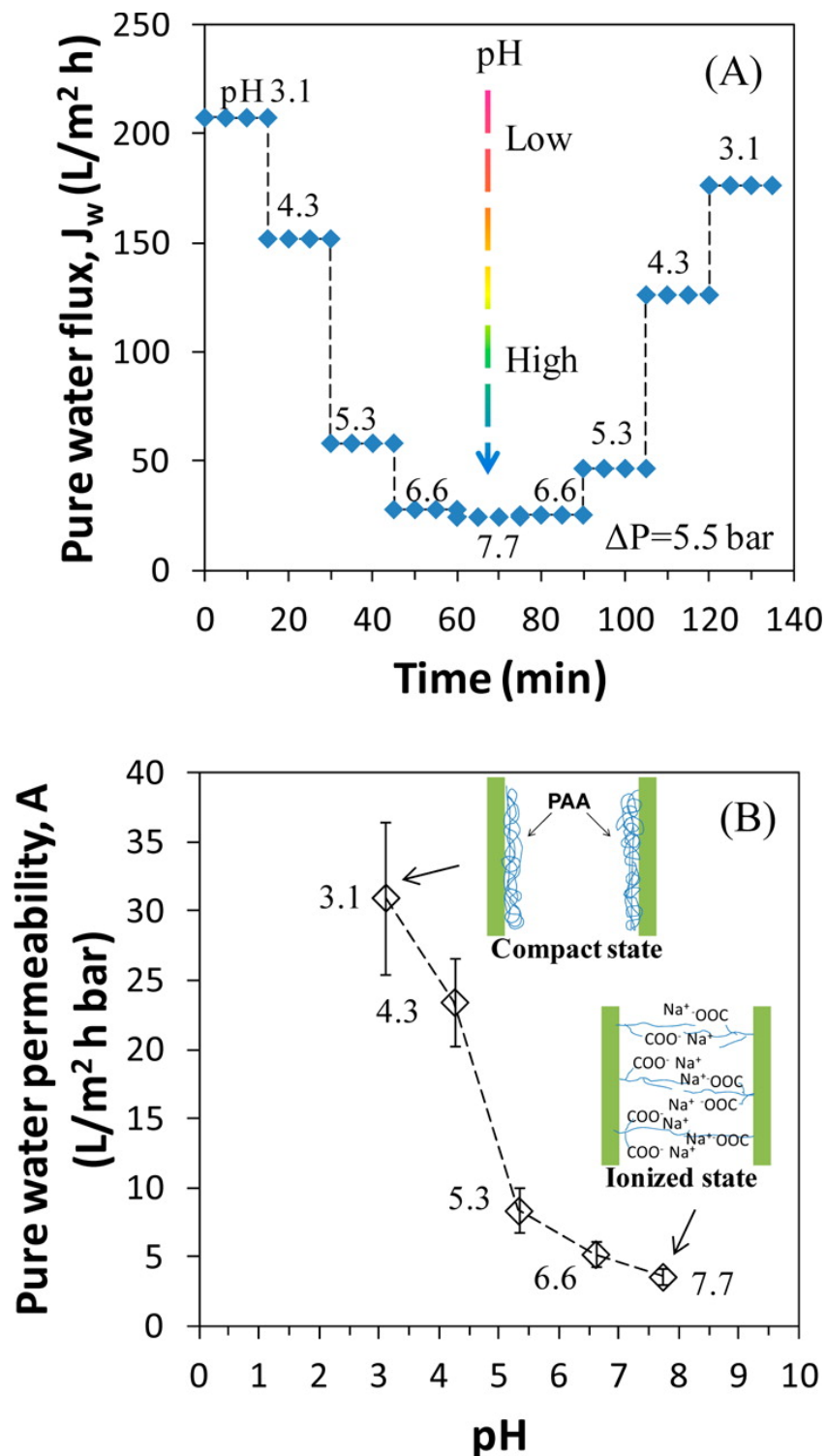
Figure 1.8: COOH functionalized membranes: pH responsive behavior of poly acrylic acid (PAA) functionalized bench-scale PVDF membranes is demonstrated by water permeation tests. (A) Water flux is determined at 5.5 bar and (B) pure water permeability. Thickness of PVDF membranes: 125 μm. (Reprinted with permission from [59]. Copyright (2013) American Chemical Society).
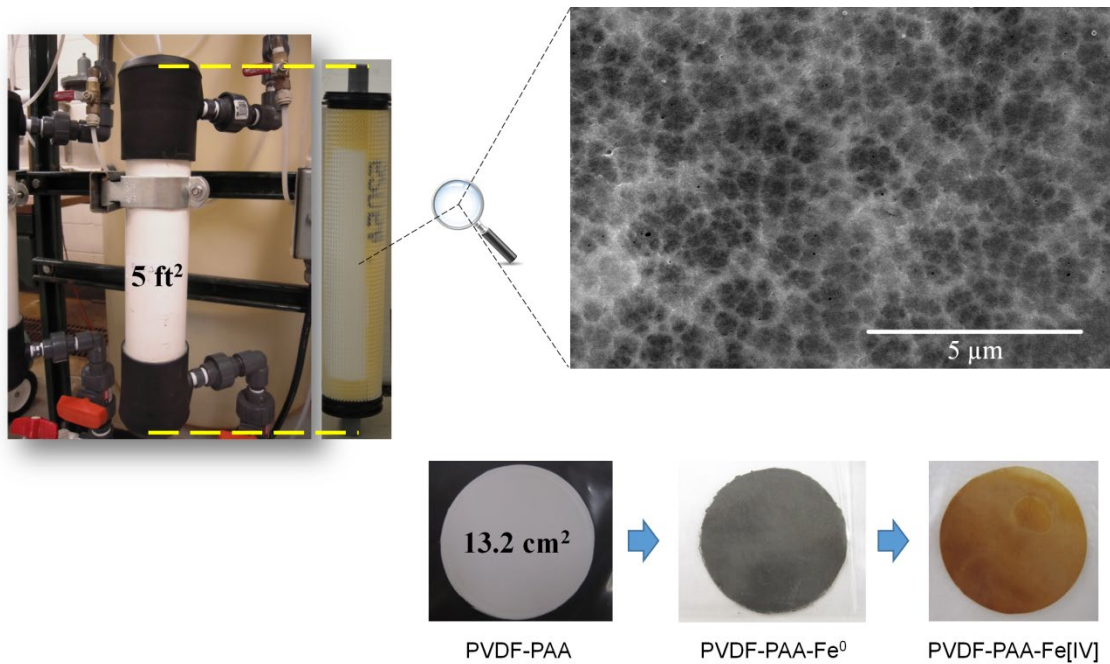
Figure 1.9: Top: Full-scale PVDF-PAA Functionalized Membrane and Module (Nanostone Water Inc.). Bottom: PVDF-PAA functionalization with zero-valent iron and iron oxide NPs. (Reprinted with permission from [158]. Copyright (2016) Elsevier).
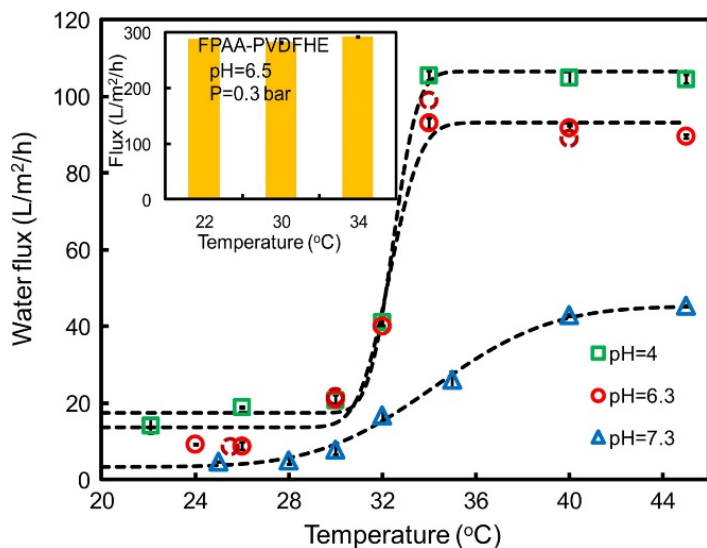
Figure 1.10: pH and temperature responsive behavior of PAA-co-PNIPAm functionalized full-scale PVDF membranes is demonstrated by water permeation tests. Water flux is determined at 0.3 bar. Sharp flux transition is seen at 32 °C. Insert shows flux behavior of membrane without PNIPAm constant pH of 6.5. (Reprinted with permission from [31]. Copyright (2014) Journal of Membrane Science).
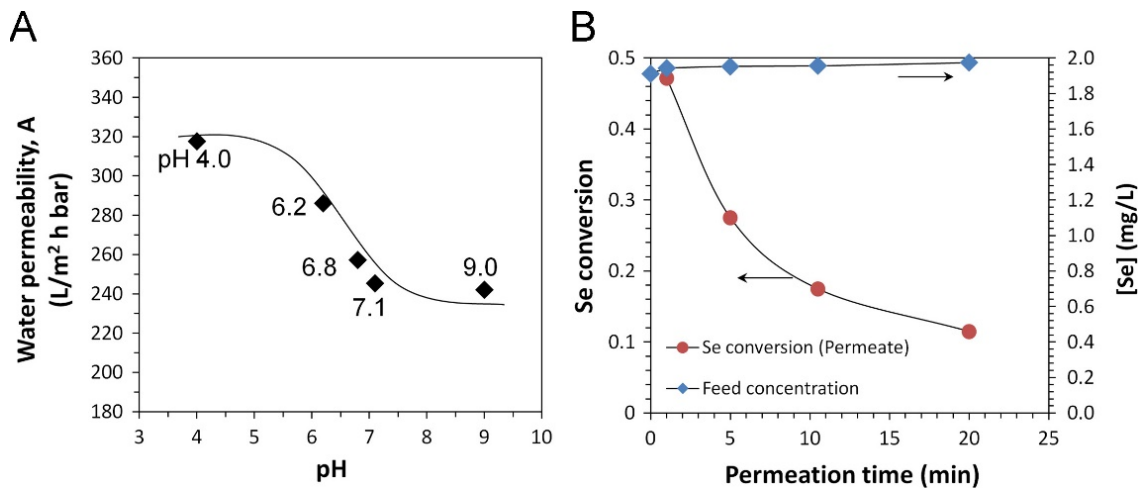
Figure 1.11: Full-scale PVDF-PAA membrane module water flux and reactivity in selenium oxyanion removal. (A) Water permeability with pH at 25 °C; (B) selenium removal results by passing synthetic selenium solution through iron immobilized module convectively, [Fe]0 = 0.68 g, [Se(VI)]0 = 1.00±0.05 mg/L, [Se(IV)]0 = 1.00±0.05 mg/L (2.0±0.1 mg/L in total) in synthetic feed solution. pH = 6.2, Jw=110.4 L/(m2·h) and τ =1.2 s. Effective membrane area: 0.465 m2. In the pH responsive study, water flux was measured after being stabilized for 15 min. (Reprinted from [62]. Copyright (2015) Elsevier).
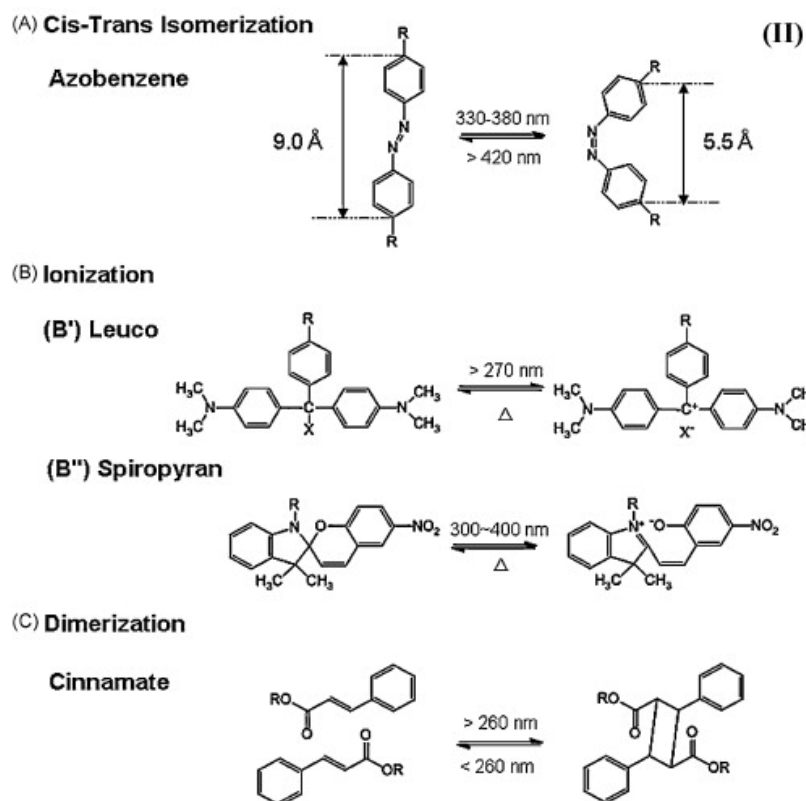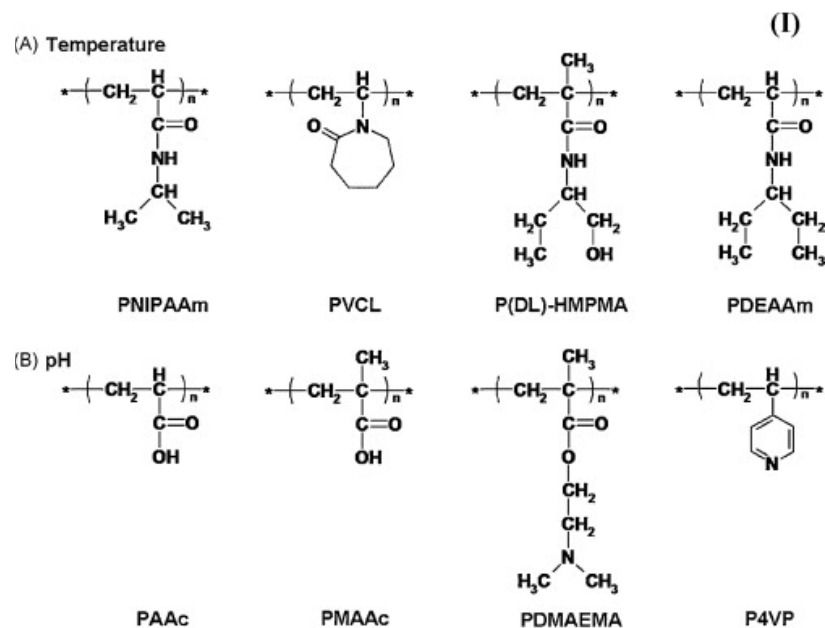
Figure 1.12: Examples of molecular structures of photoresponsive monomers: cis-trans isomer of azobenzene (A); ionization monomers of leucos (B') of spiropyran (B"); dimerization of monomer of cinnamate (C), (Reprinted with permission from [49]. Copyright (2010) Elsevier).
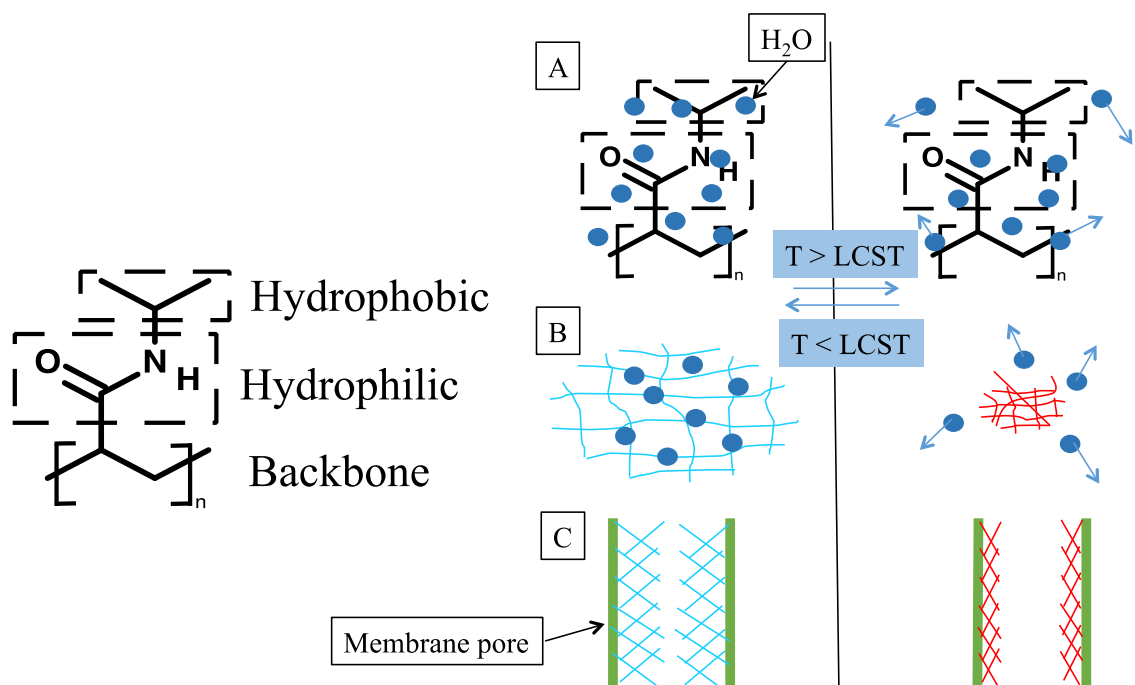
Figure 1.13: Schematic of thermo-responsive behavior of PNIPAm hydrogels and PNIPAm-functionalized membranes in aqueous environment: (A) isopropyl groups followed by polymer backbone are the first to dehydrate when temperature is raised above LCST (B) PNIPAm hydrogels swell and expand in aqueous environment below LCST (C) effective pore opening of a PNIPAm-functionalized membrane is larger when the polymer is in the collapsed state above its LCST. Reprinted from [155].

CHAPTER 2: RESEARCH OBJECTIVES

The primary objectives are the use of temperature responsive PNIPAm and its properties in order to achieve reversible adsorption of perfluoroorganic contaminants and secondly, to enhance PCB degradation via bimetallic polymeric membrane system. Multiple sub-objectives were pursued in order to achieve the primary objective. PNIPAm was synthesized in hydrogel form, and also incorporated into PVDF membrane pores in order to study its characteristics. Interaction parameters of PNIPAm and contaminant functional groups were used to describe adsorption/desorption phenomena. Furthermore, Fe-Pd bimetallic nanoparticle immobilization in membrane pores and subsequent characterization yielded degradation model characteristics. Understanding adsorption and diffusion of PCB into the polymeric PNIPAm-functionalized membrane is important in evaluating the effect of incorporating PNIPAm on PCB degradation. The structures of the polymers used in this study, specifically PNIPAm and PMMA, and of the contaminants examined, specifically PFCs and PCBs, are displayed in Figure 2.1 and a schematic of research goals can be found in Figure 2.2. The specific objectives of this research are divided into the following categories:

Synthesis and characterization of polymeric membranes and Fe-Pd nanoparticles:

- Development of temperature and pH responsive membrane by filling pores with responsive polymers

- Characterization of PNIPAm swelling and transmembrane flux at various thermal conditions for reaction model characteristics

- Immobilization of Fe-Pd nanoparticles in PVDF membrane pores via ion exchange methods

- Characterization of the bimetallic nanoparticles within membrane pores for reaction model characteristics

PFC treatment in water via reversible adsorption:

- Determination of the adsorption isotherms of PFOA onto PNIPAm hydrogels

- Determination of the adsorption and desorption kinetics of PFOA onto PNIPAm hydrogels in water around PNIPAm's LCST using a pseudo-second order adsorption kinetics model

- Evaluation of the interaction properties between PNIPAm and PFOA versus PFOS in order to describe the relationship between interaction parameters of the functional groups involved in adsorption and desorption

- Performance of temperature swing adsorption using PNIPAm-functionalized PVDF membranes for continuous adsorption and desorption over multiples cycles

PCB degradation in water via PNIPAm-PMMA functionalized PVDF membrane with reactive Fe-Pd nanoparticles:

- Evaluation of the effect of introducing PNIPAm into the reactive membrane domain on PCB adsorption at various thermal conditions

- Evaluation of the effect of introducing PNIPAm into the reactive membrane domain on PCB diffusion at various thermal conditions

- Evaluation of the effect of introducing PNIPAm into the reactive membrane domain on PCB degradation rates at various thermal conditions

- Combination of transmembrane flux data at various thermal conditions, nanoparticle characterization, and PCB degradation data in order to effectively model the reaction

PVDF

Bisacrylamide-crosslinked
PNIPAm-co-PMMA

PFOA

PFOS

PCB
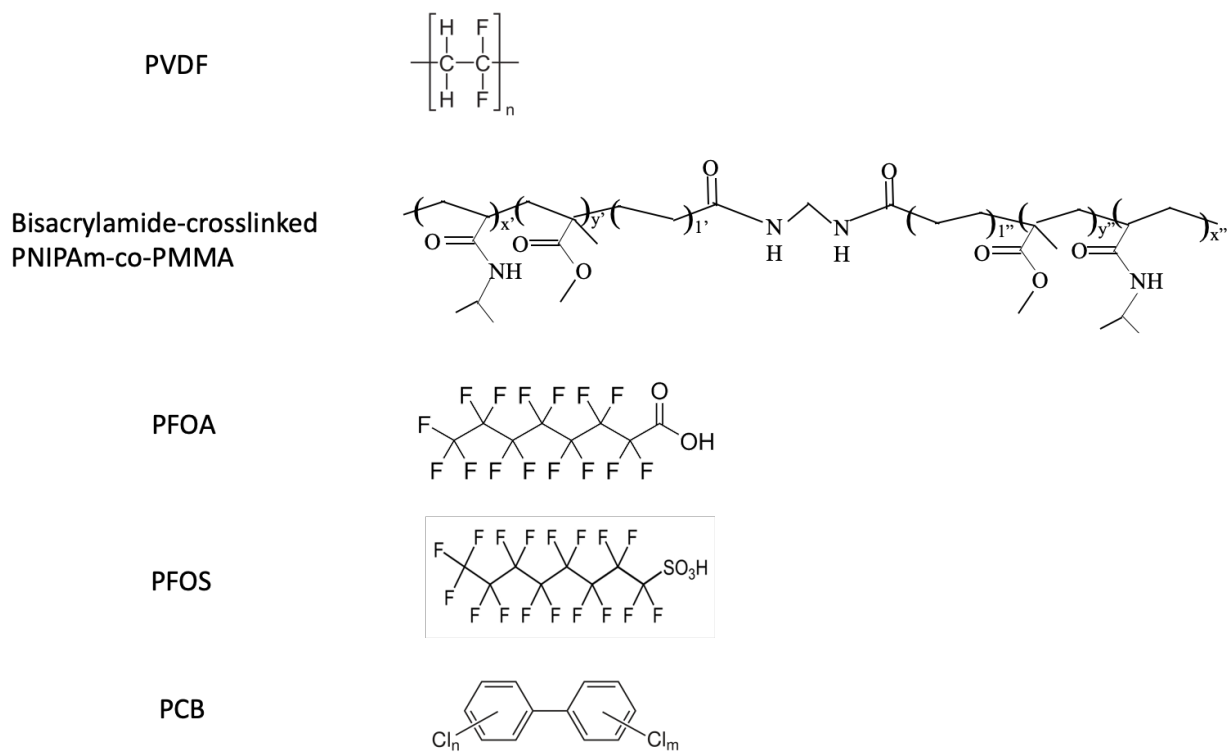
Figure 2.1: Structure of compounds used in this study
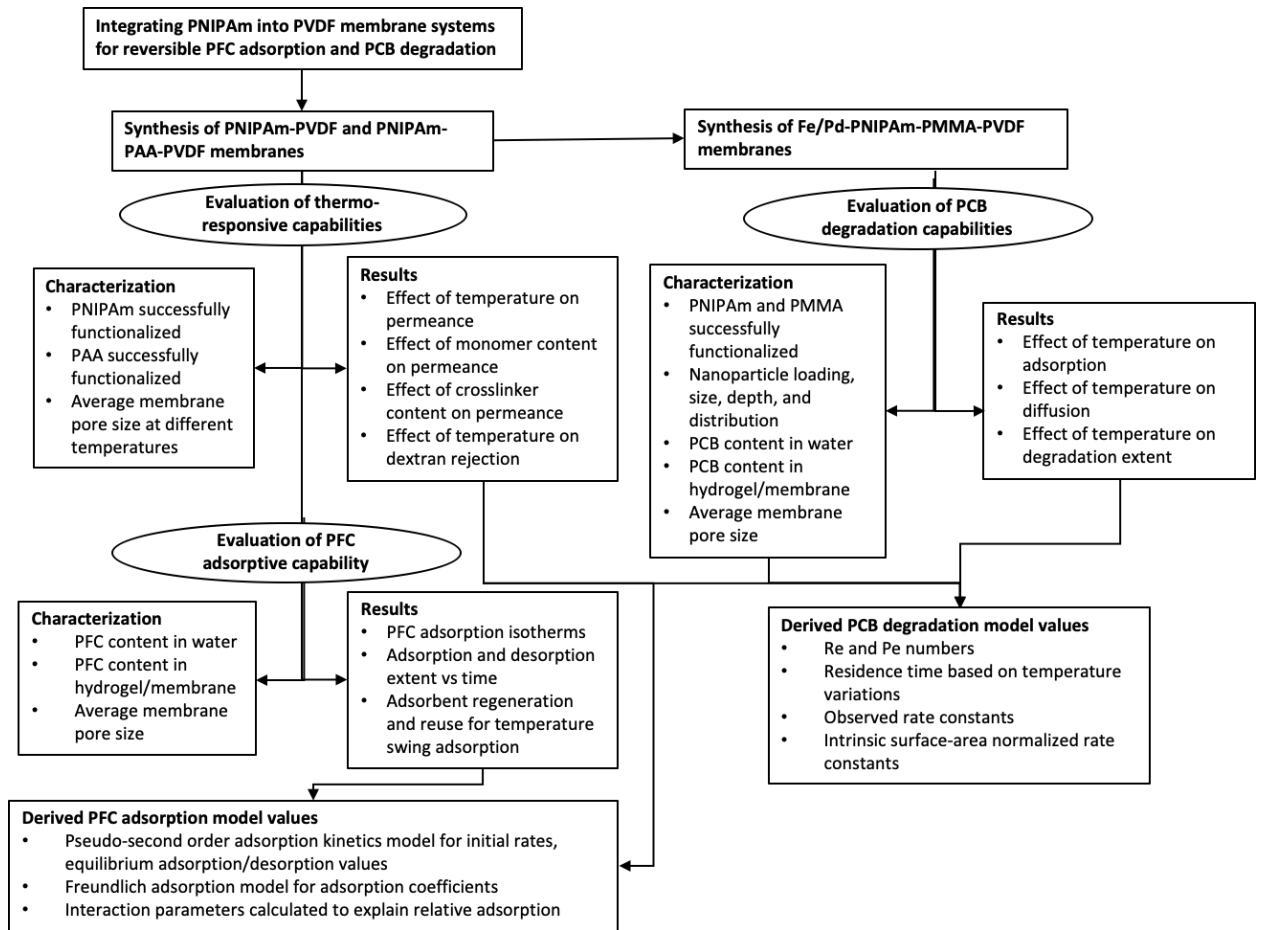
Figure 2.2: Schematic of research goals and processes

CHAPTER 3: EXPERIMENTAL

This chapter explains the experimental procedure, in detail, for each of the undertaken experiments. Details about the synthesis of polymeric hydrogels, of polymers in membrane pores, and of reactive Fe-Pd nanoparticles in membrane pores are shown. Furthermore, the analytical characterization methods, including attenuated total reflectance Fourier transform infrared, dynamic light scattering, energy dispersive X-ray spectroscopy, liquid chromatography mass spectrometry, inductively coupled plasma optical emission spectroscopy, are each explained. Experiments conducted to evaluate stimuli-responsive flux behavior, adsorption/desorption behavior, and catalytic behavior are detailed.

3.1 Materials

Full scale hydrophilized polyvinylidene fluoride 700 (PVDF-700) membranes were obtained from Nanostone Water, Inc., Oceanside, CA (average pore size: 250 nm, thickness: 0.172 mm, porosity: 0.4). All chemicals used were reagent grade. N-isopropylacrylamide (NIPAm) was purchased from VWR at 97% purity. N,N'-methylenebisacrylamide (BIS, 99%) and ammonium persulfate (APS, 98%) were received from Acros Organics. Ethanol (>99.9%), and methanol (>99.9%) were purchased form Sigma-Aldrich. Perfluorooctanoic acid (PFOA, 97%) was purchased from Alfa Aesar as Sodium perfluorooctanoate and Perfluorooctanesulfonic acid (PFOS, 98%) were obtained from Matrix Scientific as Potassium perfluorooctanesulfonate. Sodium borohydride (99.99%) and acrylic acid (99%) were purchased from Sigma-Aldrich. Sodium hydroxide (1 M), ferrous chloride tetrahydrate (FeCl2•4H2O), and

palladium(II) acetate (Pd(OAc)$_2$) were obtained from Fisher Scientific. Ultra-high purity (UHP) nitrogen gas was purchased from Scott Specialty Gases. Deionized ultra-filtered water (DIUF) was acquired from Fisher Scientific.

3.2 Synthesis:

3.2.1 Synthesis of PNIPAm hydrogels

The PNIPAm hydrogels were prepared by temperature initiated free radical polymerization. First the DIUF was purged with UHP Nitrogen for 30 minutes because the presence of oxygen affects polymerization. The pre-polymerization mixture consisted of 30 g of NIPAm monomer in 200 mL of de-oxygenated DIUF, with 3 mol% BIS cross-linker and 2 mol% APS initiator for a molar ratio of NIPAm:BIS of 97:3. The solution was placed into petri dishes in a vacuum oven at 70 °C for two hours. The hydrogels were then removed from the plates, freeze dried, and crushed using a mortar and pastel. The broken up cross-linked PNIPAm hydrogels were then placed in deionized water to wash away any unreacted NIPAm monomer.

3.2.2 Synthesis of PNIPAm-PMMA hydrogels:

The PNIPAm-PMMA hydrogels were prepared by temperature initiated free radical polymerization. The pre-polymerization mixture consisted of 13.5g of NIPAm monomer in 100mL of DIUF (deoxygenated with UHP Nitrogen for 30 minutes), and MMA and BIS crosslinker were added for a molar ratio of NIPAm:MMA:BIS of 90:5:5, along with 2 mol% APS initiator relative to NIPAm. The solution was placed into petri dishes in a vacuum oven at 70 °C for two hours. The hydrogels were then removed from the plates and washed in deionized water to remove any unreacted NIPAm and MMA monomer.

3.2.3 Synthesis of PNIPAm-functionalized PVDF membranes

PNIPAm monomer (6g, 13 wt%), BIS cross-linker (3 mol%), and APS initiator (2 mol%) were dissolved in de-oxygenated DIUF at room temperature to create the pre-polymerization mixture. The full-scale PVDF 700 membranes were developed in collaboration with Nanostone Sepro, Oceanside, CA. These hydrophilized membranes are supported by a backing fabric for increased stability, with a relatively open structure uniform geometry. The full-scale membrane sheets were cut into circles with diameters of 14 cm and were weighed prior to being mixed in the pre-polymerization mixture for 5 minutes. The pre-polymerization mixture was then passed through the membrane at least 3 times using a vacuum pump in order to ensure the mixture was inside the membrane pores rather than only on the surface. The membrane surface was then dried using UHP nitrogen gas and placed between two glass plates and heated in an oven at 70 °C while being purged with UHP nitrogen for 2 hours. The PNIPAm-functionalized PVDF 700 membrane was then removed from the oven and washed with dilute ethanol to remove any unreacted monomer and stored in DIUF overnight. The membrane's mass increased an average of 15% post-functionalization. Figure 3.1 is a schematic of the membrane functionalization process.

3.2.4 Synthesis of PNIPAm-PMMA-functionalized PVDF membranes:

NIPAm monomer (6g, 13 wt %) was mixed with MMA monomer and Methylene-bisacrylamide (MBA) cross-linker in the same ratio as the hydrogel preparation of 90:5:5, with Ammonium Persulfate initiator (1 mol %) in de-oxygenated DIUF water at room temperature. The PVDF 400 B membrane from Nanostone Sepro was weighed and mixed

in the monomer solution for 5 minutes. The solution was then passed through the membrane using a vacuum funnel to ensure coating of the membrane pores. The membrane was then placed between two glass plates and heated at 70 °C while being purged with Nitrogen for 2 hours. The surface of the functionalized membrane was then washed with water and ethanol, and stored in DIUF water overnight. Mass of membranes increased an average of 20% post-functionalization. Figure 3.2 is a schematic of the membrane functionalization process.

3.2.5 Synthesis of Fe/Pd nanoparticles in functionalized PVDF membrane pores:

The bimetallic nanoparticles were immobilized in the functionalized membrane pores via an ion exchange method developed by our lab [99]. Functionalized PNIPAm-PMMA-PVDF membranes were soaked in a 70 mM NaCl solution with an adjusted pH of 11.5 overnight to enhance ion exchange capability with Fe^{2+}. The high pH enabled the carboxyl groups of the PMMA chains to chelate with Na^+ and release H^+. A drop in pH of the solution confirms the presence of ion exchange. Next, an aqueous solution containing 4 mM Fe^{2+} as $FeCl_2 \cdot 4H_2O$ was passed through the membrane using a pressurized permeation cell several times to ensure ion exchange within the membrane pores. The membranes were then placed in an aqueous 25mM $NaBH_4$ solution for 30 minutes to reduce the Fe^{2+} to Fe^0. The membranes were then washed, and then a water:ethanol solution with a molar ratio of 10:90 containing Pd as $Pd(OAc)_2$ was passed through the membrane several times to coat the Fe^0 particles with Pd. The Pd concentration was 3 mol% of the Fe solution previously used. The membranes were washed with deionized water and stored in ethanol to avoid oxidation. The Fe content in each membrane was calculated using inductively coupled plasma (ICP) spectroscopy,

where Fe solution concentration was measured before and after the ion exchange process, and immobilization content determined via mass balance. Figure 3.3 is a schematic of the ion exchange method and degradation reaction scheme.

3.3 Characterization and analytical methods

3.3.1 Attenuated total reflectance Fourier transform infrared (ATR-FTIR)

Attenuated total reflectance Fourier transform infrared (ATR-FTIR Varian 7000e) was used in order to confirm the presence of PNIPAm in the PVDF membrane. Samples of PNIPAm hydrogels as well as non-functionalized and PNIPAm-functionalized PVDF 700 membranes were analyzed to confirm successful polymerization of the blank PVDF membranes. PVDF membrane's CF_2 group's characteristic absorption band would be found at 1120-1280 cm^{-1} [31, 159]. NIPAm's –NH and –C=O groups' characteristic absorption bands would be found at 1540 cm^{-1} and 1650 cm^{-1}, respectively [31, 160-162].

3.3.2 Dynamic Light Scattering (DLS) for particle size

Dynamic light scattering (DLS) was used in order to determine the apparent number average hydrodynamic diameter of the hydrogels, and the temperature was varied from 25 ºC to 35 ºC for 7 cycles to observe swelling behavior. The crosslinking density of the hydrogels was then increased and DLS was used to determine the average hydrodynamic diameter by raising the temperature above the LCST for 3 cycles. The swelling capacity was then compared to the less cross-linked hydrogel.

3.3.3 Energy dispersive X-ray spectroscopy (EDS) analysis of PNIPAm hydrogels with PFOA

After PFOA adsorption, PNIPAm hydrogel samples were dried and analyzed using energy dispersive X-ray spectroscopy (EDS, Oxford Instruments X-Max^N 80 detector). Hydrogel samples were freeze dried and mounted on the holder inside the scanning electron microscope chamber (FEI Helios Nanolab 660) and EDS analysis was performed in order to find the relative ratios of carbon, nitrogen, oxygen, and fluorine. Using the atomic ratios of fluorine, which only exists in PFOA, versus nitrogen, which only exists in PNIPAm, the adsorbed amount can be loosely predicted and compared to the equilibrium adsorption data.

3.3.4 Liquid Chromatography Mass Spectrometry (LC-MS/MS)

All PFOA and PFOS samples were analyzed by liquid chromatography mass spectrometry (LC-MS/MS) separation. UPLC coupled electrospray ionization tandem mass spectrometry was used in this study. A bench top binary prominence Shimadzu chromatograph (Model: LC-20 AD) equipped with SIL 20 AC HT autosampler that was interfaced with an electrospray ionization (ESI) of AB SCIEX Flash Quant mass spectrometer (MS/MS) (Model: 4000 Q TRAP). Filtered and diluted water samples were spiked with 64 ng/L isotopic mass labeled surrogate perfluoro-n-[1,2,3,4-$^{13}C_4$] octanoic acid (SS) and 30 ng/L isotopic mass labeled internal standard perfluoro-n-[1,2,3,4-$^{13}C_4$] heptanoic acid (IS) were added to 1.0 mL volume of sample solution. SS spiked samples, continuous calibration verification (CCV), reagent blank and IS-blank were used as

quality controls (QC). Target analyte concentrations and QC performance of the method were determined using IS based calibration curves.   A gradient elution of mobile phase containing 20 mM ammonium acetate in pure water (A) and pure methanol (B) was used with a Macherey Nagel analytical column EC 125/2 NUCLEODUR C18 Gravity packed with 5 µm particle (length 125 x 2 mm ID) at a constant flow rate of 0.4 mL/min. A 13.51 min gradient with composition of B was started 40% at 0.01 min, 65% at 1 min, 90% at 6 min, 95% at 11.5 min, 40% at 13.51 min with 2 min equilibration time. A volume of 5 µL of standard or samples was injected. Data were collected in negative multiple reaction monitoring (MRM) mode with monitoring of quantitation and qualifier ions for PFOA and PFOS, SS and IS. Data acquisition and process were performed using AB Sciex Analyst version 1.4.2 and Multiquant version 3.0, softwares, respectively. The precursor and product ions monitored were PFOA 412.912 > **368.7**, 168.7 m/z; PFOS 498.88 > **79.9**, 98.8 m/z; SS 416.946 > **371.9** 171.7 m/z; IS 366.897 > **321.7**, 171.6 m/z were obtained. Bold face indicates the quantitation ions. The PFOA, PFOS, SS and IS were eluted from column at retention times of 4.24, 4.78, 4.22, 3.73 min, respectively. Average spiked SS recovery was for 108.5% and CCV was 97.5%. Limit of detections (LOD) for target analytes were 0.25 ng/L at S/N= 4. Seven calibration points with linear dynamic range (LDR) were 2.5 - 320 ng/mL with R^2 values of 0.99968. MS was operated with curtain gas 30 psi, negative ESI 4500 volt, temperature 300^0C, and ion sources gas (GS1/GS2) 30 psi.

3.3.5 Metal loading analysis using ICP-OES

In order to measure the Fe content in solution, inductively coupled plasma optical emission spectroscopy ICP-OES, VARIAN) was used. Firstly, when preparing the aqueous Fe solution for ion exchange, samples were taken before and after the ion exchange process and analyzed in order to determine the change in Fe concentration. Using mass balance, the amount of Fe immobilized in the membrane was determine. As a secondary check, after using the membrane for PCB degradation, the membrane was digested in dilute nitric acid using heat, and the Fe/Pd content in the entire membrane could be measured using ICP-OES.

3.3.6 Characterization of Fe/Pd nanoparticles inside functionalized membranes:

In order to analyze nanoparticle sizes within membrane pores, a lamella was prepared using FIB-SEM (FEI Helios Nanolab 660) [109, 110]. The lamella sample was imaged using the scanning electron microscope (FEI Helios Nanolab 660) and the Fe nanoparticles could be observed directly. Elemental composition of the lamella was determined using energy dispersive X-ray spectroscopy (EDX Oxford Instruments X-Max^N 80 detector) in order to confirm the presence of Fe as the corresponding particles in the lamella.

3.3.7 PCB-1 and Biphenyl analysis:

PCB-1 and Biphenyl analysis was conducted using a gas chromatograph (GC, Varian-3900), which was equipped with an ion-trap mass spectrometer (MS, Saturn-2100T). Hexane was used as the extractant for both PCB-1 and Biphenyl. An equal volume of hexane was added to each aqueous sample and shaken for 2 hours to reach extraction equilibrium prior to moving 1 mL of hexane with extracted PCB-1/Biphenyl

into a 2-mL analysis glass vial. Biphenyl-d10 was used as an internal standard (10 ppm). The internal standard was injected into the aqueous solution prior to hexane extraction to ensure extraction efficiency. External standards of PCB-1 and Biphenyl were used to prepare calibration curves, which were linear over the concentration range of 0.1-5 ppm ($R^2 > 0.99$) using a 6-point calibration.

3.4 Swelling studies for PNIPAm-PMMA hydrogels:

Swelling studies were conducted using the PNIPAm hydrogels in order to verify their thermo-responsive behavior in an aqueous solution. Hydrogels were weighed and placed in water baths at 25 °C and 35 °C. The hydrogels were then removed, wiped to remove any water on the surface, and weighed. Five samples were used at each temperature, and the swelling ratio (Q) was calculated for each individual sample as $Q = W_s / W_d$, where W_s is the mass of the swollen samples and W_d is the mass of the dry sample.

3.5 Temperature-responsive flux measurements for PNIPAm-PVDF membranes:

The PNIPAm-functionalized membrane was placed in a stirred cell acquired from Millipore in order to study its temperature responsive flux behavior. The cell was filled with DIUF and temperature was maintained using electrical heating tape. The cell had a digital thermocouple that enabled continuous monitoring of the temperature of the DIUF inside the cell. UHP nitrogen was used to pressurize the cell, which had a maximum pressure limit of 5.5 bars. Whenever the pressure was varied, water flux through the membrane was allowed to reach steady state before any samples were taken. When the temperature was varied, samples were only taken once the permeated water temperature was equal to the cell's internal temperature. Triplicate samples were taken to measure

water flux by measuring permeated volume versus permeation time. Final runs were always conducted at conditions equal to the first run in order to test reversibility. Flux tests were performed using pure water at both 22 ºC and at 35 ºC with varying pressure in order to test the stability of the membrane. In order to further examine the temperature responsive nature of the PNIPAm functionalized membrane, the pressure was held constant and flux was measured as temperature was varied from 22 ºC to 40 ºC.

3.6 Temperature and pH-responsive flux measurements for PNIPAm-PMMA-PVDF membranes:

PNIPAm-PMMA-functionalized membranes were placed in a dead-end stirred cell acquired from Millipore in order to examine thermo-responsive transmembrane permeance. The cell was filled with DIUF water and wrapped with an electrical heating tape with a temperature controller and digital thermocouple to measure temperature inside the cell. The cell was pressurized with UHP nitrogen with a limit of 6 bars. Pressure was varied and flow through the membrane was allowed to reach steady state before samples were collected in allotted time intervals. Three samples were taken at each pressure in order to use permeated volume and time to calculate transmembrane flux. When temperature was varied, samples were taken once the permeated water temperature was equal to the water temperature inside the cell, and three samples were taken at each point. Flux tests were performed by varying pressure at constant temperature to test membrane stability. Temperature was then varied at constant pressure and pH, from 20 °C to 40 °C to test thermo-responsivity. Finally, temperature was varied again at a different pH to test the pH responsive nature of the membrane because of the

PMMA, which deionizes at pH values above the pKa of PMMA (about 4.5), causing

increased interaction with the water and lower transmembrane permeance.

3.7 PFOA and PFOS equilibrium adsorption onto PNIPAm hydrogels

Adsorption of aqueous perfluorooctanoic acid (PFOA) using PNIPAm hydrogels

was studied in order to determine the equilibrium adsorption values for aqueous PFOA-

PNIPAm systems at near freezing (4ºC), ambient (22ºC), and above LCST (35ºC)

temperatures. Aqueous PFOA solutions (20 mL) were made using DIUF with

concentrations ranging from 25 mg/L to 250 mg/L and adsorption was conducted using

0.5 g of PNIPAm hydrogels in each 20 mL vial. Three independent samples were

analyzed for each concentration point, at each temperature. By plotting the equilibrium

amount of PFOA adsorbed onto the hydrogels (q_e) versus the equilibrium PFAO

concentration remaining in the aqueous phase (C_e), equilibrium adsorption curves can be

experimentally determined for each isotherm.

The equilibrium adsorption isotherms of PFOA and PFOS were compared to

calculated interaction parameter values. The different functional groups in the

compounds yield different interaction parameters for the compounds. The apparent

hydrogen bonding and dispersion interaction parameters of the various functional groups

can be compared to the adsorption extent at temperatures above and below PNIPAm's

LCST in order to explain relative adsorption behavior.

3.8 PFOA adsorption/desorption kinetics using PNIPAm hydrogels

The ability of PNIPAm particles to adsorb PFOA was studied as a function of time to determine the adsorption and desorption rates. Two grams of PNIPAm hydrogels were placed in 500 mL of water concentrated with 1000 ppm PFOA and shaken at 100 rpm in a temperature-controlled shaker set at 35 ºC, with samples taken at various time intervals up to 24 hours. After reaching equilibrium, the hydrogels were removed from the aqueous PFOA solution and placed in DIUF and shaken at 100 rpm at 20ºC, with samples taken at various time intervals up to 18 hours. A sample volume of 1 mL was used in order to minimize the impact on the total solution concentration. Triplicate samples were always taken. Once taken, the sample was then analyzed using LCMS. Knowing the concentration of the aqueous phase at each point, the amount of adsorbed PFOA at each time interval was calculated by mass balance.

3.9 PFOA adsorption onto PNIPAm-functionalized PVDF membranes via convective flow

The PNIPAm-functionalized membrane was placed in a stirred cell acquired from Millipore in order to study its ability to adsorb and reversibly desorb PFOA as it is passed convectively through the membrane. In order to study adsorption, the cell was filled with 80 mL of DIUF concentrated with PFOA (0.5 mg/L) while the temperature was maintained at 35 ºC using electrical heating tape. The cell had a digital thermocouple that enabled continuous monitoring of the temperature of the DIUF inside the cell. UHP nitrogen was used to pressurize the cell to 3.5 bar, yielding an average flux of 11 LMH. 80 mL of aqueous PFOA was passed through the membrane and the permeate was all

collected in approximately 10 mL aliquots and PFOA concentrations were analyzed by LCMS using triplicate samples from each aliquot. Using mass balance, the amount of PFOA adsorbed in the membrane at each point could be calculated. Next, 80 mL of DIUF was placed in the cell at 22 ºC with the pressure maintained at 3.5 bar in order to force the entire volume through the membrane to measure its desorption ability. Again, the entire permeate was collected in approximately 10 mL aliquots and the associated concentrations were analyzed using LCMS in order to determine the amount of desorbed PFOA. This adsorption/desorption study was repeated 5 times in order to test the long-term stability of the membrane and explore its ability for temperature swing adsorption.

3.10 Adsorption/desorption of PCB-1 in PNIPAm-PMMA hydrogels:

Hydrogels were placed in 20mL aqueous PCB-1 and Biphenyl solutions and shaken for 24 hours at 25 °C and 35 °C in order to determine relative adsorption. PNIPAm-PMMA-functionalized PVDF membranes, as well as pristine PVDF membranes with no functionalization, were also placed in the same volume and concentration of PCB and Biphenyl at 25 °C and 35 °C and shaken for 24 hours. Three independent samples were taken for each material, at each of the two temperatures. Samples before and after adsorption were analyzed using GCMS-MS, and adsorbed quantity was calculated via mass balance. Next, vials with PNIPAm hydrogels and 20 mL of aqueous PCB-1 that were shaken at 35 °C were then shaken at 25 °C for 24 hours, and samples were analyzed for any changes in PCB-1 concentration, and therefore in adsorbed PCB-1. The vials were then shaken at 35 °C again for 24 hours to measure any subsequent change, and temperature was varied above and below the LCST over three

cycles to determine whether adsorption/desorption was reversible. There was no head space in the vials to avoid PCB-1 and Biphenyl loss due to their semi-volatile nature.

3.11 Diffusion of PCB-1 through Fe-Pd-PNIPAm-PMMA-functionalized PVDF membranes:

The diffusivity of PCB-1 was measured in order to understand the mass transport influence in PCB batch and convective flow degradation. Two metal diffusion cells were used with a thin membrane in between. One one side, a 300-mL aqueous PCB-1 solution was injected on one side (the feed side), while 300 mL of pure water was simultaneously injected in the other side (the permeate side). As soon as the solutions were injected, PCB-1 started to diffuse through the membrane to the permeate side. A PNIPAm-PMMA-PVDF membrane of area 3.5 cm^2 with immobilized Fe particles was used, without the presence of Pd to avoid any reaction. Triplicate samples were taken from both sides simultaneously at various time points. All samples were mixed with an equal volume of hexane for extraction, along with naphthalene d_8 internal standard, followed by analysis using gas chromatography mass spectrometry. Diffusion experiments were conducted at 25 °C and 35 °C.

3.12 2-chlorobiphenyl degradation:

3.12.1 Convective flow degradation:

For the convective flow degradation, a piece of PNIPAm-PMMA-functionalized PVDF membrane with immobilized Fe/Pd was placed in a dead-end filtration cell (surface area of 13.2 cm^2) surrounded with an electric heating tape, connected to a temperature controller. Aqueous PCB-1 was also pre-heated or cooled to the desired temperature of the experiment. An initial PCB-1 solution of 5ppm in water was placed in

the cell and was pressurized through the reactive membrane. The solution was pressurized through the membrane until the temperature of the permeate was equal to the temperature of the filtration cell prior to conducting experiments. Pressure was varied in 10-minute intervals and permeate was collected in triplicate samples at each pressure. Transmembrane flux was measured at each pressure in order to determine residence time in the membrane. Aqueous permeate was collected in 5 mL samples, which were placed in 5 mL of hexane for extraction of unreacted PCB-1 for analysis via GCMS-MS. Residence time was varied by changing pressure within the range of 0.7 to 3.5 bars. Triplicate samples were collected at each of 4 different pressures for each given temperature. Degradation was conducted at four different temperatures: 15 °C, 25 °C, 35 °C, and 45 °C.

3.12.2 Batch degradation:

2-chlorobiphenyl (PCB-1) was degraded in a batch experiment using the PNIPAm-PMMA-functionalized PVDF membranes with Fe/Pd nanoparticles. An initial PCB-1 solution of 5ppm in water was used, due to solubility limits, in 8 mL EPA glass vials. Two pieces of reactive functionalized membranes were placed in each vial (surface area of 13.2 cm^2). Once the membranes were placed in the vials (shaken at 200 rpm), the reaction started. In order to end the reaction at various time points, the membrane was removed from the vial, and the unreacted PCB-1 and Biphenyl product was extracted by mixing the 8 mL of aqueous PCB-1 with 8 mL of hexane for analysis via GCMS-MS. In addition to using the Fe/Pd-PNIPAm-PMMA-PVDF membranes, experiments were also conducted with PNIPAm-PMMA-PVDF membranes with only Fe, and without any membrane at all as controls. A temperature-controlled shaker was used to shake the vials

during the experiments in order to be able to control the environmental temperature of the reaction and evaluate thermo-responsive behavior. Batch degradation experiments were conducted at 25 °C and 35 °C. Three samples were taken at each time point for each experiment. There was zero head space in the vials during the degradation experiment in order to avoid any biphenyl loss due to its semi-volatile nature.
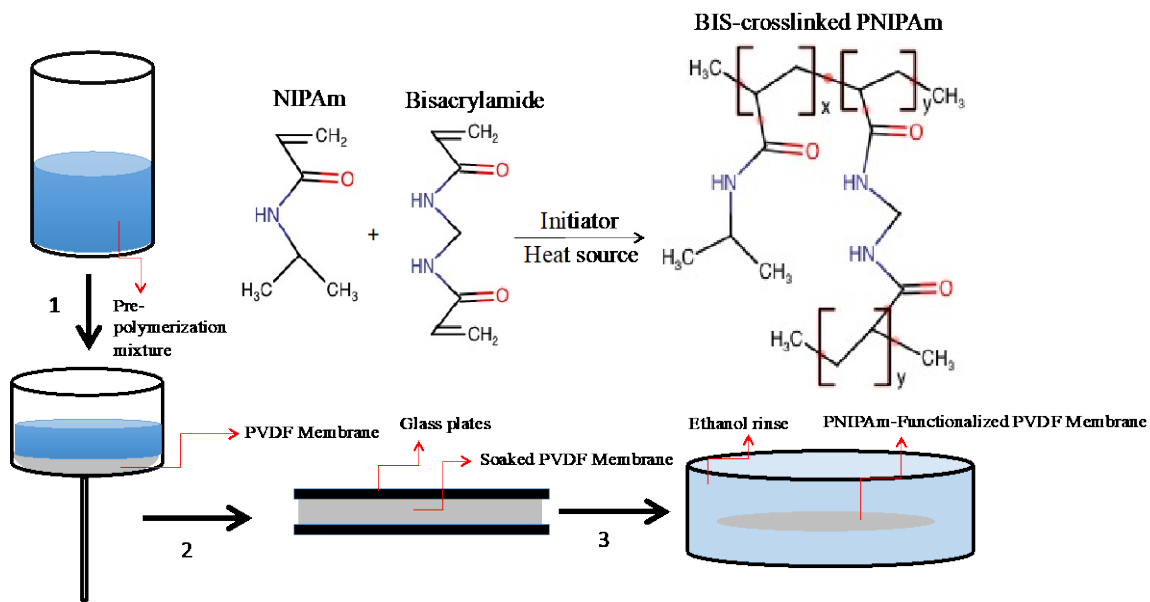
Figure 3.1: Schematic of the membrane functionalization process for PNIPAm-functinoalized PVDF membrane with BIS crosslinker. In step 1, the pre-polymerization mixture is passed through the PVDF membrane in order to wet the pores. In step 2, the soaked membrane is placed between two glass plates and heated at 70 ºC for two hours. In step 3, the functionalized membrane is washed in ethanol to remove unreacted monomer. Reprinted from [155].
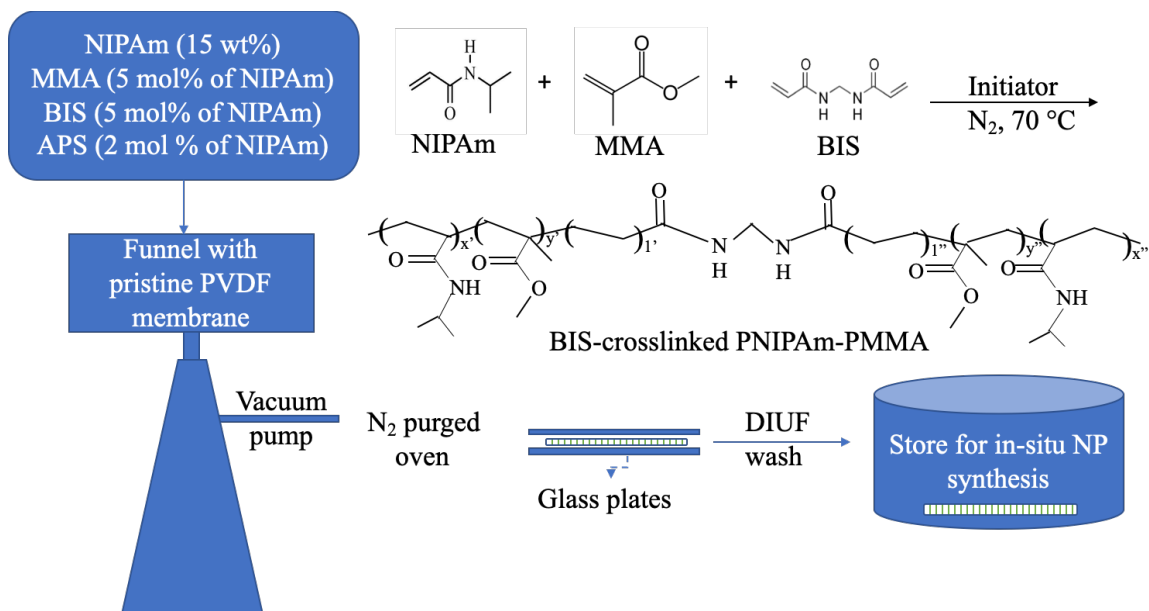
Figure 3.2: Schematic of the in-situ membrane functionalization process for PNIPAm-PMMA-functionalized PVDF membrane with BIS crosslinker.

COOCH$_3$

COOCH$_3$

COOCH$_3$

NaCl
pH 10

COONa

COONa

COONa

FeCl2·4H2O
N$_2$ purge

Fe^{2+} COO$^-$

COO$^-$

Fe^{2+} COO$^-$

NaBH$_4$

COO$^-$

COO$^-$

COO$^-$

Pd(OAc)$_2$

COO$^-$

COO$^-$

COO$^-$

Fe^{2+}

e$^-$

H$_2$O

H$_2$

Fe$_0$

Pd$_0$
(Fe^0 + Pd^{2+} → Fe^{2+} + Pd^0)

H*

C$_{12}$H$_9$Cl

C$_{12}$H$_{10}$ + Cl$^-$

Fe^0 + 2H$_2$O $\longrightarrow$ Fe^{2+} + H$_2$ + 2OH$^-$

H$_2$ $\xrightarrow{\text{Pd}}$ 2H*

PCB + 2nH* $\longrightarrow$ Biphenyl + nH$^+$ + Cl$^-$
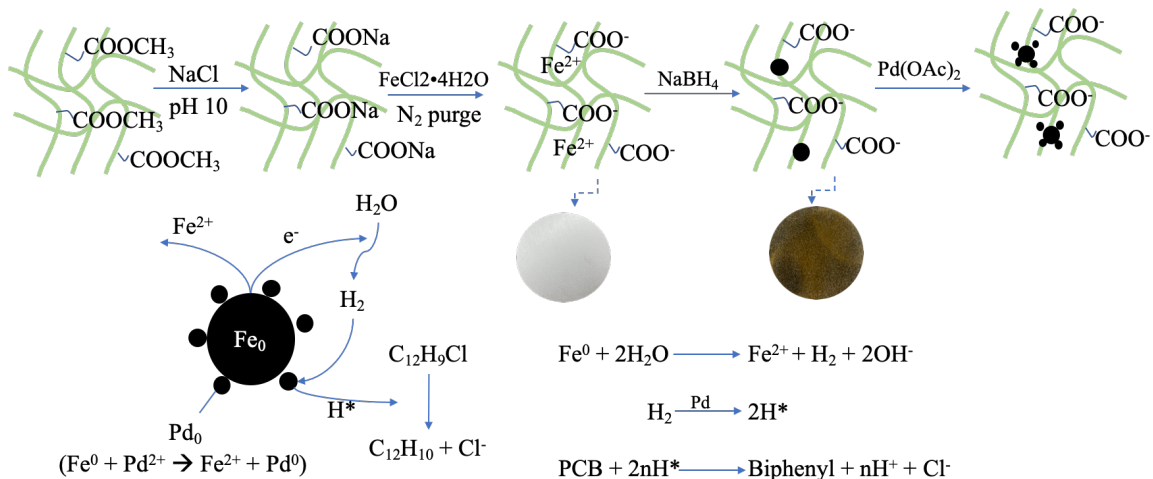
Figure 3.3: Schematic of in-situ nanoparticle immobilization process through ion exchange with PMMA functional groups to immobilize Fe/Pd nanoparticles for PCB degradation along with reaction scheme for PCB dechlorination via oxidative pathway.

CHAPTER 4: SYNTHESIS OF STIMULI RESPONSIVE PNIPAm HYDROGELS
AND MEMBRANES AND Fe-Pd NANOPARTICLES

This chapter details the development of temperature and pH responsive membrane by filling pores with responsive polymers. Temperature and pH responsive membranes are synthesized by functionalizing PVDF membranes with thermo-responsive PNIPAm and pH-responsive PAA/PMMA. The stimuli-responsive nature of the polymers is first tested in hydrogel form, before being polymerized in PVDF membrane pores to create stimuli-responsive membranes with effective pore size control. Stimuli-responsive character is evaluated through characterization of polymer swelling and transmembrane flux at various thermal and pH conditions. The stimuli-responsive functionality is then leveraged for the rejection of dextran, a model compound used for size-based rejection. Next, Fe-Pd bimetallic nanoparticles are immobilized in membrane pores via ion exchange and characteristics are evaluated.

4.1. Swelling studies of PNIPAm hydrogels using dynamic light scattering

When the diameters of the 3 mol% crosslinked PNIPAm hydrogels were measured, the apparent hydrogel diameter decreased approximately by a factor of 10 when the temperature of the water was raised above its LCST. As shown in Figure 4.1, the hydrogel diameter decreased from about 1000 nm to about 100 nm, indicating the successful polymerization and formation of the thermoresponsive PNIPAm hydrogels, and also indicating the repeatable thermoresponsive behavior of the hydrogels over several cycles. Adding a crosslinker is necessary for the stability of the hydrogels, and higher crosslinking density leads to more rigid particles [163]. Xiao et al. showed that even though 0.5 mol% BIS crosslinker enabled the greatest swelling change, a more stable polymer network was required to avoid the polymer chain being washed out when

formed within membrane pores [31]. Wu et al. compared individual linear PNIPAm chains to corsslinked PNIPAm gels and found that crosslinked gels have a higher transition temperature [164]. While Tanaka et al. claimed that chains located in loosely crosslinked domains deform significantly upon swelling compared to chains in densely crosslinked domains, Varga et al. showed that crosslinking density distribution within gels does not affect the VPT temperature, but rather only the system swelling capacity [165-167]. The crosslinking density of the PNIPAm hydrogels was varied in order to determine the effect on swelling capacity, which can be described as:

$$S = \frac{d_{swollen}}{d_{unswollen}} \qquad (4\text{-}1)$$

Here, S represents the swelling capacity as the ratio of the apparent diameter of the hydrogels in the swollen state (25 ºC) versus their apparent diameter in the un-swollen state (35 ºC). The average swelling capacity was observed to be 10.3 for the hydrogels formed with 3 mol% crosslinker and 3.4 for the hydrogels formed with 10 mol% crosslinker, indicating that the swelling capacity of PNIPAm hydrogels is inversely related to crosslinking density. Furthermore, average diameter was larger for hydrogels made with higher cross-linking density in both swollen and collapsed states. The large standard deviation of hydrogel diameters in the swollen state can be attributed to the complexity of the chain entanglements, which will not always swell to the same extent.

4.2 Swelling studies of PNIPAm-PMMA hydrogels:

PNIPAm-PMMA hydrogels were successfully formed with a molar ratio of NIPAM:MMA:BIS of 90:5:5. The addition of the BIS crosslinker is necessary for hydrogel stability. Increasing the BIS molar ratio would lead to more rigid and inelastic hydrogels, with 0.5 mol% enabling the greatest swelling capacity, but a higher percentage

necessary to avoid the polymer being washed away when functionalizing membrane

pores [31, 163]. The swelling ratio (Q) was calculated for 5 hydrogels formed in water

baths with temperatures of 25 °C and 35 °C. Upon raising the temperature above the

LCST of PNIPAm, molecular dynamic simulations have shown that the isopropyl groups

dehydrate first, causing the backbone to bend and collapse, and the hydrophilic amide

groups preferentially release bound water and hydrogen bond with each other [92-96].

The average Q for hydrogels placed in water was calculated to be 1.4 at 25 °C and 3.6 at

35 °C. Hydrogel particles were then freeze dried and crushed into very small pieces in

order to analyze swelling capacity using dynamic light scattering. The dynamic light

scattering machine has a temperature controller and can analyze hydrodynamic diameter

of small hydrogel particles in aqueous solution. The hydrogels were placed in the

chamber and temperature was varied from 25 °C to 35 °C over 5 cycles, shown in Figure

4.2. Here, instead of using a swelling ratio (W_s/W_u), swelling capacity (S) was found to

be 5.3.

4.3 Characterization of PNIPAm-functionalized PVDF membranes

4.3.1 Attenuated total reflectance Fourier transform infrared radiation (ATR-FTIR)

      The characterization of the PNIPAm hydrogel, blank PVDF 700 membrane, and

PNIPAm-functionalized PVDF 700 membrane by ATR-FTIR is shown in Figure 4.3.

Line 1 indicates the presence of CF_2 in the blank PVDF membrane due to its

characteristic adsorption band at 1120-1280 cm^{-1}, which is not present in the spectrum of

the PNIPAm hydrogel [31, 159]. Line 2 indicates the presence of PNIPAm's isopropyl

group, with characteristic adsorption bands at 1366-1466 cm^{-1} corresponding to isopropyl

group bonds [31]. Lines 3 and 4 indicate the presence of the N-H (amide I) and C=O

(amide II) stretching of the O=C-NH groups of the PNIPAm chains, respectively, with characteristic adsorption bands at 1540 cm^{-1} and 1650 cm^{-1} [31, 160-162]. The presence of the characteristic peaks of PNIPAm's functional groups in the spectrum of the functionalized PVDF membrane confirms the polymerization of PNIPAm inside the PVDF membrane pores.

4.3.2 Functionalized membrane morphology characterization by SEM

The morphologies of a blank PVDF membrane and PNIPAm-functionalized PVDF membrane were analyzed via SEM, shown in Figure 4.4. The blank PVDF membrane shows a highly porous structure with predominantly circular-shaped non-uniform pores. After functionalization with PNIPAm, the membrane is much less porous with smaller effective pore sizes. The PNIPAm hydrogels formed within the membrane pores did not leach and were not washed away, indicating strong attachment of the PNIPAm hydrogels in the PVDF membrane pores [168]. The effect of temperature on the functionalized membrane was also examined. When temperature was increased from 25 °C to 40 °C, a conformational change occurs with the PNIPAm chains, and pore size can be seen to be larger. When temperature is below the LCST, PNIPAm hydrogels in the membrane pores swell and occupy more space, resulting in a smaller unoccupied pore volume.

4.4 Temperature responsive water flux through PNIPAm-functionalized PVDF 700 membranes

PNIPAm is known to exhibit a conformational change as temperature is raised above its LCST of 32 ºC. As temperature is increased, the isopropyl and methylene groups dehydrate, causing the backbone to collapse and causing the hydrophilic

functional groups in the PNIPAm to release bound water and hydrogen bond with each other instead. When functionalized within membrane pores, the collapsing of PNIPAm chains at higher temperatures results in larger effective pore diameters. The linearity of the flux tests at constant temperature while varying pressure indicates membrane stability, and yielded fluxes of 1.6 LMH/bar at 22 ºC and 28.8 LMH/bar at 35 ºC, shown in Figure 4.5.

4.4.1 Membrane Permeance aspects

Due to laminar flow through membrane pores and assuming no slip at the wall, the Hagen-Poiseuille equation can be used to estimate relative pore diameters:

$$J_w = \frac{N \pi \Delta P}{A 8 \eta L} \left(\frac{D}{2} \right)^4 \qquad (4\text{-}2)$$

Here, ΔP represents the pressure differential (3.5 bar), N represents the number of pores, A represents the area of permeation (45 cm^2), η represents viscosity of water, L represents the membrane thickness (0.172 mm), and D represents the pore diameter. The viscosity of water is adjusted for temperature over the temperature range using the following equation:

$$\eta = 2.414 \times 10^{-5} \times 10^{\frac{247.8}{T-140}} \qquad (4\text{-}3)$$

Here, T represents temperature in Kelvin. Number of pores can be related to pore diameter and membrane void fraction:

$$N = \frac{V_m \varepsilon}{\pi \left(\frac{D}{2} \right)^2 L} \qquad (4\text{-}4)$$

Here, V_m is the total volume of the membrane, defined as the membrane surface area

multiplied by the length of the membrane, and ε is the membrane void fraction.

Combining equations 2, 3, and 4, we get the following relationship:

$$J = \left(\frac{\Delta P V_m \varepsilon}{A 8 L^2}\right)\left(2.414 \times 10^{-5} \times 10^{\frac{247.8}{T-140}}\right)^{-1}\left(\frac{D}{2}\right)^2 \qquad (4\text{-}5)$$

The relative pore diameters can then be estimated from the flux data, and constant values

such as V_m, A, L cancel out, operating under the assumption that number of pores and

membrane length are constant.

Number of pores and pore length are assumed to be constant, confirmed by measuring

membrane thickness across the temperature range. The recorded water permeance values

increased with temperature, displaying a sharper increase of over 2-fold from between 28

ºC and 34 ºC, shown in Figure 4.6. The estimated relative effective pore diameters over

the temperature range are also shown, demonstrating an increase of about 3.5-fold. This

perceived coil-to-globule transition is explained by Oliveira et al., who show that the

radius of gyration for PNIPAm decreases by a factor of about two when the temperature

is raised above the LCST, but only when the number of monomer repeat units in the

polymer chain is at least 32 [169].

4.4.2 Effects of PNIPAm crosslinking extent in membrane

The effect of PNIPAm cross-linking extent was investigated as it relates to the

functionalized membrane's flux response to changes in temperature. Permeance data was

adjusted for water viscosity changes due to temperature, and was normalized to

viscosity at 25 ºC. The content of methylene bisacrylamide crosslinker was varied

from 0.1 mol % to 2 mol % relative to NIPAm when functionalized in PVDF membranes. For each membrane, transmembrane flux was measured at constant pressure at both 30 ºC (below LCST) and 34 ºC (above LCST), which is can be found in Figure 4.7. The ratio of permeance above the LCST versus permeance below the LCST is referred to as the valve ratio, since it is representative of the change in pore size, and therefore also of the compounds that would be rejected. The valve ratio increased until it reached a value of 15 at 0.5 mol% crosslinker content, and then decreased as crosslinker was further increased.

Even though 0.5 mol% crosslinker content achieved the largest valve ratio, there are other factors to consider when determining the optimal crosslinker content for PVDF membrane functionalization. The PVDF membranes are functionalized with PNIPAm via a pore filling method, where the monomer solution is polymerized in situ in the PVDF membrane pores, without covalent attachment. An increase in permeance by 15 times could cause the polymer to be washed out. When crosslinker content is increased above the 0.5 mol% value, permeance is not as drastically affected by temperature variations, which results in a more stable network. The increased crosslinker content reduces the movement of PNIPAm chains within the PVDF membrane pores and reduces swelling capacity of PNIPAm hydrogels. There are also other considerations when determining crosslinking content, such as its effect on contaminant diffusion through the functionalized membrane. If the functionalized membrane system is used to immobilize reactive nanoparticles for chlorinated organic degradation, too high a degree of crosslinking could lead to diffusion limitations and ultimately reduced reaction rate.

4.4.3 Effects of monomer concentration

Monomer concentration in the PNIPAm pre-polymerization mixture can also impact permeance when functionalized in PVDF membrane pores. NIPAm concentration in the pre-polymerization mixture is varied, with constant methylene bisacrylamide cross-liking density and persulfate initiator content. Transmembrane permeance decreased as NIPAm concentration was increased. It has been proven that NIPAm concentration is directly correlated to grafting amount when concentration is in the range of 0 – 15 % by weight [170]. Since more polymer is occupying the PVDF membrane pores, water permeability is reduced. Figure 4.8 shows the effect of NIPAm monomer concentration on effective pore diameter, calculated using the Hagen Poiseuille equation, where an increase in monomer concentration from 1 to 5 % by weight led to a reduction in calculated effective pore diameter from 230 nm to 100 nm. Manipulating monomer concentration yields control over the pore coverage by PNIPAm hydrogels, thereby enabling effective pore size control as well as further regulation of PNIPAm's thermo-responsive behavior when functionalized in membrane pores.

4.5 Temperature and pH responsive water flux through PNIPAm-PMMA-functionalized PVDF membranes:

PNIPAm has been known to exhibit a thermo-responsive conformational change around its LCST of 32 ºC, as shown in the PNIPAm-PMMA hydrogel swelling studies. When functionalized in membrane pores, the thermo-responsive behavior of PNIPAm can be used to control effective pore diameter and therefore transmembrane permeance. The introduction of PMMA into the polymeric membrane matrix, in order to be able to immobilize Fe-Pd nanoparticles through ion exchange methods, additionally provides

pH-responsive functionality. With a pKa of about 4.5, PMMA is deprotonated at high pH and protonated at low pH, thereby displaying increased hydrophilicity at low pH values and consequently increased swelling in an aqueous environment. Incorporating a pH responsive polymer has been known to aid in reducing membrane fouling because fouling properties are correlated with surface charge, which can be selectively tuned by controlling pH [57]. A PNIPAm-PMMA functionalized PVDF membrane was placed in a dead-end filtration cell, and permeance was measured across a range of temperatures for three distinct pH values. As temperature is raised around PNIPAm's LCST of 32 ºC, the isopropyl groups begin to dehydrate and initiate a chain collapse, increased effective diameter and transmembrane flux. Figure 4.9 shows the increase in permeance across the temperature range, with the largest increase occurring between 28 ºC and 35 ºC. At lower pH values, when the PMMA is in its protonated collapsed state, the PNIPAm chain collapse is less restricted and therefore exhibits a much larger change in transmembrane permeance (about 4-fold at pH=2.5). However, at high pH, when PMMA is in its deprotonated swollen state, PNIPAm chain collapse is more restricted resulting in a smaller change in transmembrane permeance (about 2-fold at pH=10). The increase in transmembrane permeance due to the PNIPAm chain collapse into a hydrophobic state provides an opportunity for enhanced adsorption of hydrophobic contaminants into the polymer matrix as they pass through the membrane. Furthermore, the reduced water content in the polymer matrix provides an ideal environment for the degradation capacity of Fe nanoparticles that have been proven to deactivate over time through oxidation due to oxygen content in the water.

4.6 Dextran rejection through PNIPAAm–PVDF membranes

The ability to manipulate effective pore size of PNIPAm-functionalized PVDF membranes by controlling temperature can be leveraged to create a gating functionality in order to separate compounds of different sizes. Dextran was used as a model compound to evaluate the effect of temperature on separation ability. Dextran's molecular weight is 2,000,000 g/mol, and the feed concentration used was 2 g/L. As temperature is increased above PNIPAm's LCST, solution flux increases through the membrane and dextran rejection decreases. Raising temperature leads to a larger effective pore size due to collapse of the PNIPAm chains, thereby allowing greater amounts to pass through. GPC experiments were conducted to measure dextran concentration in the feed and in the permeate. Monomer concentration was also varied in order to evaluate its effect on dextran rejection. As monomer concentration was raised, increased pore filling led to smaller effective pore sizes, thereby leading to increased dextran rejection. At 30 ºC, dextran rejection was almost 100% when a 5 % NIPAm monomer concentration was used in the pre-polymerization mixture. When temperature was raised above the LCST to 34 ºC, rejection fell to below 40%. At both temperatures, when NIPAm concentration was reduced from 5 % to 3 %, rejection fell by about a factor of 3. These results are shown in Figure 4.10.

PVDF membranes were also functionalized with both PNIPAm and PAA in order to evaluate the effect of not only temperature, but also of pH as it relates to dextran rejection. As pH is increased above PAA's pKa value of about 4.5, the carboxylic groups in the PAA chains deprotonate and swell in an aqueous environment, thereby reducing effective membrane pore size. Figure 4.11 shows that as pH was increased from 4 to 7.3

at constant temperature, dextran rejection increased due to reduced effective pore opening and increased mass transfer resistance caused by PAA polymer chain swelling. Dextran rejection was also tested in a PVDF membrane functionalized with the same quantity of PAA, but without PNIPAm, which showed no rejection at pH values of 4 and 6, but showed 9% rejection at pH 7.3. The addition of the formed PNIPAm chains significantly increases rejection through the membrane.
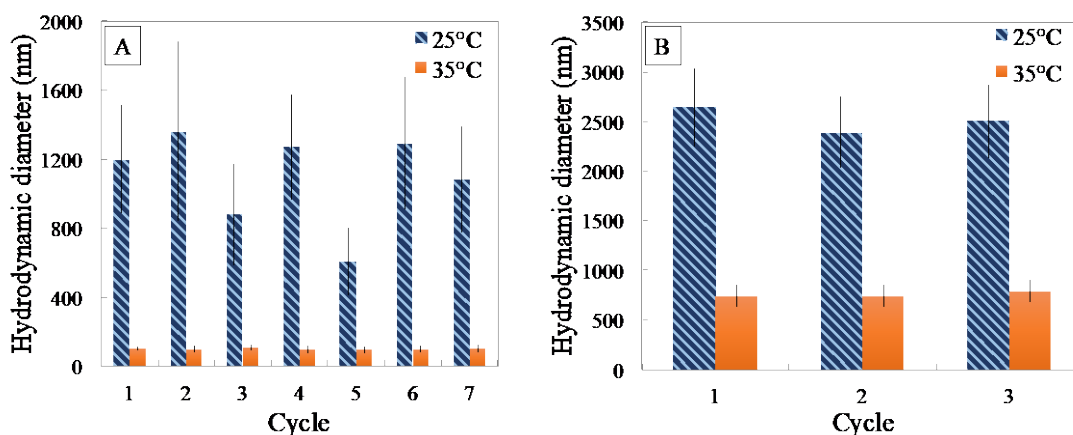
Figure 4.1: (A) Hydrodynamic diameter (number average) of PNIPAm hydrogels (13 wt% NIPAm, 3mol% Bisacrylamide crosslinker, 2 mol% APS initiator) in aqueous solution measured using DLS changing the solution temperature from 25 ºC to 35 ºC over seven cycles. (B) Hydrodynamic diameter (number average) of PNIPAm hydrogels (13 wt% NIPAm, 10 mol% Bisacrylamide crosslinker, 2 mol% APS initiator) in aqueous solution measured using DLS changing the solution temperature from 25 ºC to 35 ºC, over three cycles. Reprinted from [155].
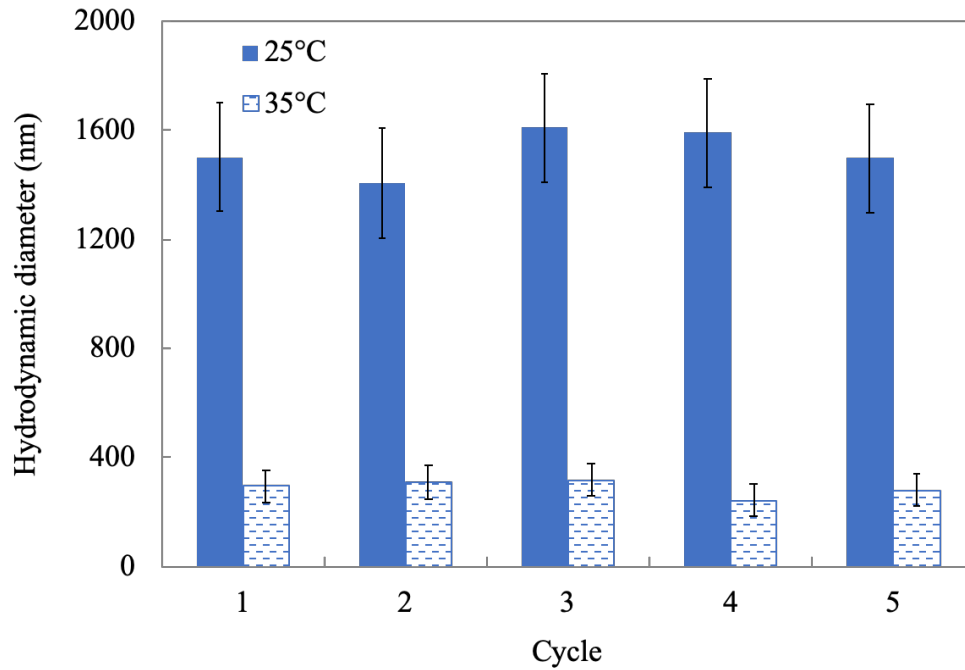
Figure 4.2: Hydrodynamic diameter (number average) of PNIPAm-PAA hydrogels (15 wt% NIPAm, 5 mol% Acrylic Acid, 5 mol% Bisacrylamide crosslinker, 2 mol% APS initiator) in aqueous solution measured using DLS changing the solution temperature from 25 ºC to 35 ºC over five cycles.
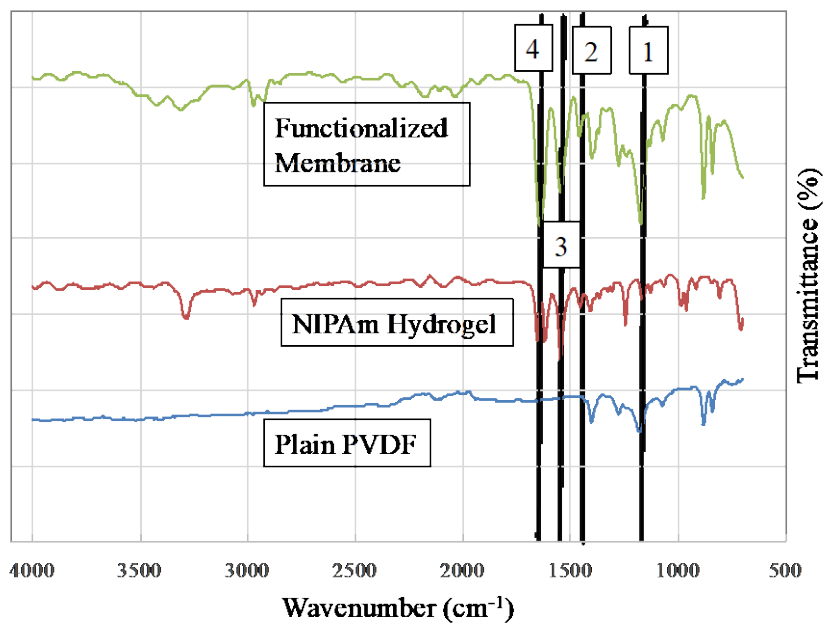
Figure 4.3: ATR-FTIR spectrum of PNIPAm hydrogel, blank PVDF 700 membrane, and PNIPAm-functionalized PVDF 700 membrane. Reprinted from [155].
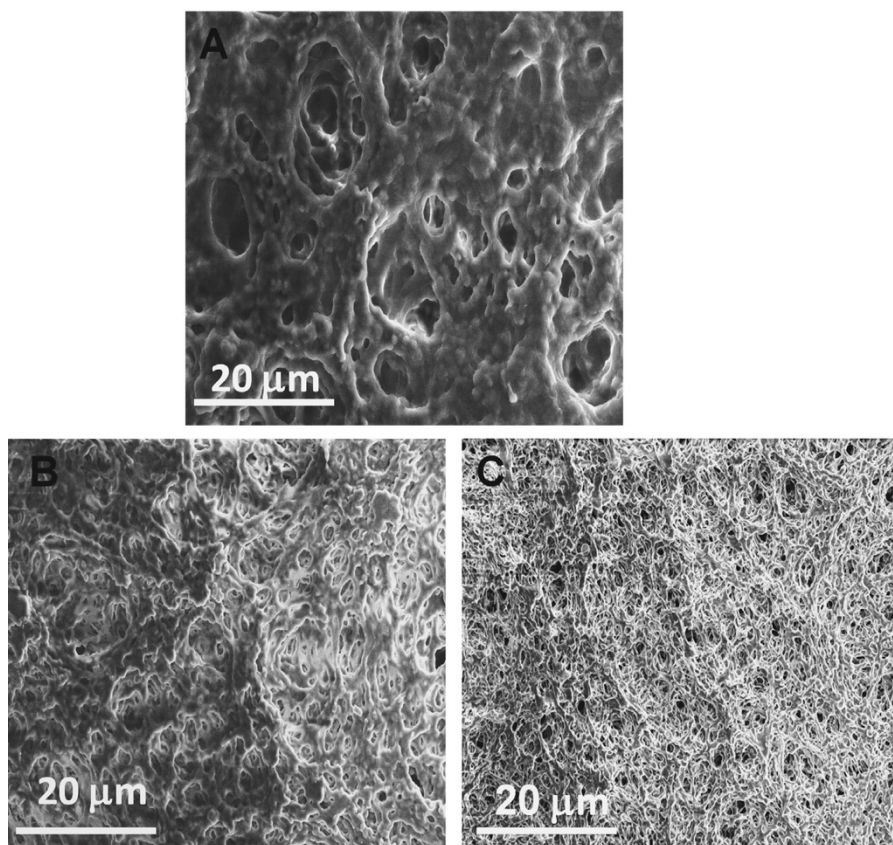
Figure 4.4: SEM images of blank PVDF (A) and PNIPAAm–PVDF Millipore membranes (B: 25 °C (below LCST); C: 40 °C (above LCST)). (Reprinted with permission from [31]. Copyright (2014) Journal of Membrane Science).
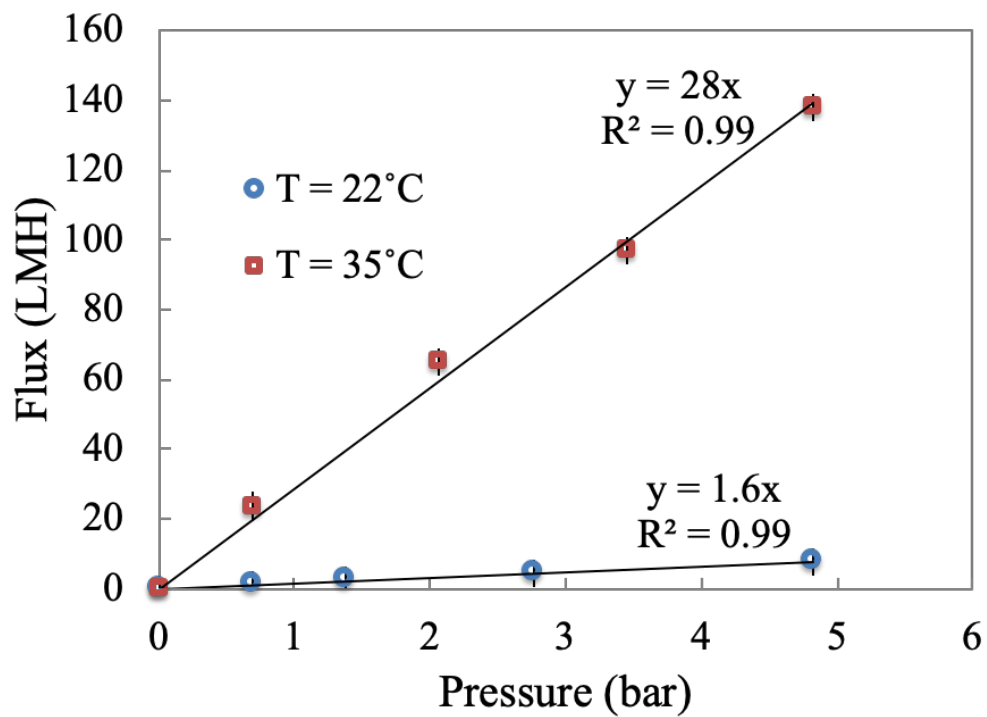
Figure 4.5: PNIPAm-functionalized PVDF membrane (15 wt% PNIPAm in water, 3 mol% Bisacrylamide crosslinker relative to NIPAm, 2 mol% APS initiator, area of 45 cm2) demonstrates stability with linear flux relationship to pressure at 22 °C and 35 °C with flux values of 1.6 LMH/bar and 28 LMH/bar respectively. Reprinted from [155].
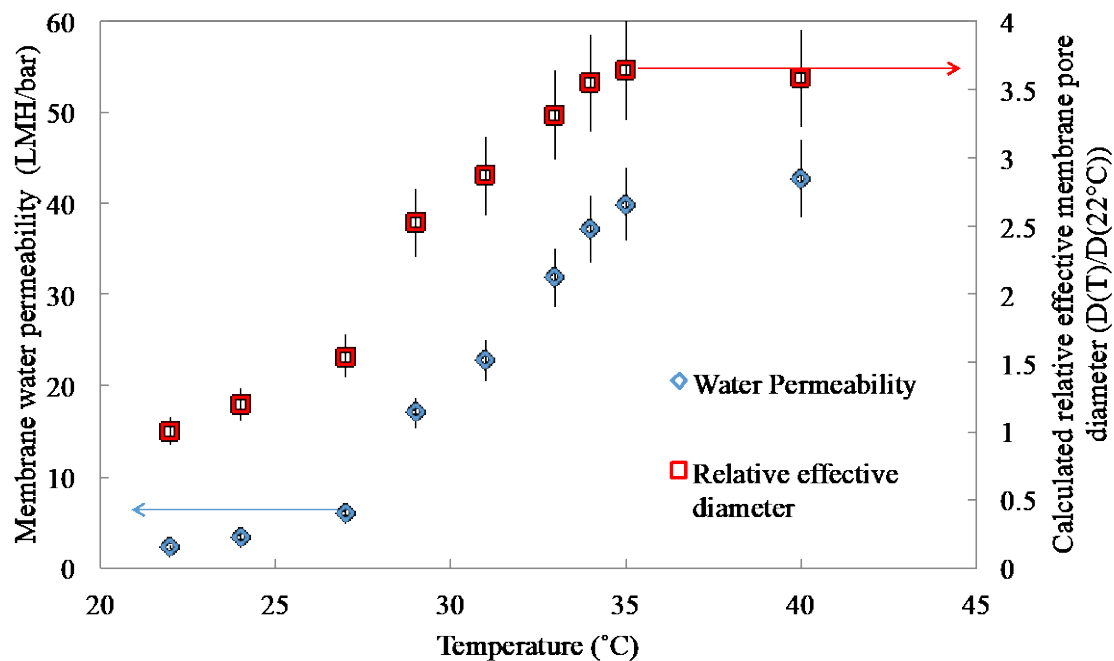
Figure 4.6: The effect of temperature on the viscosity-corrected water permeation and effective membrane pore size of a PNIPAm-functionalized PVDF membrane (15 wt% PNIPAm in water, 3 mol% Bisacrylamide crosslinker relative to NIPAm, 2 mol% APS initiator, area of 45 cm^2). As temperature is gradually increased form 22 °C to 41 °C at 3.5 bar, a sharp permeance increase (approximately 2-fold) occurs between 28 °C and 34 °C , and relative effective membrane pore opening increases over 3-fold for the temperature range. Reprinted from [155].
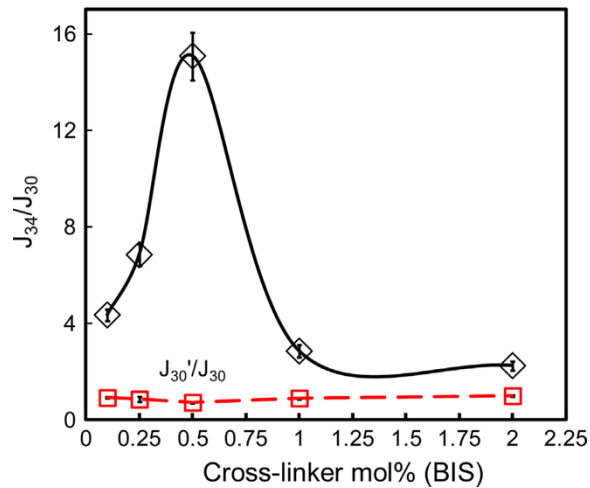
Figure 4.7: Dependence of thermal on-off ratio on the cross-linker amounts in the range from 0.1 to 2.0 mol% for PNIPAAm–PVDF Millipore membrane (P1⁄41.4 bar). For all the membranes, the NIPAAm concentration for polymerization solution was 5 wt%. Data was corrected with viscosity and normalized by permeability at 30 ºC. (Reprinted with permission from [31]. Copyright (2014) Journal of Membrane Science).
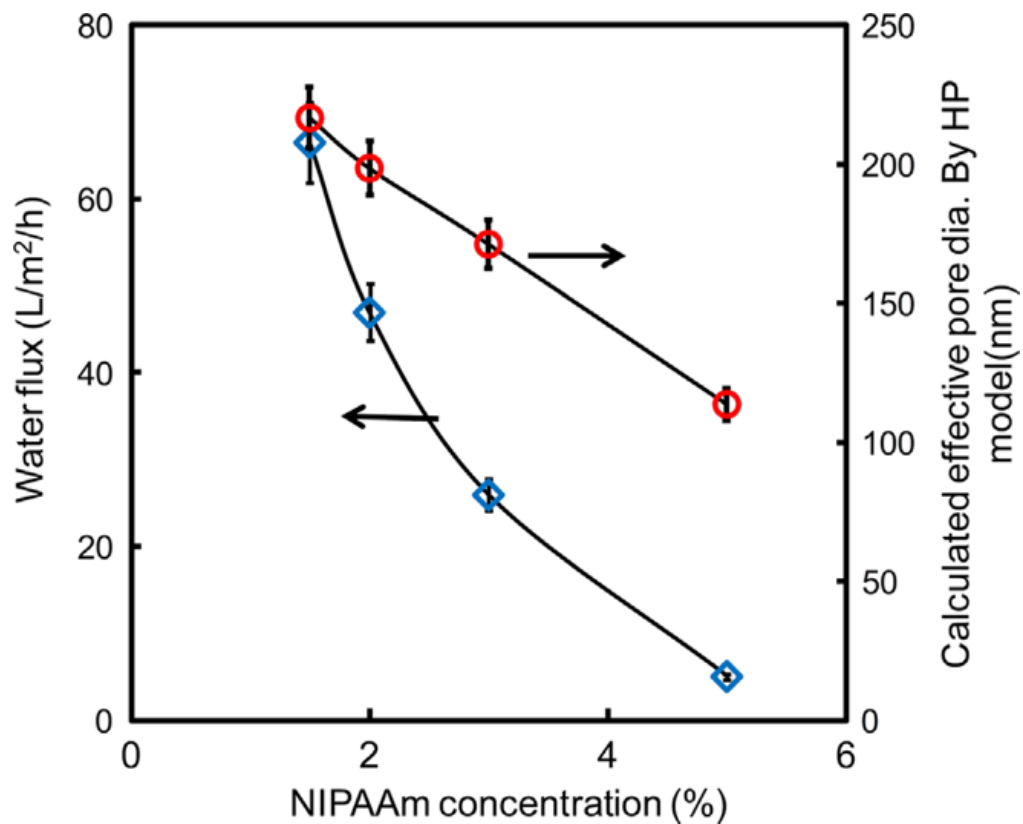
Figure 4.8: Effect of monomer (NIPAAm) concentration on water flux at 1.4 bar and calculated effective pore size for PNIPAAm–PVDF Millipore membrane (cross-linker concentration = 1 mol%). (Reprinted with permission from [31]. Copyright (2014) Journal of Membrane Science).
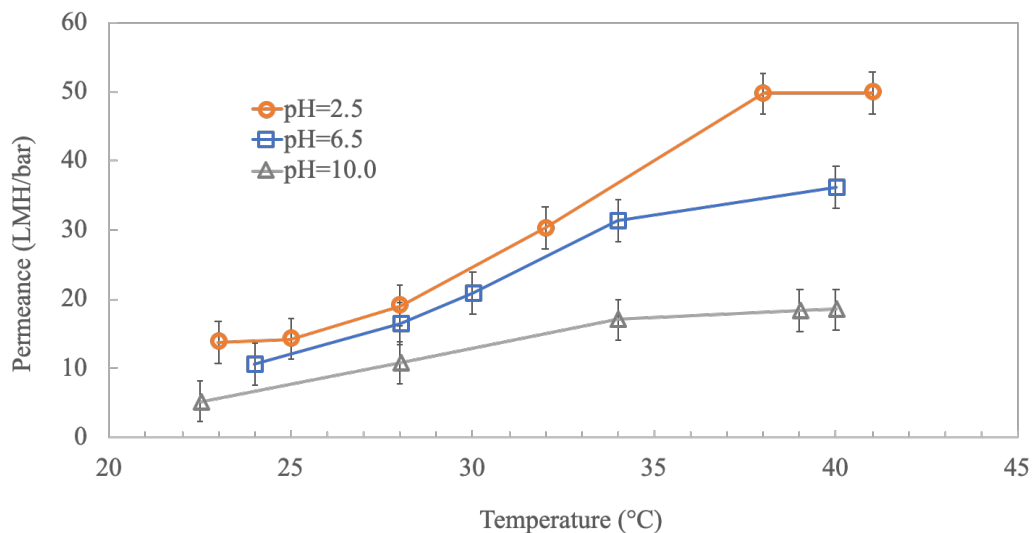
Figure 4.9: The effect of temperature and pH on the viscosity-corrected water permeation of a PNIPAm-PMMA-functionalized PVDF membrane (15 wt% NIPAm in water, 5 mol% MMA, 3 mol% Bisacrylamide crosslinker, 2 mol% APS initiator, area of 14 cm^2). As temperature is gradually increased form 22 ºC to 41 ºC at 1.7 bar, permeance increases. Decreasing the acidity of the water causes swelling of the PMMA and decreased permeance, as well as a minimized temperature effect on permeance.
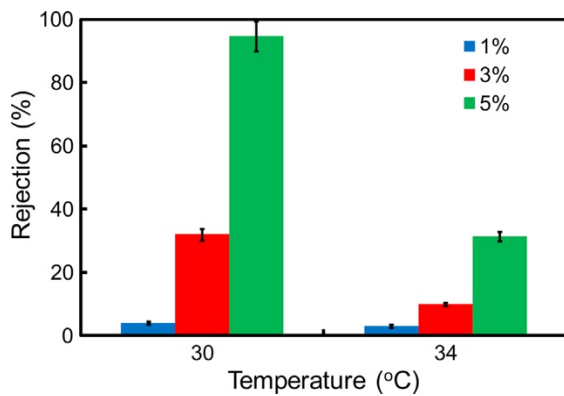
Figure 4.10: The effects of temperature and monomer concentration on dextran rejection with PNIPAm-PVDF Millipore membrane (5 mol% crosslinker) (M_W = 2,000,000 g/mol; Stokes radius r_s=26.1 nm, calculated from r_s=0.27$M_w^{0.498}$). (Reprinted with permission from [31]. Copyright (2014) Journal of Membrane Science).
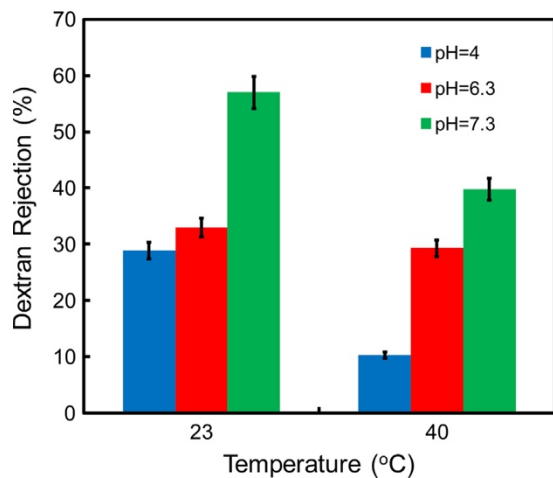
Figure 4.11: The effects of temperature and pH on dextran rejection of PNIPAm-PAA-PVDF membrane (M_w=2,000,000 g/mol; Stokes radius r_s=26.1 nm, calculated from r_s=0.27$M_w^{0.498}$). (Reprinted with permission from [31]. Copyright (2014) Journal of Membrane Science).

CHAPTER 5: THERMO-RESPONSIVE ADSORPTION-DESORPTION OF PFOA FROM WATER

In this chapter, the thermo-responsive nature of PNIPAm hydrogels, examined in the previous chapter, is leveraged for reversible contaminant adsorption in both hydrogel form and when functionalized in PVDF membrane pores. While commercial adsorbents, such as GAC, are available for the adsorptive treatment of PFCs from wastewater, the use of stimuli responsive PNIPAm is examined to address current adsorbent recycling and reuse issues. In order to evaluate adsorptive ability and the effect of temperature thereon, equilibrium adsorption isotherms are found, followed by determination of adsorption and desorption kinetics. In order to more quantitatively describe relative adsorption of compounds onto PNIPAm in its different conformational states, interaction parameters are calculated for the PFCs and for PNIPAm's exposed functional groups. The ability to use PNIPAm to conduct temperature swing adsorption over multiple cycles is then examined to test the reversibility of the adsorption mechanism.

5.1 PFOA equilibrium adsorption onto PNIPAm hydrogels

Adsorption of PFOA onto PNIPAm hydrogels was evaluated at various PFOA concentrations for three different temperatures. Due to relatively low water solubility, PFOA concentrations were varied between 25 and 250 ppm. For this low concentration range, the adsorption isotherms can be fitted using a Freundlich isotherm equation, which empirically describes adsorption of solutes from a liquid onto a solid.

$$q_e = K_d C_e^{1/n} \qquad (5\text{-}1)$$

Here, q_e (mg/g) represents the amount of solute (PFOA) adsorbed per unit weight of solid (PNIPAm) at equilibrium, in units of mg/g, while C_e (mg/L) represents the

equilibrium concentration of solute in solution (water) when the adsorbed amount is equal to q_e, and K_d (L/g) is the distribution coefficient, and n is the correction factor. While, the Freundlich isotherm does not predict that adsorption maximum, this experiment explores the linear part of the isotherm.

The observed isotherms fit the experimental data well, as shown in Figure 5.1. The K_d values increased significantly as temperature was raised, with a larger jump between 20 ºC and 35 ºC due to the polymer's LCST value of 32 ºC. Freundlich adsorption isotherms for PFOA on PNIPAm gels yields K_d values of 0.073 L/g at 35 °C, 0.026 L/g at 22 °C, and 0.007 L/g at 4 °C. As temperature is increased, the isopropyl groups of the PNIPAm particles dehydrate fast, and increase adsorption of PFOA due to its hydrophobic tail. This behavior, where hydrophobic contaminants will partition into the more dehydrated parts of the polymer, is shown in Figure 5.1.

The large increase in hydrogel adsorption capacity of PFOA from 4 °C to 22 °C cannot be attributed to the LCST conformational change of PNIPAm and therefore requires another explanation. Futscher et al. studied the conformational changes of PNIPAm versus its NIPAm monomer using Fourier transform infrared spectroscopy to probe changes, and found that NIPAm exhibits a nearly linear change with temperature compared to PNIPAm, which displays a discontinuous shift across the LCST [171]. The presence of NIPAm in the hydrogels is a reasonable explanation for the difference. Xiao et al. demonstrated decreased partitioning of hydrophilic orange II onto PNIPAm hydrogels by raising temperature. There was a significant change in partitioning when temperature was raised in the region below PNIPAm's LCST [43]. PFOA however is structured like a surfactant with a long hydrophobic tail and a hydrophilic carboxylic

head, leading to interaction with both the hydrophobic and hydrophilic functional groups of PNIPAm. Another explanation could be the effect of temperature on ionization, where increasing temperature increases Ka and decreases pKa, thereby increasing ionization in weak acids. The counter ion for PFOA in these experiments is Na^+, which has been shown to interact with the amide group of PNIPAm, showing greater interaction at higher temperatures [172].

5.2 PFOA adsorption/desorption kinetics using PNIPAm hydrogels

In order to further understand and model the adsorption kinetics, a pseudo-second order (PSO) model that has been used to explain sorption rate whereby adsorption capacity is proportional to sorbent active sites occupied was used [173].

$$\frac{\partial q_t}{\partial t} = k_2 (q_e - q_t)^2$$ (5-2)

Here, q_t and q_e (mg/g) represent the amount of PFOA adsorbed at time, t (hrs), and at equilibrium respectively, while k_2 is the second order adsorption rate constant and ϑ_0 is the initial adsorption rate (mg/g/h). By integrating from time 0 to time t, equation 4 can be rearranged as follows:

$$\frac{t}{q_t} = \frac{1}{k_2 q_e^2} + \frac{t}{q_e} = \frac{1}{\vartheta_0} + \frac{t}{q_e}$$ (5-3)

By plotting t/q_t vs. t, a linear fit enables the determination of q_e and k_2 values for both adsorption and desorption, as shown in Table 5.1 along with values for other adsorbents for comparison. These plots are shown in Figure 5.2. Kinetic adsorption and desorption values were calculated, and then used to calculate adsorption and desorption data points to compare with the experimental data, which are shown in Figure 5.3. Over half of the adsorbed amount adsorbs in the first hour, and over half of the desorbed

85

amount desorbs within the first hour. There is no longer any appreciable adsorption or desorption after 15 hours.

Here, the q_e values can be compared to the equilibrium isotherm experimental data for consistency, and fall within 20% of the predicted value from the adsorption isotherms. The initial desorption rate was greater than the initial adsorption rate, both in the same range as PFOA adsorption onto GAC, reported as 16.2 mg/g/h [75], even though the distribution coefficients are lower.

5.3 EDS analysis of PNIPAm hydrogels with adsorbed PFOA

The molar ratio of Nitrogen (N) to Fluorine (F) is a good indicator of the amount of PFOA adsorbed, since Nitrogen is only present in the PNIPAm hydrogel and Fluorine is only present in the PFOA molecules. The approximate molar ratio of N:F is 52:1, and since there is 1 N present per PNIPAm monomer, and 15 F present per PFOA molecule, the molar ratio of PNIPAm monomers in the hydrogel to PFOA molecules can be approximated as 780:1, yielding an estimated 4.7 mg/g adsorbed. In the experimental equilibrium adsorption data found in Table 5.2, the amount adsorbed for that hydrogel was 3.5 mg/g, which is on the same order of magnitude. This analysis confirms the presence and adsorption of PFOA onto the PNIPAm hydrogels, but should not be used as a quantitative tool because of the high standard deviation of values between the three different sites of the sample. Table 5.3 shows full EDS analysis results of three different sample sites. The standard deviation for F content is 0.37 for the three sites, indicating that F is not evenly distributed throughout the hydrogel.

5.4 Adsorption of PFOA and PFOS onto PNIPAm hydrogels using interaction parameters

The adsorption of contaminants such as PFOA and PFOS onto PNIPAm in an aqueous environment can be explained using interaction parameters. When the temperature is below PNIPAm's LCST, the polymer swells with bound water (to its hydrophilic amide functional groups) and bulk water [171]. Therefore, the adsorption of PFOA and PFOS onto the hydrogel will can be partly explained by the difference between 1) the hydrogen bonding interaction (δ_h) between the polymer's hydrophilic functional group and the hydrophilic groups of PFOA and PFOS (carboxylic and sulfonate groups respectively) and 2) the hydrogen bonding interaction (δ_h) between the hydrophilic functional groups of PFOA and PFOS and the water. As temperature is raised and the isopropyl groups dehydrate to initiate chain collapse, adsorption can be partly explained by the difference between 1) the dispersion interaction (δ_d) between the hydrophobic functional groups of PNIPAm (isopropyl) and of the target perfluorinated compound (fluorinated carbon tail) and 2) the hydrogen bonding interaction (δ_h) between the hydrophilic functional groups of PFOA and PFOS (carboxylic and sulfonate groups respectively) and the water. The difference occurs because the amide groups in PNIPAm will release the bound water and interact with other PNIPAm amide groups following chain collapse. Any ionization effects on interaction are not considered here. These basic interactions between the aqueous environment, PFOA, and PNIPAm hydrogels are depicted in Figure 5.4.

The effective interaction parameters for various compounds can be calculated using a group contribution method developed by Hansen and Beerbower [174]. Barton found that it is convenient and reliable to use structural combination methods to estimate

interaction parameters, and assumes additive cohesion parameter components for groups present in a molecule [174].

Ferrell et. al used a similar method for calculating solubility parameters of functional groups to quantify interaction between water and poly(styrene sulfonate) [175]. The molar attraction constant was observed by Scatchard and Small by plotting the square root of the product of the molar cohesion energy and molar volume versus chain length and realizing a linear relationship, yielding the F-method, where: [174]

$$\delta_d = \sum_z F_{d,z} / \sum_z V_z \qquad (5\text{-}4)$$

Here, V (cm^3/mol) is the molar volume and F (J$^{1/2}$ cm$^{3/2}$ mol^{-1}) is the molar attraction constant.

The F-method is not applicable directly to calculating δ_h. Assume hydrogen bonding cohesive energy is additive. Using estimates of U$_h$ (J/mol), δ_h can be estimated [174].

$$\delta_h = \left(\sum_z U_{h,z} / \sum_z V_z \right)^{1/2} \qquad (5\text{-}5)$$

The reported group contribution values of molar attraction constants, molar volumes, and molar cohesive energy can be found in Table 5.4, while calculated values for solubility parameter values of interest can be found in Table 5.5 and Table 5.6, as well as reference values of compounds with similar structures [176].

In order to compare the impact of these described interaction parameters on adsorption capacity, adsorption of PFOA and PFOS was compared. The hydrophobic fluorinated tail of both PFOA and PFOS are the same, and the dispersion interaction parameter associated with the tail is predicted to be around 20.8 MPa$^{1/2}$. However, the hydrophilic head groups of the two molecules differ. PFOA has a carboxylic group, which has a hydrogen bonding interaction parameter of 13.2 MPa$^{1/2}$ while PFOS has a

sulfonate group, which has a higher hydrogen bonding interaction parameter. Sulfonic

groups' affinity to form hydrogen bonds with OH groups has been shown to increase the

interaction of compounds with polar solvents upon sulfonation [175, 177]. Therefore, it

would be expected that PFOS would partition less into the PNIPAm hydrogels than

PFOA because of the stronger hydrogen bonding interaction between its sulfonate head

group and the surrounding aqueous environment. The lack of measured cohesive energy

density (CED) values for sulfonated polymers causes uncertainty in using group

contribution calculations to determine interaction parameters [175]. Adsorption isotherm

data for PFOS can be found in Figure 5.5, with K_d values for PFOA and PFOS are

detailed in Table 5.7. The ratio of K_d values for PFOS adsorption at 35 ºC versus 20 ºC is

only 1.1, compared to a much larger ratio of 2.8 for PFOA. While equilibrium adsorption

of PFOS by PNIPAm is higher than adsorption of PFOA below the LCST, much like

PFOS adsorption onto GAC and other adsorbents, it is much lower above the LCST due

to the presence of the sulfonate group [73-75]. Therefore, conducting temperature swing

adsorption of PFOS using PNIPAm would not provide any new information.

5.5 Predicting aqueous PFOA solution concentrations:

Using the adsorption isotherm values, the potential to concentrate aqueous PFOA

solutions can be examined. Given an initial aqueous PFOA concentration, the equilibrium

adsorption isotherm can be used to determine the extent of adsorption by computing q_e

and C_e from equations 5-6 and 5-7:

$$q_e = K_d C_e^{1/n} \qquad\qquad (5\text{-}6)$$

$$C_i V_w = q_e m_h + C_e V_w \qquad\qquad (5\text{-}7)$$

Equation 5-6 represents the adsorption isotherms. In equation 5-7, C_i is the initial aqueous PFOA concentration, V_w is the total water volume, and m_h is the hydrogel mass. Equation 7 can be combined with equation 8 in order to determine both C_e and q_e values if the other values (V_w, m_h, C_i) are known, and then equation 5 can be used to find q_t versus t values in order to predict adsorption versus time data.

Assuming 1g of PNIPAm hydrogels were placed in 20 mL of 20 mg/L aqueous PFOA and allowed to reach equilibrium at 35 °C, the K_d values indicate that 0.31 mg/g would be adsorbed, resulting in a final equilibrium concentration of 4.3 mg/L. Assuming the PNIPAm hydrogels with adsorbed PFOA are then removed and placed in 3 mL of pure water at 22 °C, the K_d values would indicate that 0.28 mg/g would remain adsorbed, resulting in a final equilibrium concentration of 11 mg/L. The final equilibrium concentration achieved was 10 mg/L, agreeing with the adsorption isotherm experiments.

5.6 Membrane Adsorption/Desorption:

PNIPAm-functionalized membrane adsorption and desorption of PFOA is plotted in Figure 5.6. Using the hydrogel equilibrium isotherms, a value of 0.5 mg/L for C_e would yield q_e values of 0.04 mg/g for the PFOA adsorption isotherm. The upper limit of functionalized membrane adsorption of PFOA is on the same order of magnitude. Desorption was conducted with pure DIUF water at 20 °C. After 300 mL of pure DIUF water was permeated, 80% of previously adsorbed PFOA was desorbed. The initial rates were calculated in terms of mg PFOA adsorbed/L of solution permeated. The initial adsorption rate was 0.14 mg/L, while the initial desorption rate was 0.17 mg/L. It was shown that after 80 mL of permeated solution (aqueous 0.5 mg/L PFOA for adsorption and pure DIUF for desorption), both adsorption and desorption rates were much lower.

Therefore, for conducting temperature swing adsorption studies, only 80 mL was used for each adsorption and desorption cycle.

Temperature swing adsorption was conducted over 5 cycles, shown in Figure 5.7. About 0.01 mg of PFOA was adsorbed after 80 mL of 0.5 mg/L of aqueous PFOA was permeated through the membrane at 3.5 bar and 35 °C, meaning that about 25% of the 0.04 mg of permeated PFOA was adsorbed. Residence time would have an impact on membrane adsorption performance, but this paper focuses on the ability to regenerate the membrane and perform temperature swing adsorption. When 80 mL of pure water was passed through the membrane at the same pressure of 3.5 bar, at a temperature of 20 °C, about 60% of the adsorbed PFOA was desorbed. For the next 4 cycles, adsorption capacity seemed to be constant after passing 80 mL of aqueous PFOA through the membrane at the same 3.5 bar pressure. Also, desorption was relatively constant at between 50-60% of the adsorbed amount. After the first adsorption/desorption cycle, however, more than 90% of the PFOA adsorbed in consequent adsorption cycle was desorbed in each following desorption cycle, indicating promise for the use of PNIPAm-functionalized membranes for temperature swing adsorption. While the pressure was held constant, the flux was maintained throughout each cycle with little deviation. Every time the temperature was raised to 35 °C for adsorption, the flux was around 10.6 LMH, while the flux dropped to around 1.2 LMH when the temperature was dropped to 20 °C, with standard deviations of 0.5 LMH and 0.1 LMH, respectively. The ability to quickly and easily desorb contaminant from the functionalized membrane is encouraging for use as an adsorbent with greater regeneration ability than other adsorbents.

In order to confirm that desorption using pure water must be conducted below LCST, two adsorption/desorption cycles were conducted using 0.5mg/L aqueous PFOA for each adsorption cycle and pure DIUF for each desorption cycle, shown in Figure 5.8. In both cases, adsorption was conducted above PNIPAm's LCST, while the first desorption cycle was conducted below PNIPAm's LCST. However, for the second desorption cycle, pure DIUF at 35 °C was used rather than at 20 °C to prove that desorption is insignificant if T > LCST. For the first cycle, 0.016 mg of PFOA was adsorbed, followed by about 60% desorption using pure water at 20 °C. A second adsorption cycle yielded the same adsorption capacity as the first cycle. However, only 13% of adsorbed PFOA was desorbed using water above LCST, compared to 60% with 20 °C water, thereby proving that LCST behavior plays a role in enhancing desorption. In the control run, where PFOA was permeated through a blank PVDF membrane, less than 1% was adsorbed, indicating that adsorption takes place in the polymeric PNIPAm domain. Flux above LCST was constant at 37 LMH, while flux below LCST was 2.5 LMH. Pressure was set at 2.75 bar because the functionalized membrane used was not as tight as the one used for the temperature swing adsorption cycles.

Table 5.1: Pseudo-second order adsorption/desorption kinetic rate values derived from experimental data with comparisons to other studied adsorbents

Adsorbent	q_e (mg/g)	k_2 (g/mg/h)	ϑ_0 (mg/g/h)	R^2
PNIPAm-PVDF membrane adsorption at 35 °C	48	0.012	28	0.99
PNIPAm-PVDF membrane desorption at 20 °C	11	0.31	41	0.99
Anion exchange resin [75]	22.2	0.63	313	1.00
Multi-walled carbon nanotube [75]	12.4	0.049	7.6	0.99
Granular actiated carbon [75]	22.7	0.032	16.2	1.00

Table 5.2: EDS elemental ratio analysis of PFOA (A) and of the PNIPAm hydrogel with adsorbed PFOA (B)

(A) PFOA		(B) PNIPAm hydrogel with PFOA	
Element	At %	Element	At %
F	62.0	C	66.4
C	28.8	N	18.7
Na	7.2	O	14.3
O	2.0	F	0.49

Table 5.3: EDS analysis of a PNIPAm hydrogel sample post PFOA adsorption. The hydrogel used was taken from the experiment in Figure 5, where 1 g of hydrogel was placed in 20 mL of 250 mg/L aqueous PFOA solution and allowed to reach equilibrium.

Weight Percentage (%)					
Element	Site 1	Site 2	Site 3	Average	Standard Deviation
Carbon (C)	66.1	65.5	67.6	66.4	1.08
Nitrogen (N)	19.7	18.8	17.6	18.7	1.05
Oxygen (O)	13.7	15	14.1	14.3	0.67
Fluorine (F)	0.06	0.7	0.7	0.49	0.37

Table 5.4: Values of molar volume, molar attraction constants, and molar cohesive energy for the prediction of functional group solubility parameter values.

Functional group		V (cm^3/mol)	F_d (J$^{1/2}$cm$^{3/2}$mol^{-1})	U_h (J mol^{-1})
-CONH		16.8	516	5985
-COOH		27.8	530	4887
-SO$_3$H		23.6	597	11347
-OH		10	210	20000
-	2 x CH$_3$	31.7	419	0
isopropyl	1 x CH$_2$	16.6	270	0
-C$_7$F$_{15}$	7 x C	-19.2	-70	0
	15 x F	18	221	0

Table 5.5: Predicted dispersion interaction parameters of functional groups involved in hydrophobic interaction.

Component	δ_d (MPa$^{1/2}$)
Water	15.6
Methanol	15.1
Isopropyl	13.8
-C$_7$F$_{15}$	20.8

Table 5.6: Predicted hydrogen bonding interaction parameters of functional groups involved in hydrophilic interaction.

Component	δ_h (MPa$^{1/2}$)
Water	42.3
Methanol	22.3
CONH	18.9
COOH	13.2
*Sulfonate	23.3

*The lack of measured CED values for sulfonated polymers causes uncertainty in using

group contribution calculations to determine interaction parameters [175].

Table 5.7: Freundlich distribution coefficients of PFOA and PFOS onto PNIPAm hydrogels above and below PNIPAm's LCST.

	K_d at 20 °C (L/g)	K_d at 35 °C (L/g)
PFOA	0.026	0.073
PFOS	0.041	0.047
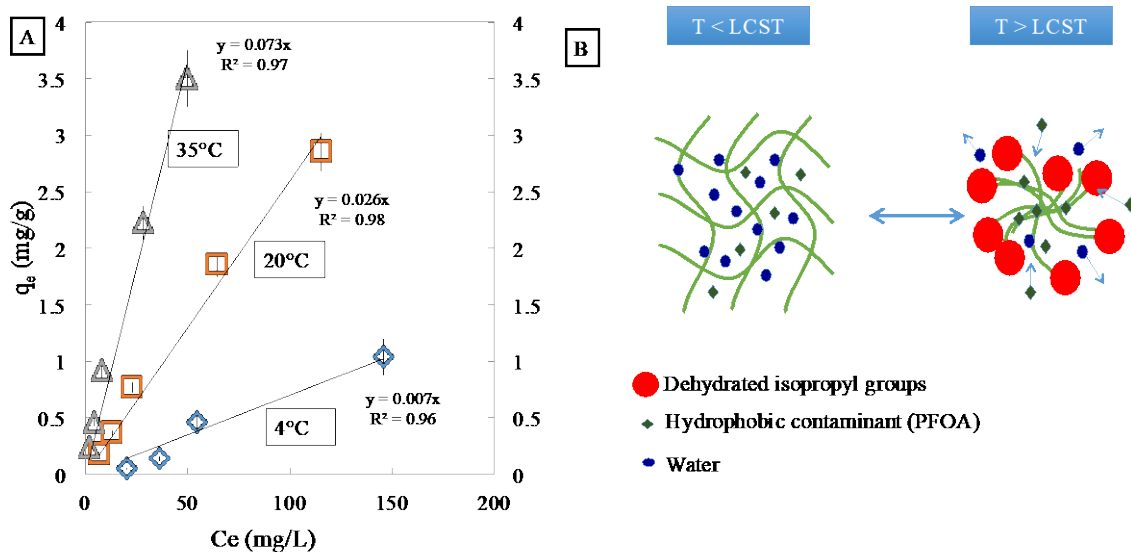
Figure 5.1: (A) Adsorption isotherms of PFOA onto PNIPAm hydrogels in water. Initial aqueous PFOA samples had concentrations ranging from 25 mg/L to 250 mg/L, with 0.5g of PNIPAm hydrogels (13 wt% NIPAm, 3 mol% BIS crosslinker, 2 mol% APS) and shaken at 100 rpm until equilibrium. Experimental data is fitted with Freundlich isotherms. (B) Schematic of adsorption of hydrophobic contaminants onto PNIPAm hydrogels in water above PNIPAm's LCST, where PFOA's hydrophobic tail preferentially resides in the dehydrated isopropyl groups of PNIPAm. Reprinted from [155].
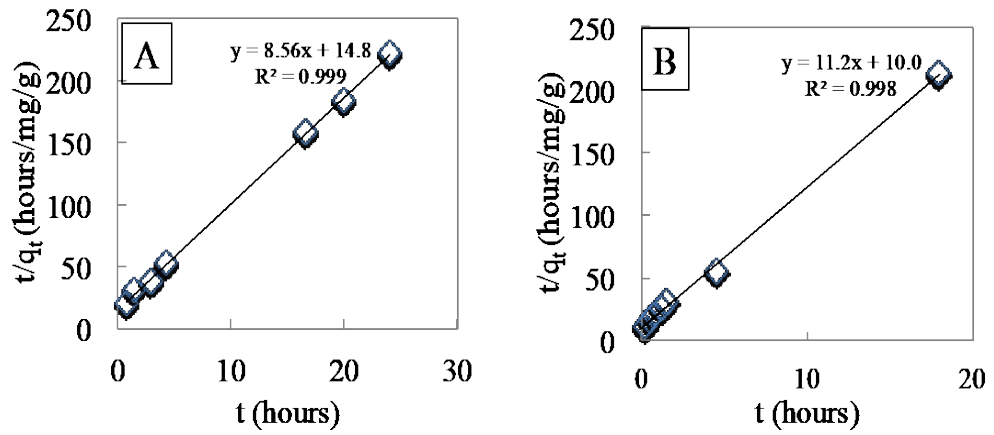
Figure 5.2: Fitting second order adsorption equation to experimental data to determine adsorption rate constants, including initial adsorption/desorption rates and second order rate constants. (A) Adsorption (35 °C) of PFOA using 2 g of PNIPAm hydrogels (d=1000 nm at 20 °C) in 500 mL of water with initial concentration of 1000 mg/L and (B) desorption (20 °C). Reprinted from [155].
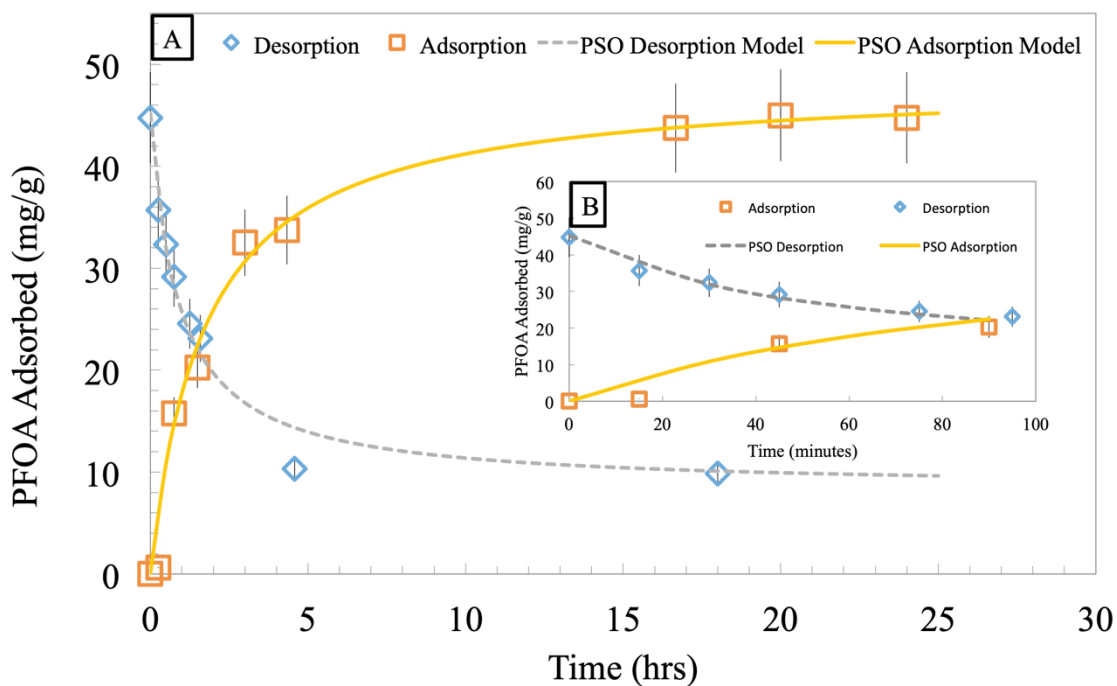
Figure 5.3: Adsorption (35 °C) and desorption (20 °C) of PFOA using 2 g of PNIPAm hydrogels (d=1000 nm at 20 °C) in 500 mL of water with initial concentration of 1000 mg/L. PSO model was fit to the experimental data. (A) PFOA adsorption and desorption over one day and (B) Zoomed in PFOA adsorption and desorption for the first 100 minutes. Reprinted from [155].
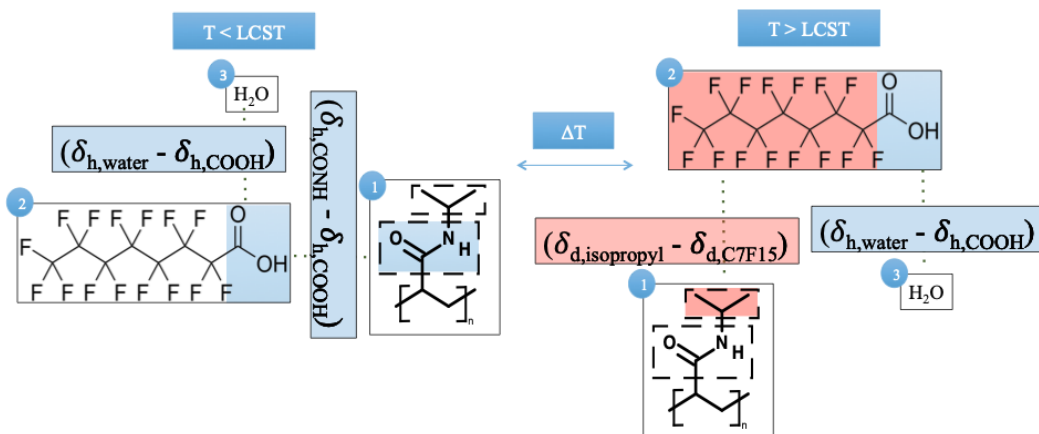
Figure 5.4: Schematic depicting interaction of hydrophilic and hydrophobic functional groups for the adsorption and desorption of aqueous PFOA onto PNIPAm, above and below its LCST. The compound labeled 1 refers to PNIPAm, while compounds 2 and 3 refer to PFOA and water respectively. The hydrogen bonding interaction parameters are labeled using δ_h, while the dispersion interaction parameters are labeled using δ_d. Reprinted from [155].
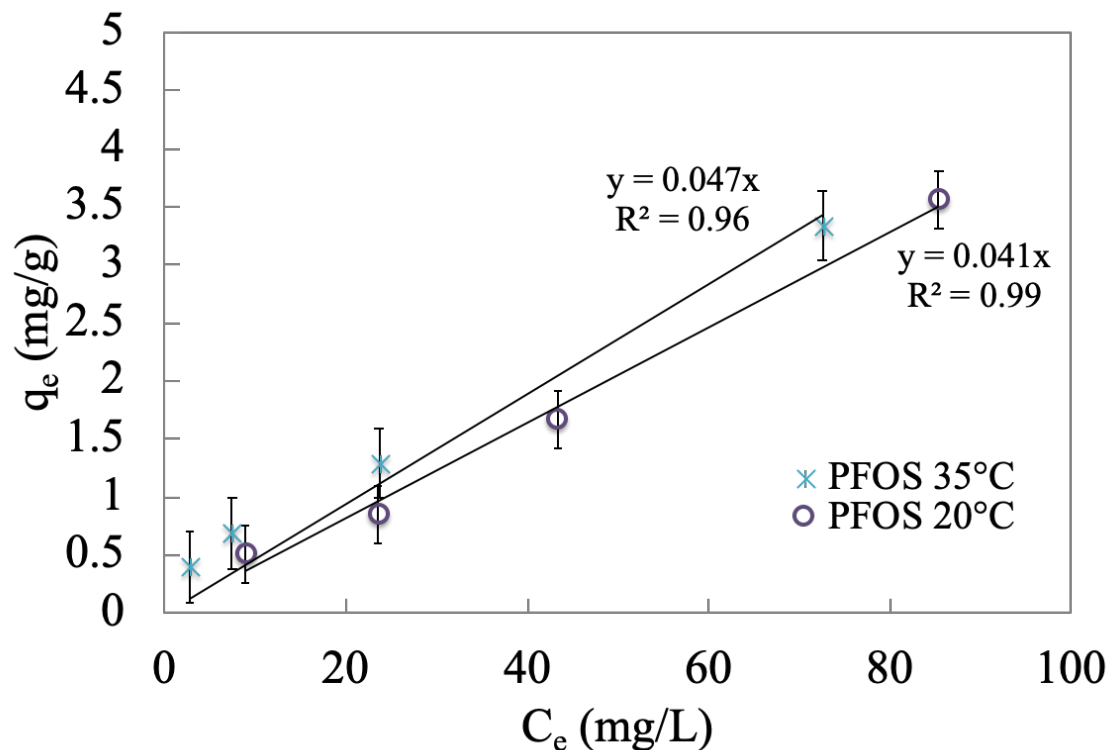
Figure 5.5: Adsorption of PFOS onto PNIPAm hydrogels in water at various temperatures. Initial aqueous PFOA samples had concentrations ranging from 25 mg/L to 200 mg/L, with 0.5g of PNIPAm hydrogels (15wt% NIPAm, 3 mol% BIS crosslinker, 2 mol% APS) and shaken at 100 rpm until equilibrium. Experimental data is fitted with linear isotherms. Reprinted from [155].
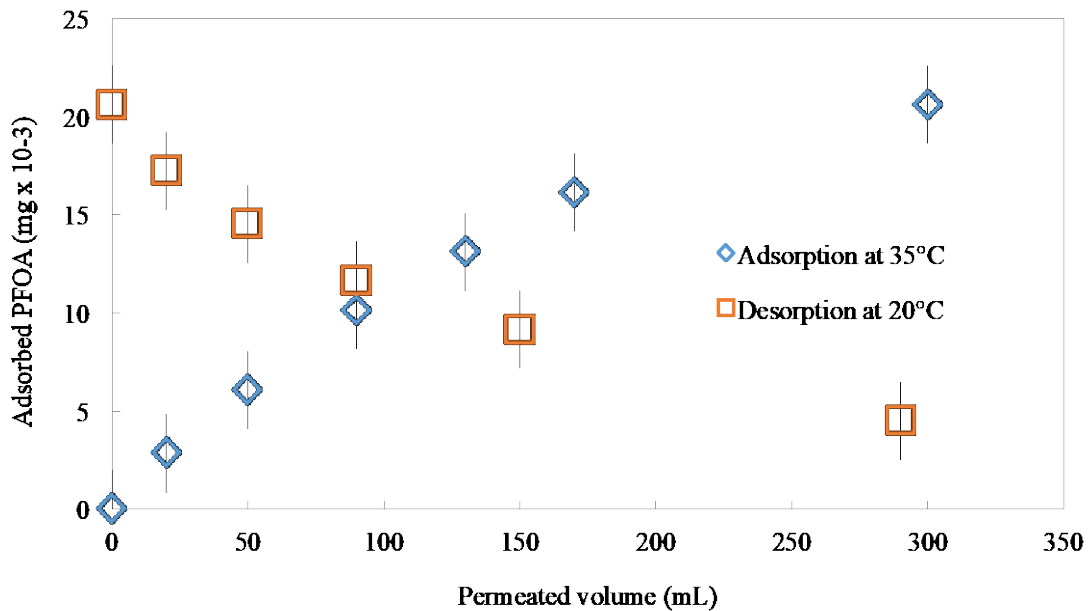
Figure 5.6: Adsorption and desorption of PFOA using PNIPAm functionalized PVDF 400 membrane (17% weight gain post polymerization, area of 45 cm^2) by convective flow at constant pressure of 3.5 bar in a dead-end filtration cell. The functionalized membrane adsorbed 20 μg after 300 mL of 0.5 mg/L aqueous PFOA was permeated at 35 °C. 80% of adsorbed PFOA was desorbed after 300 mL of pure DIUF water was permeated. Reprinted from [155].
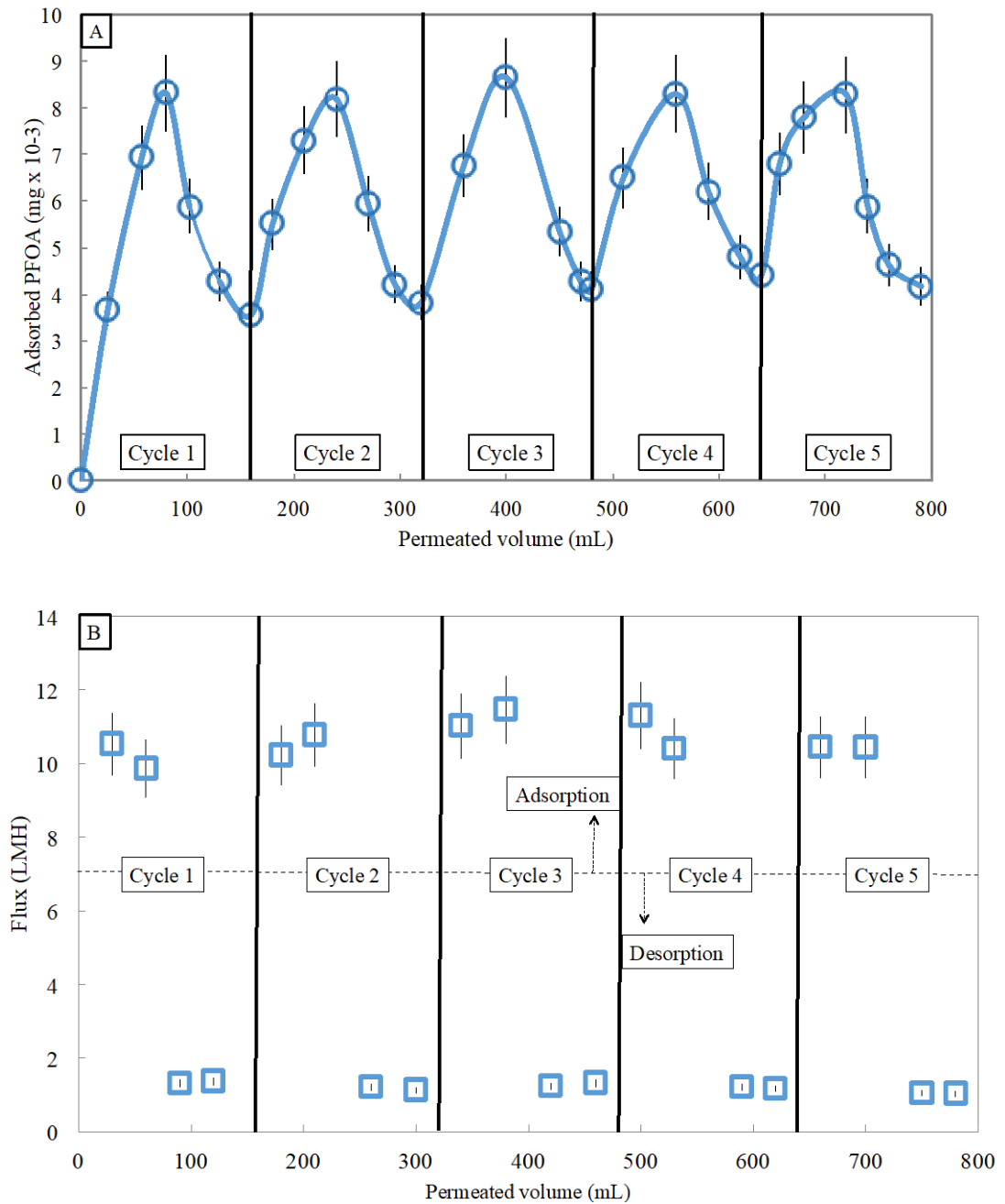
Figure 5.7: Adsorption and desorption of PFOA using PNIPAm functionalized PVDF 400 membrane (17% weight gain post polymerization, area of 45 cm^2) by convective flow over five adsorption/desorption cycles of 0.5 mg/L aqueous PFOA solution followed by pure water, at constant pressure of 3.5 bar. (A) Five adsorption/desorption cycles demonstrate consistent temperature swing adsorption. (B) Average flux above LCST is 10.6 LMH, while flux below LCST is 1.2 LMH, and is not affected by the presence of PFOA. Reprinted from [155].
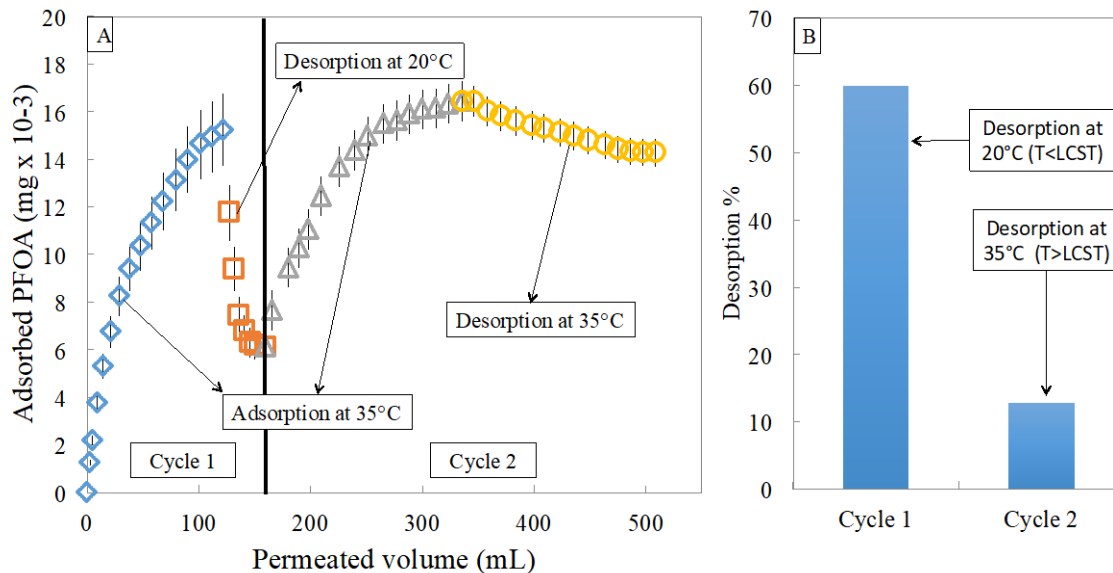
Figure 5.8: (A) Two adsorption/desorption cycles of PFOA using PNIPAm functionalized PVDF 700 membrane (15% weight gain post polymerization, area of 45 cm^2) by convective flow at constant pressure of 2.75 bar. Desorption in cycle 1 was conducted at 20 °C compared to 35 °C in cycle 2, both with pure DIUF. (B) Comparison of desorption percentage using pure water at 20 °C versus pure water at 35 °C shows much higher desorption using pure water at 20 °C as expected from LCST behavior. Reprinted from [155].

107

CHAPTER 6: NANOPARTICLE INTEGRATED CATALYTIC DEGRADATION OF PCB

In this chapter, the thermo-responsive adsorptive ability of PNIPAm functionalized in membrane pores, shown in the previous chapter, is used to enhance catalytic degradation of PCB. While PCB has been degraded using bimetallic Fe-Pd immobilized in membrane pores, the incorporation of stimuli-responsive materials could enhance degradation through increased contaminant adsorption and diffusion. The effect on introducing PNIPAm into the reactive Fe/Pd-PMMA-PVDF membrane system is evaluated at various thermal conditions for its effect on PCB adsorption and diffusion. Next, its effect on PCB-1 degradation via oxidative pathway is evaluated in convective flow mode (negligible mass transfer resistance) and in batch mode (increased mass transfer resistance). Transmembrane flux data and nanoparticle characterization data, examined in chapter 4 for various thermal conditions, is combined with PCB degradation data to effectively model the reaction.

6.1 Adsorption/desorption of biphenyl and PCB-1 onto PNIPAm-PMMA hydrogels and functionalized membranes:

The ability of PNIPAm functionalized membranes to selectively and reversibly adsorb and desorb hydrophobic contaminants by varying temperature was demonstrated using perfluorooctanoic acid (PFOA) in our previous publication [155]. It was shown that the apparent interaction parameter of PNIPAm varies according to its exposed functional groups, depending on its conformational state. Therefore, adsorption of compounds also varies when temperature is changed and PNIPAm changes conformation accordingly. In its swollen state, surrounding water is much more exposed to PNIPAm's amide group, thereby reducing the polymer's interaction with hydrophobic compounds. As the

temperature is raised, the isopropyl groups dehydrate first, and attract hydrophobic

compounds into the polymeric PNIPAm domain. We have shown the potential for

temperature-swing adsorption using PNIPAm functionalized membranes as a means of

providing a new avenue for contaminant adsorption by adsorbents that can easily release

the contaminant and are therefore easier to clean than commercial adsorbents currently

used [155]. The increased hydrophobic contaminant adsorption capacity of PNIPAm is

used here to increase adsorption of PCB-1 with the goal of increasing degradation

efficiency.

Apparent interaction parameters of PNIPAm and PCB-1 can be used to

qualitatively explain changes in adsorption as temperature is varied. In our previous

publication, the change equilibrium Freundlich distribution coefficients of

perfluorooctanoic acid (PFOA) onto PNIPAm-functionalized membranes was related to

changes in apparent interaction parameter values [155]. In this case, the PCB contaminant

is a conjugated aromatic compound compared to the previously studied perfluorinated

carboxylic acid. Furthermore, carboxylic groups are now present in the polymeric domain

due to the presence of PMMA. As temperature is raised, PNIPAm's apparent hydrogen

bonding parameter decreases significantly as the hydrophilic functional groups collapse

and bond with themselves. Raising temperature causes PNIPAm's apparent dispersion

interaction parameter to increase, as the isopropyl groups dehydrate and attract

contaminants with similar dispersion interaction. The PMMA groups, unlike PNIPAm,

have exposed hydrophilic carboxylic groups when temperature is raised, thereby reducing

the hydrophobicity of the polymeric domain. Nevertheless, the dehydration of the

isopropyl groups caused by the thermo-responsive collapse of PNIPAm affect the

apparent hydrophobicity of the polymeric domain substantially enough that PCB-1 preferentially adsorbs as temperature is raised above 32 ºC.

Using an initial 5 mg/L solution of PCB-1 in water, both PNIPAm-PMMA hydrogels as well as PNIPAm-PMMA functionalized PVDF membranes were used to quantify relative adsorption above and below PNIPAm's LCST of 32 ºC, depicted in Figure 6.1.

The PNIPAm-PMMA hydrogels showed a significant increase in equilibrium adsorption (Q_e) of PCB-1 adsorption, from about 40% (0.035 mg PCB-1 / g hydrogel) to about 70% (0.062 mg PCB-1 / g hydrogel), when temperature was raised from 25 ºC to 35 ºC. The PNIPAm-PMMA functionalized membranes also showed an increase in PCB-1 adsorption, from about 6% of total PCB-1 to 10%, while adsorption onto the pristine PVDF membrane without any PNIPAm remained approximately constant over the temperature range. The increased interaction of the hydrophobic phenyl groups with the isopropyl groups of PNIPAm as they dehydrate when temperature is raised causes increased partitioning into the PNIPAm domain. As temperature is then lowered back down below PNIPAm's LCST of 32 ºC, the polymer rehydrates and exposes its amide functional groups, releasing some of the adsorbed contaminant. The adsorption/desorption mechanism is reversible and repeatable over multiple cycles. Using PNIPAm-PMMA hydrogels, temperature is varied from 35 ºC to 25 ºC and repeated over 5 adsorption/desorption cycles, demonstrating the reversible nature of thermo-responsive adsorption using PNIPAm, as has been demonstrated with PFOA in our previous publication [155]. Adsorption of PCB-1 is constant at approximately 70% (0.07 mg PCB-1 / g hydrogel), while desorption releases approximately 40% of the adsorbed 70% over

each cycle, as shown in Figure 6.2. Trans-membrane permeation was also measured using PNIPAm-PMMA functionalized PVDF membranes before and after PCB-1 adsorption in order to determine the effect of adsorbed PCB-1 on the polymeric conformation. Permeation was consistent in both cases indicating that adsorption of PCB-1 did not substantially affect polymer conformational properties.

Controlling the aqueous environment around polymers containing reactive nanoparticles can yield control over reaction conditions, since the presence of oxygen causes nanoparticle oxidation and consequent deactivation of reactivity. Controlling adsorption into the reactive polymeric domain can also yield control over reaction conditions, by increasing partitioning of PCB-1 into the nanoparticle-immobilized polymeric domain.

6.2 Nanoparticle immobilization and characterization:

Fe and Pd nanoparticles were immobilized within the membrane pores through the ion exchange method. In order to determine nanoparticle size distribution within membrane pores, a scanning electron microscope (FEI Helios Nanolab 660) was used to acquire images and ImageJ software was used to automatically analyze particle size distribution for 100 nanoparticles. The particle sizes are summarized in Figure 6.3 for the Fe/Pd-PNIPAm-PMMA-PVDF membrane, which also shows the corresponding energy dispersive x-ray image of Fe, indicating that the nanoparticles shown are in fact Fe. The mean particle diameter was found to be 16 nm with a standard deviation of 6 nm. These particle properties are important for determining PCB degradation model values. The particle sizes and distribution were very similar to those properties determined in our previous study where the bimetallic nanoparticles were immobilized in PAA-PVDF

membranes, which examined nanoparticle size and distribution on the surface, shown in Figure 6.4, and at various depths through the membrane, shown in Figure 6.5 [110]. The consistency of nanoparticle size and distribution throughout the membrane enables the assumption that particles are uniformly distributed for the PCB degradation model. In order to verify the immobilization of Pd, a membrane was functionalized with much higher Pd content (10 wt% compared to 3 wt% of Fe) in order to eliminate noise interference. The presence of Pd is confirmed and shown in Figure 6.6.

6.3 Diffusion of PCB-1 and Biphenyl through Fe/Pd-PNIPAm-PMMA-PVDF membranes:

Bulk diffusion can readily be calculated using the Stokes-Einstein equation,

$$D_S = \frac{k_B T}{6\pi\mu r} \qquad (6\text{-}1)$$

Here, D_s is the bulk diffusion coefficient, k_B is Boltzmann's constant, μ is the dynamic viscosity of solvent ($\mu_{water} = 8.9 \times 10^{-4} \, Pa \cdot s$), and r is the particle radius. The radius can be calculated for PCB-1 using its molar volume. At 25 °C, D_s for PCB-1 was calculated to be 6.0 x 10^{-10} m^2/s. Diffusion is inherently reliant on temperature as shown in equation 2. Therefore, an increase in temperature is expected to increase the diffusion coefficient. At 35 °C, D_s was calculated to be 6.2 x 10^{-10} m^2/s, displaying a small increase of just over 3%. However, PCB-1 diffusion through the functionalized membrane is expected to be much slower due to the hindrances and constraints caused by the crosslinked PNIPAm and PMMA chains and the PVDF matrix. In order to determine diffusion coefficients at 25 °C and 35 °C, data was fit to the equation derived by Yang et al [178].

$$\frac{C_{PCB}}{C_{PCB,initial}} = \left[\frac{DH}{l}\right]\left(\frac{A}{V}\right)\left(t - \frac{l^2}{6D}\right) \qquad (6\text{-}2)$$

Here, D is the diffusion coefficient (m^2/s), H is the partition coefficient, A refers to the membrane area (m^2), V refers to the permeate solution volume (m^3), and l refers to the membrane thickness (m). By plotting the change in concentration versus time, shown in Figure 6.7, the lag time ($l^2/6D$) can be found from the x-intercept and the diffusion coefficient can be derived from the slope and intercept. There was negligible change in the feed side, while the permeate side increased linearly with time. The diffusion coefficients for PCB-1 were derived to be 6.6 x 10^{-11} m^2/s and 8.7 x 10^{-11} m^2/s at 25 °C and 35 °C, respectively.

As expected, the transmembrane diffusion coefficients are significantly lower than the bulk diffusion coefficients. The change in temperature led to an increase in transmembrane diffusion coefficient for PCB-1 of 25% compared to an increase in bulk diffusion coefficient of 3%. As temperature is raised above PNIPAm's LCST of 32 °C, the isopropyl groups dehydrate first and cause PNIPAm chains to collapse in an aqueous environment. PNIPAm's apparent hydrogen bonding interaction parameter decreases above its LCST, making it closer to that of PCB-1 [155]. Simultaneously, the PNIPAm chain collapse results in larger apparent membrane pore diameters. The large increase in transmembrane diffusion coefficient could be utilized to increase PCB degradation efficiency in systems where diffusion plays a role. The partition coefficient values were also calculated using equation 3, resulting in a ratio of partition coefficient at 35 °C to partition coefficient at 25 °C of 1.3.

6.4 Convective flow degradation of PCB-1:

The residence time (τ) within the membrane was varied by changing pressure within the range of 0.7 to 3.5 bar. Residence time can be calculated by dividing the void volume in the membrane (V_{void}) by the transmembrane flux (J_w) multiplied by the area, where the void volume is available space within the membrane pores, which can be calculated from the mass difference between a dry and wet Fe/Pd-PNIPAm-PMMA-PVDF membrane.

$$\tau = V_{void} / (J_w A) \qquad (6\text{-}3)$$

$$V_{void} = \emptyset V_{membrane} \qquad (6\text{-}4)$$

Here, $\emptyset$ represents surface porosity, which can also be described as the area of all membrane pores divided by the total membrane area:

$$\emptyset = \frac{n_{pores} \pi R^2}{A_M} \qquad (6\text{-}5)$$

For Re << 1, there is laminar flow through cylindrical pores:

$$u(r) = 2u_0 (1 - \frac{r}{R})^2 \qquad (6\text{-}6)$$

Here, R is the radius of the membrane pore, r is the point of interest in the pore's radius, u_0 is velocity at the pore center, and $u(r)$ is the velocity at radius point r. The average velocity through a pore can then be defined as:

$$u_{pore} = \frac{\int_0^R u(r) 2\pi r \, dr}{\pi R^2} \qquad (6\text{-}7)$$

Total flux through the membrane can then be defined as the number of pores, multiplied by the average pore velocity, divided by the membrane area (A_M).

$$J_w = \frac{n_{pores} \int_0^R u(r) 2\pi r \, dr}{A_M} = \frac{\emptyset u_0}{2} \qquad (6\text{-}8)$$

The pore mean velocity $(\bar{u})$ can then be defined as:

$$\bar{u} = \frac{J_w A_M}{n_{pores} \pi R^2} = \frac{J_w}{\emptyset} = \frac{u_0}{2} \qquad (6\text{-}9)$$

The residence time can then be related to pore length (L=75 μm) and velocity:

$$\tau = \frac{V_{void}}{J_w A_M} = \frac{2L}{u_0} \qquad (6\text{-}10)$$

Unlike our previous publication where membrane void fraction was unchanging [109, 110], the thermo-responsive collapse of PNIPAm chains at higher temperatures causes void fraction to grow as relative effective pore diameter increases. This is accounted for in calculating velocity through the pore, where the ratio of pore areas is estimated. By using the Hagen-Poiseuille equation due to laminar flow through cylindrical pores, relative pore diameters can be found based on membrane permeance data and change in area can therefore be calculated. The permeability data for the convective flow runs can be found in Figure 6.8, along with a comparison to permeability through the same membrane prior to the addition of the nanoparticles. The permeability is lower with the presence of nanoparticles, and the effect of temperature on flux is reduced due to additional restrictions on PNIPAm chain expansion. An increase in viscosity-corrected permeability is shown with temperature increases for the Fe-Pd-PNIPAm-PMMA-PVDF membrane with 5 mol% crosslinking. Rather than seeing a sharp step change at PNIPAm's LCST, the stimuli-response is gradual for the membrane with immobilized

nanoparticles, which is incorporated into the reaction model. Liu et al. recently showed that PNIPAm thin films are sensitive to humidity that can affect temperature dependence behavior based on interfacial boundary condition properties [179].

With laminar flow through membrane pores and assuming no slip at the wall, the following Hagen-Poiseuille equation can be used to estimate relative pore diameters.

$$J_w = \frac{N\pi\Delta P}{A8\eta L}\left(\frac{D}{2}\right)^4 \tag{6-11}$$

Here J_w refers to the transmembrane flux, N is the number of pores, By knowing the flux values at the different temperatures, ΔP refers to the pressure differential, A is the membrane area, η is the viscosity, which is adjusted for temperature, L is the membrane thickness, and D is the effective pore diameter. When temperature is changed, N, ΔP, A, L are all constant. Viscosity can be corrected for temperature according to the following equation:

$$\eta = 2.414\times10^{-5}\times10^{\frac{247.8}{T-140}} \tag{6-12}$$

Once adjusted for viscosity, the flux ratio at two different temperatures is proportional to the respective ratio of diameters to the fourth power. After finding relative diameter, relative void fraction can be calculated because relative void fraction is proportional to the ratio of the square of relative diameters. Relative diameter and void fraction calculations can be found in Table 6.1. These void volumes are also necessary for the calculation of metal loading density because unlike batch degradation, the volume being reacted is confined to the void volume within the reactive membrane pores, detailed in Table 6.2.

In order to determine final concentration, a first order reaction is assumed, and is integrated along the pore axial distance, z. In order to determine whether mass diffusion (D_M) can be neglected, the Peclet number is calculated as follows:

$$Pe = \frac{Lu}{D_M} \qquad (6\text{-}13)$$

Since Pe is large ($>10^3$), D_M can be neglected. Using equation 6-14, derived in our previous publication by averaging the mass balance for first order reaction across the pore radius, pseudo-first order reaction rate constant ($k_{obs} = k_{sa}\rho_m a_s$) can be determined [110]:

$$\bar{C}_{final} = \frac{\bar{C}_{initial}\tau^2 \left[k_{obs}^2 (\int_{\frac{k_{obs}\tau}{2}}^{\infty} \frac{e^{-t}}{t} dt) + e^{-\frac{k_{obs}\tau}{2}} (4\frac{1}{\tau^2} - 2\frac{k_{obs}}{\tau}) \right]}{4} \qquad (6\text{-}14)$$

Unlike in our previous publication [110], stimuli responsive PNIPAm causes a dependence of residence time on temperature through its effect on void fraction due to PNIPAm's changing conformation. Average rate constants (k_{obs}) were determined at 15 ºC, 25 ºC, 35 ºC, and 45 ºC. At each temperature, pressure was varied four times, with three samples taken at each given pressure in order to determine an average observed rate constant. These determined rate constants were then used to plot an expected extent of degradation for each temperature across residence times ranging from 0 to 40 s, shown in Figure 6.9. At a residence time of 10 s, 70% of PCB-1 remains unreacted at 15 ºC while only about 10% remains unreacted at 45 ºC and the drastic effect of temperature on reactive efficiency can be seen. In order to find k_{SA}, the observed rate constants must be divided by nanoparticle loading capacity (ρ_m) and the surface area to mass ratio (a_s). In order to determine ρ_m (g/L), metal loading of 2 mg Fe per membrane is divided by the void volume in the membrane, which varies with temperature as shown in Table 6.1 and

Table 6.2. Like in batch degradation, a_s is calculated using average spherical nanoparticle size from TEM imaging (16nm) and iron density of 7870 g/L. MatLab was used to calculate the observed rate constant for each sample point for each temperature. Equation 6-14 can be used to determine rate constant values given feed concentration, permeate concentration, and residence time. MatLab was used to create a loop where an initial rate constant was assumed, permeate concentration was calculated, and the loop changed the rate constant until the calculated permeate concentration was equal to the experimental one. For each temperature, the average calculated rate constant was found. Surface area-normalized reaction rate constants (k_{SA}) were then calculated by dividing the observed rate constants by nanoparticle surface area to mass ratio (a_s) and by the corresponding ρ_m value found in Table 6.2. Calculations for k_{SA} can be found in Table 6.3.

The determined k_{SA} values are 0.13 L/m^2/g, 0.28 L/m^2/g, 0.72 L/m^2/g, and 1.36 L/m^2/g at 15 ºC, 25 ºC, 35 ºC, and 45 ºC, respectively. Solution phase degradation of PCB-1 was conducted at 20 ºC using Fe-Pd nanoparticles (0.5 wt% Pd) yielding a k_{SA} value of 0.12 L/m^2/h [157]. Multiple control runs were carried out using PNIPAm-PMMA-functionalized membranes with only Fe and no Pd in order to measure any potential PCB loss not attributed to dechlorination via the reductive pathway. Control runs yielded <5% PCB-1 loss indicating minor potential adsorption onto the membrane. Furthermore, biphenyl recovery was measured for 4 points, resulting in product recovery values of 88%, 85%, 80%, 81% at 15 °C, 25 °C, 35 °C, and 45 °C, respectively, resulting in an average recovery value of 84%. The slight biphenyl product loss can be attributed to membrane adsorption, as well as minor evaporative losses due to the semi-volatile nature of biphenyl, especially as temperature is raised.

According to the Arrhenius equation, rate constants will naturally vary with temperature without the increased adsorptive ability of PNIPAm present,

$$\ln\left(\frac{k_2}{k_1}\right) = -\frac{E_a}{R}\left(\frac{1}{T_2} - \frac{1}{T_1}\right) \qquad (6\text{-}15)$$

Here, k refers to the k_{SA} values, E_a is the activation energy (J/mol), R is the gas constant (8.314 J/mol/K), and T is the temperature (K). By plotting the natural log of the surface area-normalized rate constant values versus the reciprocal of temperature, effective activation energy values can be determined for the reaction. Figure 6.10 shows the Arrhenius plot with a R^2 value > 0.99.

The activation energy was calculated to be 60 kJ/mol. An activation energy of 20 kJ/mol was reported with Pd content of 0.5 wt% relative to Fe [157, 180], which accounts for the difference. The purpose of incorporating thermo-responsive PNIPAm into the reactive membrane domain is to increase degradation efficiency by increasing temperature above PNIPAm's LCST of 32 ºC due to increased contaminant diffusion and adsorption into the reactive polymeric domain, whilst simultaneously increasing flow through the membrane due to the increased effective pore diameters attributed to the PNIPAm chain collapse. However, in convective flow degradation, mass transfer is negligible due to the pressurization of aqueous PCB-1 through the dead-end filtration cell, as shown by the Peclet number. Therefore, increased diffusion above PNIPAm's LCST does not enhance PCB-1 degradation in this case.

6.5 Batch phase degradation of PCB-1:

For batch phase degradation of PCB-1, PNIPAm-PMMA functionalized PVDF membranes with immobilized Fe-Pd nanoparticles were placed in vials with known concentrations of aqueous PCB-1 and degradation was conducted for multiple time points

at both 25 ºC and 35 ºC. After 40 minutes, 8% of PCB-1 remained at 25 ºC while less than 1% remained at 35 ºC. Biphenyl product was also measured, showing 90% recovery of degraded PCB-1 at 25 ºC and 85% recovery of degraded PCB-1 at 35 ºC. Adsorption of biphenyl product onto the membrane is the cause of the discrepancy between measured biphenyl product and degraded PCB-1. Others have also shown a discrepancy between expected biphenyl product and consumed PCB [110, 150]. Lower biphenyl product recovery above PNIPAm's LCST is expected. In order to account for the slight discrepancy between degraded PCB-1 and measured biphenyl product, adsorption of biphenyl onto the functionalized membrane was tested. A functionalized membrane was placed in an aqueous biphenyl (5 ppm) solution and shaken for several hours. There was no head space to ensure no biphenyl loss. The membrane was then removed, and the biphenyl was extracted from the aqueous solution using hexane for GCMS analysis. This experiment was carried out at 25 °C and 35 °C. Triplicate samples were carried out at each temperature. It was found that there was greater adsorption at 35 °C, due to hydrophobic nature of PNIPAm above its LCST. Results can be seen in Table 6.4. These adsorption values account for the discrepancy between PCB-1 degraded and biphenyl product measured.

Control runs were also conducted, where vials were sampled with no membrane at all, as well as with a PNIPAm-PMMA functionalized PVDF membrane with only Fe, and no Pd catalyst, which is required for the formation of the reactive hydrogen species in order to dechlorinate the PCB-1. Concentrations of PCB-1 and biphenyl are plotted versus degradation time in Figure 6.11, with the plot of the natural log of PCB-1 concentration versus time for determination of the observed rate constant shown in Figure

6.12. For the batch study, the PCB-1 degradation reaction can be modeled as a pseudo-first-order reaction:

$$\frac{dC}{dt} = k_{obs}C = -k_{sa}\rho_m a_s C \qquad (6\text{-}16)$$

Here, C is the PCB-1 molar concentration, k_{sa} is the surface normalized reaction rate ($L/m^2/h$), ρ_m is the nanoparticle loading density (g/L), and a_s is the surface area to mass ratio (m^2/g). The k_{sa} values are calculated for 25 ºC and 35 ºC and tabulated in Table 6.5, where a_s is calculated using average spherical nanoparticle size from SEM imaging (16nm) and iron density of 7870 g/L. In order to calculate ρ_m, metal loading of 2 mg per membrane was divided by the PCB-1 aqueous solution volume in the degradation vial.

Unlike convective flow degradation, mass transfer plays a larger role in batch degradation. However, when temperature is raised above the LCST, diffusion is less limiting than it is below PNIPAm's LCST. In order to determine whether the increased contaminant diffusion and adsorption caused by raising temperature enhances PCB-1 degradation, the activation energy of the reaction calculated from the k_{SA} values in convective flow mode can be used. In batch mode, k_{SA} was calculated to be 0.12 $L/m^2/h$ at 25 ºC. Using the activation energy of 60 kJ/mol, the expected k_{SA} at 35 ºC can be calculated using the Arrhenius equation, shown in the supporting information. The expected k_{SA} at 35 ºC was calculated to be 0.26 $L/m^2/h$. However, the actual k_{SA} found at 35 ºC was 0.35 $L/m^2/h$, approximately 35% higher than the expected value, indicating the enhanced reactivity in batch mode due to PNIPAm's presence. Increased diffusion and partitioning impact the reactivity in batch phase due to mass transfer resistance,

characterized by the ratio of PCB-1 partitioning coefficients into the polymeric domain at 35 ºC versus 25 ºC of 1.3. The partitioning of PCB-1 into the reactive polymeric matrix has an influence on the observed reaction rate constant. It is important to note that the observed batch-mode k_{SA} values were approximately half of the observed convective flow degradation k_{SA} values due to the increased diffusion limitation present in batch degradation. When there is a diffusion limitation, increasing PCB diffusion and adsorption into the reactive polymeric domain within the membrane pores by leveraging PNIPAm's hydrophobicity shift at its LCST can enhance reactivity and PCB degradation. Stimuli responsive catalytic membranes present an opportunity to enhance catalytic activity through leveraging conformational changes of the responsive material through control of external stimuli.

Table 6.1: Void fraction calculations of PNIPAm-PMMA-functionalized PVDF membranes (15 wt% NIPAm, 5 mol% MMA, 5 mol% BIS crosslinker, 2 mol% APS) with immobilized Fe-Pd nanoparticles (2 mg Fe per membrane with 3 wt% Pd) using permeance data.

Temperature (ºC)	Permeance (LMH/bar)	Relative diameter $(d_T / d_{25ºC})$	Ø (void fraction)
15	8.4	0.96	0.19
25	9.8	1	0.21
35	12.8	1.07	0.25
45	15.7	1.11	0.26

Table 6.2: Void fraction and iron loading density calculations for each temperature.

Temperature (°C)	V_{void} (L)	ρ_m (g/L)
15	0.0000964	20.7
25	0.000105	19.0
35	0.000121	16.5
45	0.000129	15.5

Table 6.3: k_{SA} calculations using experimentally determined k_{obs} values from convective flow PCB-1 degradation.

Temperature (ºC)	k_{obs} (s^{-1})	ρ_m(g/L)	a_s (m^2/g)	k_{sa} (L/m^2/h)
15	0.037	20.7	48	0.13
25	0.072	19.0	48	0.28
35	0.16	16.5	48	0.72
45	0.28	15.5	48	1.36

Table 6.4: Adsorption of Biphenyl (5 ppm) onto PNIPAm-PMMA-functionalized PVDF membrane with Fe-Pd nanoparticles.

Temperature (°C)	Adsorption for sample 1 (%)	Adsorption for sample 2 (%)	Adsorption for sample 3 (%)	Average adsorption (%)
25	11.2	10.3	9.2	10.2
35	16.1	15.4	17.3	16.2

Table 6.5: k_{SA} calculations using experimentally determined k_{obs} values from batch phase PCB-1 degradation using PNIPAm-PMMA-functionalized PVDF membranes (15 wt% NIPAm, 5 mol% MMA, 5 mol% BIS crosslinker, 2 mol% APS) with immobilized Fe-Pd nanoparticles (2 mg Fe per membrane with 3 wt% Pd).

Temperature (°C)	k_{obs} (min^{-1})	ρ_m(g/L)	a_s (m^2/g)	k_{sa} (L/m^2/h)
25	0.049	0.5	48	0.12
35	0.14	0.5	48	0.35
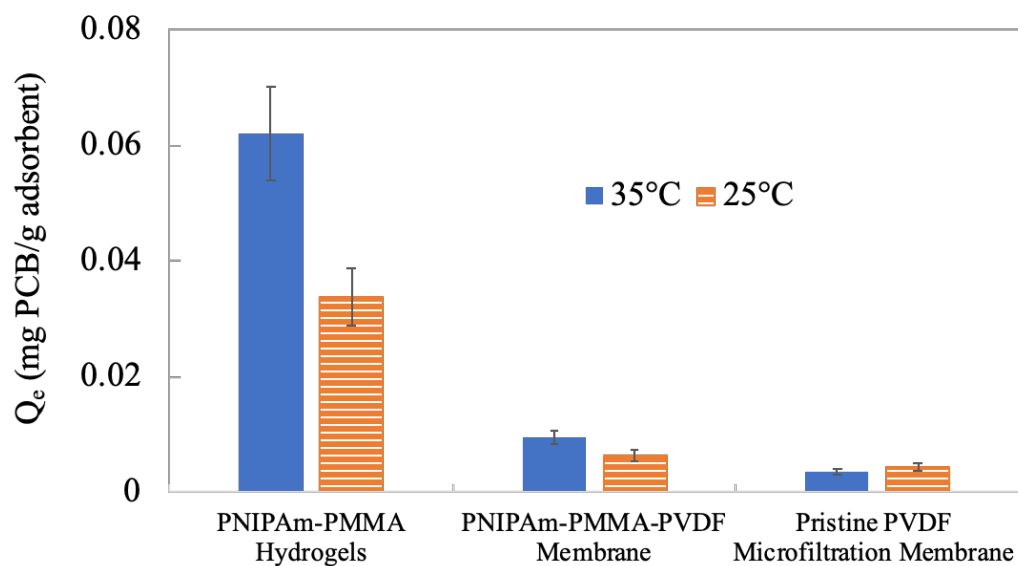
Figure 6.1: Equilibrium adsorption of PCB-1 onto PNIPAm-PMMA hydrogels, PNIPAm-PMMA-PVDF membranes, and pristine PVDF microfiltration membranes in water. Initial aqueous PCB-1 sample concentrations were 5 ppm in 20 mL. 1 g of PNIPAm-PMMA hydrogels was used (15 wt% NIPAm, 5 mol% MMA, 5 mol% BIS crosslinker, 2 mol% APS). One 14 cm^2 functionalized PVDF membrane (20% wt gain post-functionalization) and a pristine PVDF 400 membrane were used in 20 mL. Samples were shaken at 100 rpm until equilibrium.
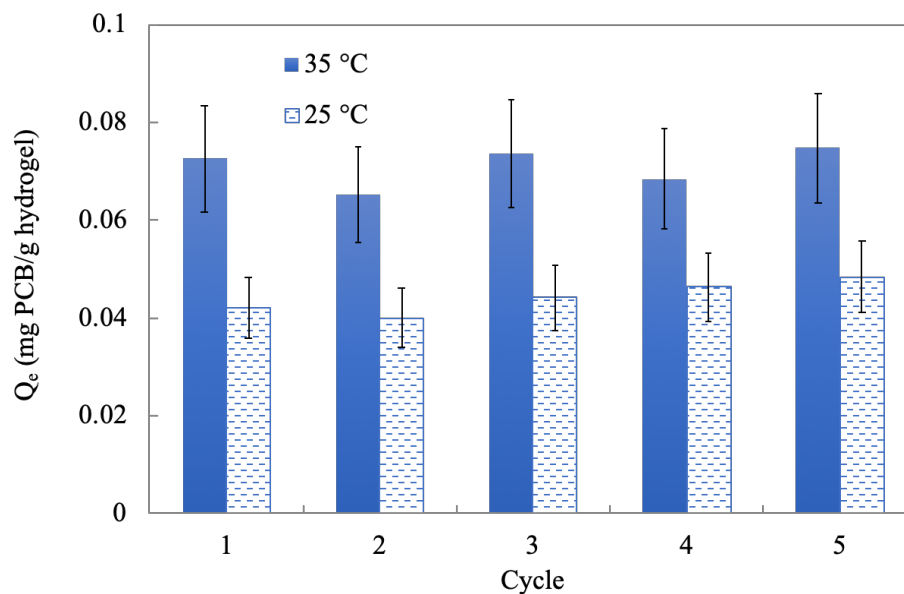
Figure 6.2: Adsorption percentage of PCB-1 onto PNIPAm-PMMA hydrogels in water followed by desorption by changing ambient temperature, repeated over 5 adsorption/desorption cycles. Initial aqueous PCB-1 sample concentration was 5ppm in 40mL. 2 g of PNIPAm-PMMA hydrogels were used per vial (15 wt% NIPAm, 5 mol% MMA, 5 mol% BIS crosslinker, 2 mol% APS). Samples were shaken at 100 rpm until equilibrium.
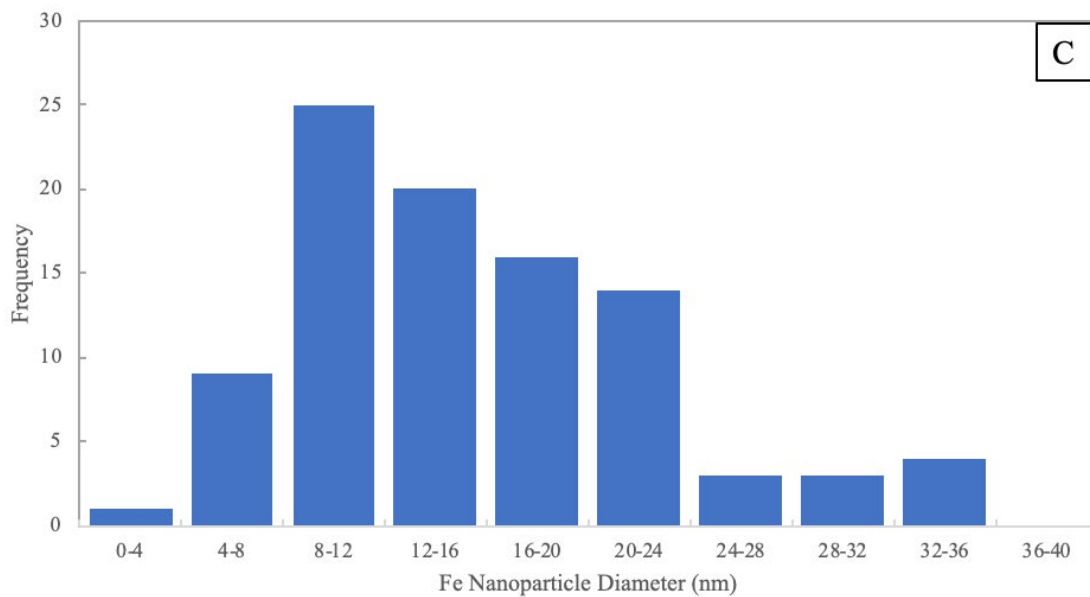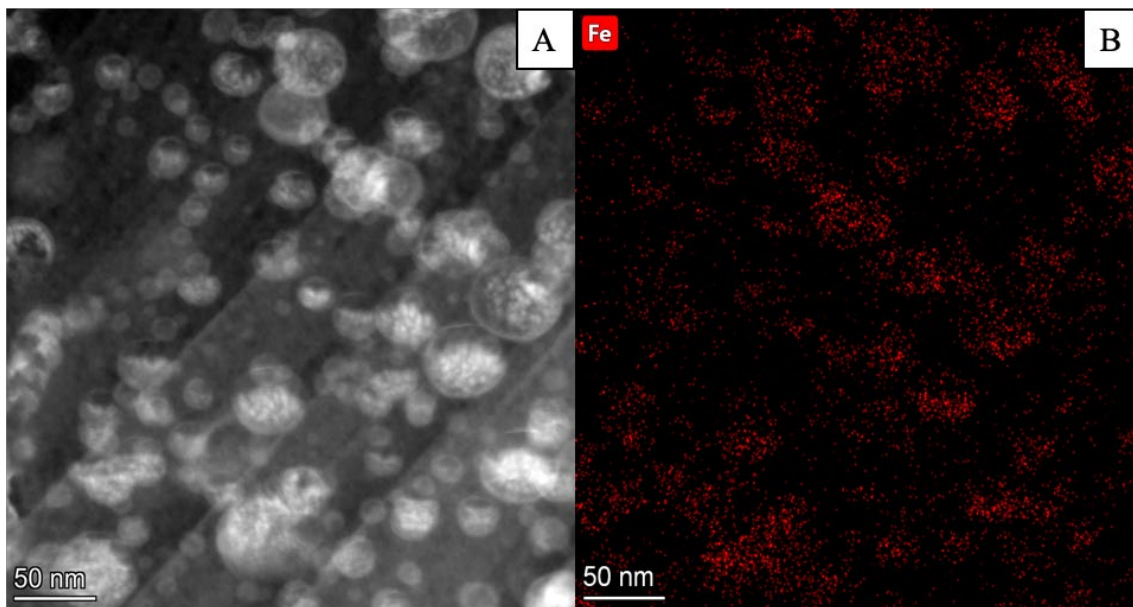
Figure 6.3: SEM image of the inside of a pore, taken from a piece 10 um below the membrane surface. (A) Sem image of Fe nanoparticles inside PNIPAm-PMMA-functionalized PVDF membrane. (B) EDX image of (A) for Fe. (C) Fe nanoparticle distribution (100 sample points) acquired using ImageJ software, with average nanoparticle diameter of 16 nm.
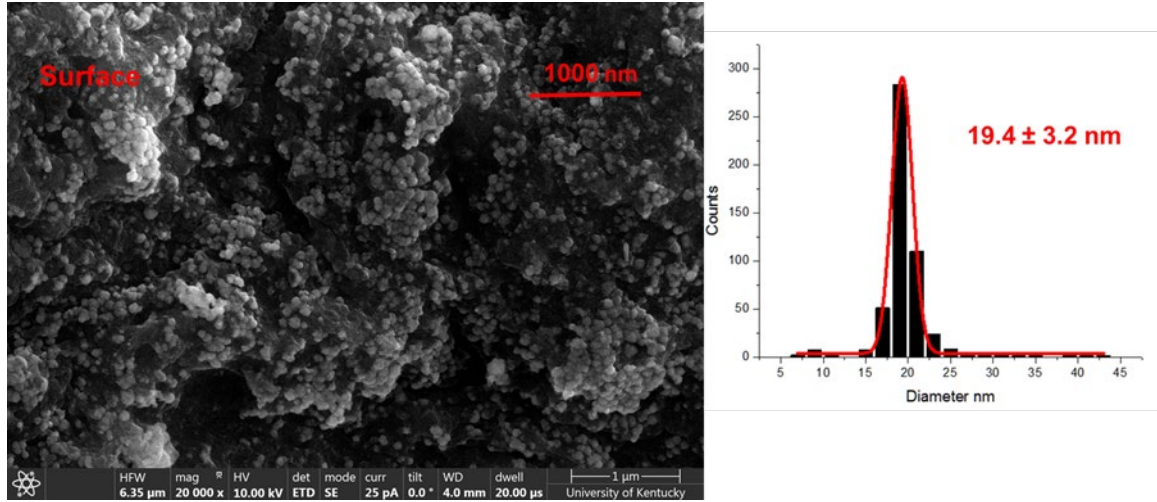
Figure 6.4: FIB-SEM image of the surface on the Fe/Pd-PAA-PVDF 700 membrane (13.4 wt % PAA, 1 mol % initiator and 1 mol % of cross-linker, 4.1 mg Fe, 1.3 wt % Pd) and the summary of observed Fe/Pd nanoparticles (more than 500 counts). (Reprinted with permission from [110], Copyright (2017) Elsevier).
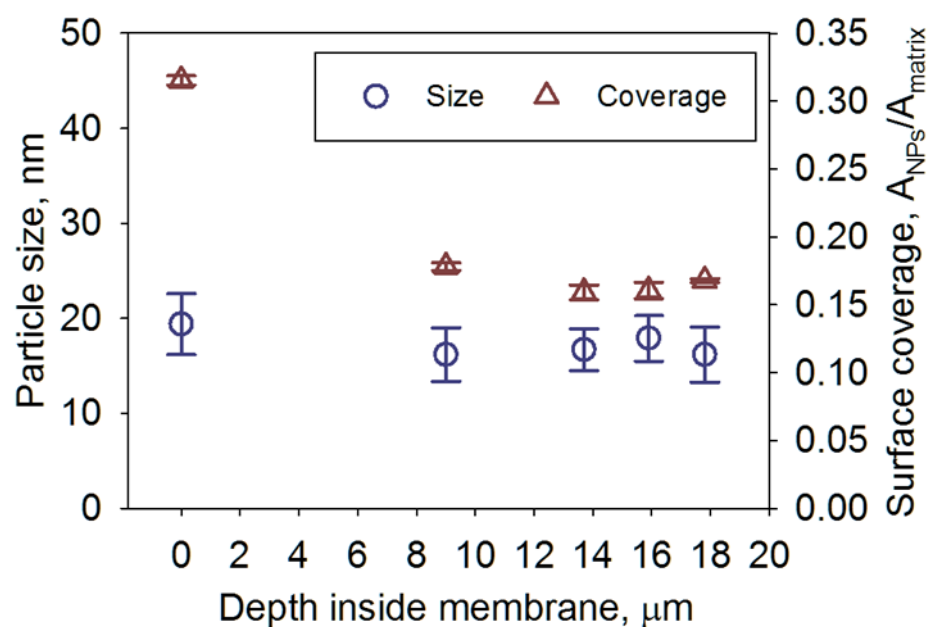
Figure 6.5: Correlation between Fe/Pd nanoparticle size, surface coverage (nanoparticle occupation of the membrane matrix) and depth under the membrane surface (more than 200 counts selected for each sample) for Fe/Pd-PAA-PVDF 700 membrane (13.4 wt % PAA, 1 mol % initiator and 1 mol % of cross-linker, 4.1 mg Fe, 1.3 wt % Pd). (Reprinted with permission from [110], Copyright (2017) Elsevier).
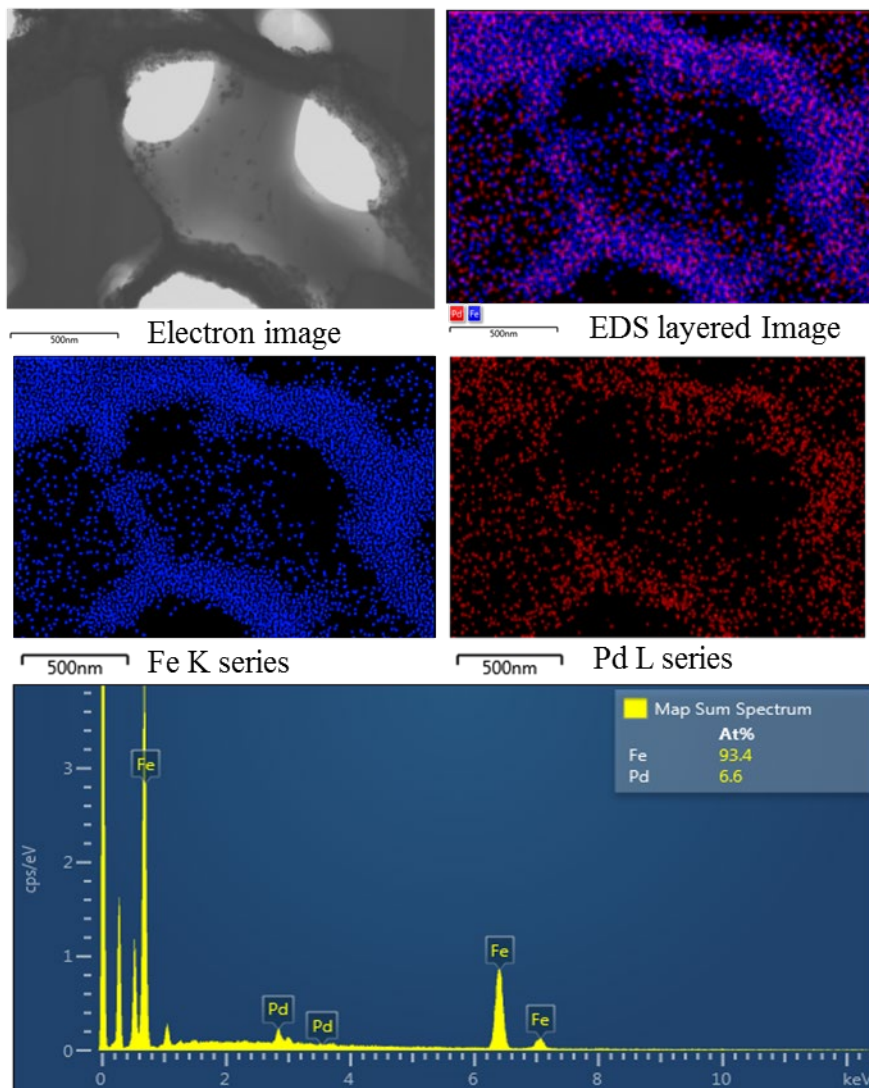
Figure 6.6: EDX mapping image of Fe/Pd-PAA-PVDF lamella sample prepared by FIB. High Pd:Fe ratio was used in this membrane to eliminate interference from noise. (Reprinted with permission from [110], Copyright (2017) Elsevier).
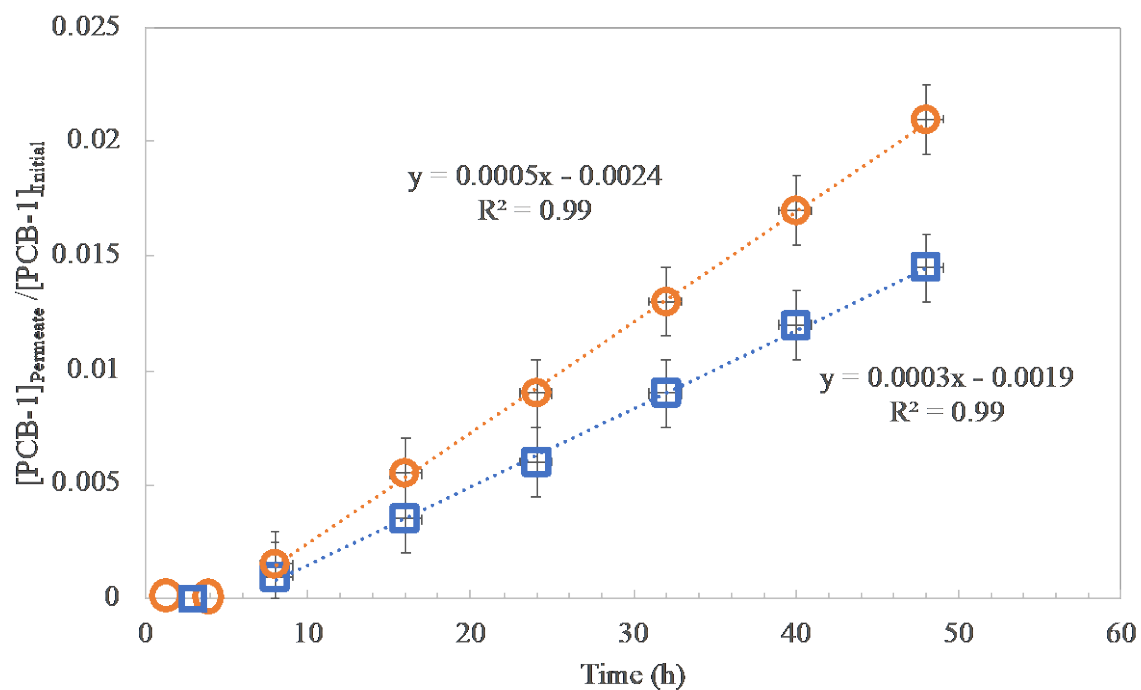
Figure 6.7: Diffusion of PCB-1 through a PNIPAm-PMMA-functionalized PVDF membrane with Fe nanoparticles. Effective surface area: 3.5 cm^2. [PCB-1]$_{Feed}$ = 25 μM. Diffusion cell volume = 300 mL. (Data points prior to breakthrough not included in linear fit to determine parameters).
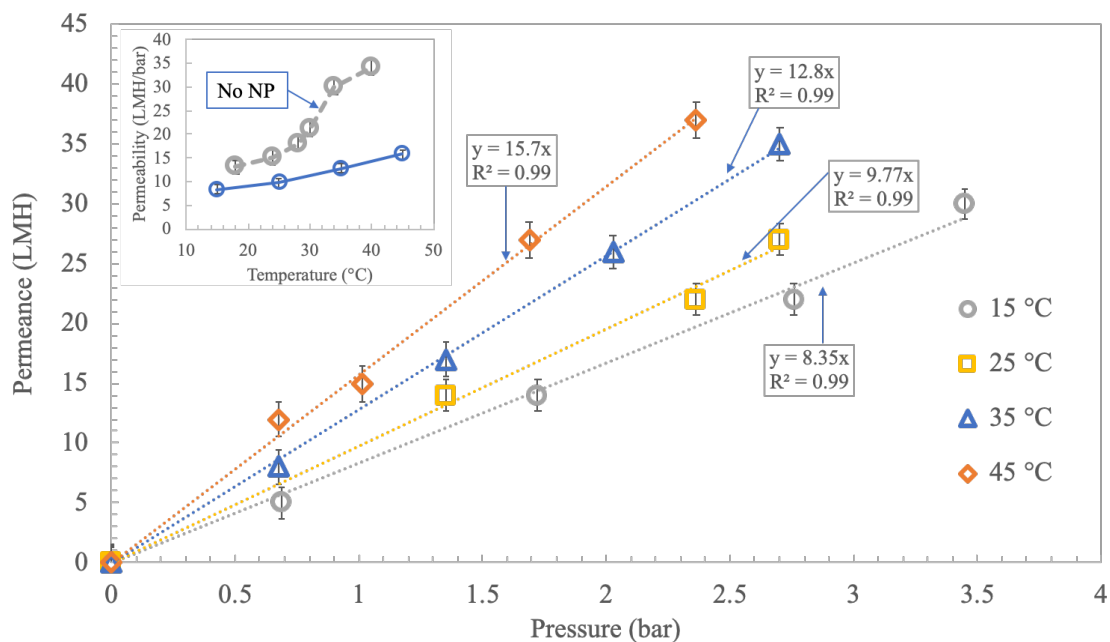
Figure 6.8: Flux through PNIPAm-PMMA-functionalized PVDF membrane (15 wt% NIPAm, 5 mol% MMA, 5 mol% BIS crosslinker, 2 mol% APS) with reactive Fe-Pd nanoparticles (2mg Fe loading, 16nm mean Fe particle diameter) at 15 °C, 25 °C, 35 °C, and 45 °C, all at pH 6.5. Effective surface area: 3.5 cm^2. [PCB-1]$_{Feed}$ = 25 µM. (Insert: Permeability as a function of temperature, compared with permeability as a function of temperature for the same membrane without nanoparticles).
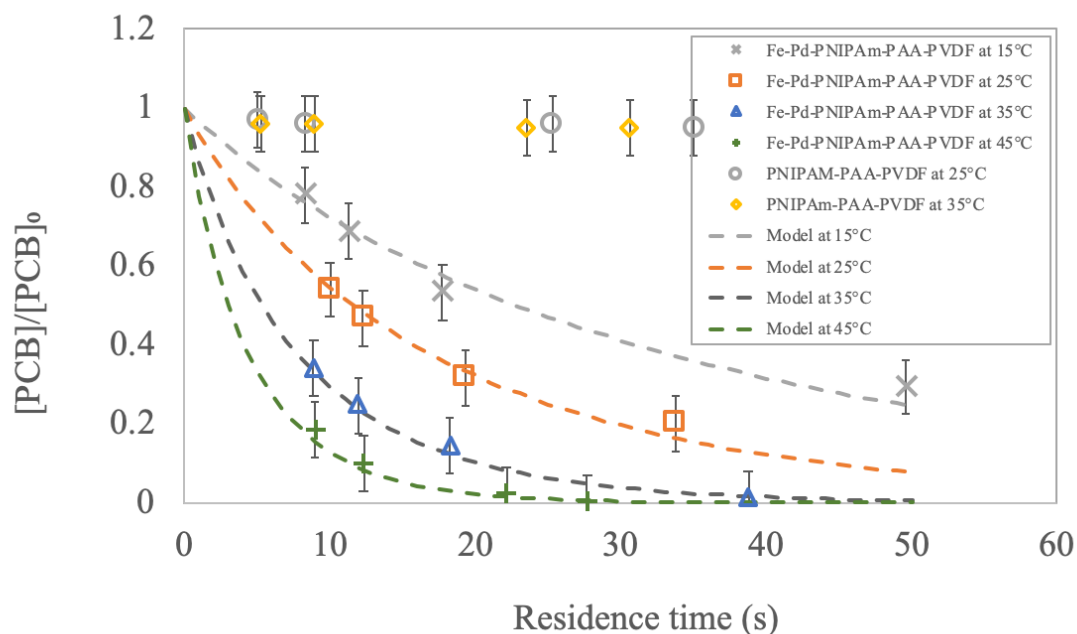
Figure 6.9: Convective flow study of PCB-1 degradation by PNIPAm-PMMa functionalized PVDF 400 membranes with Fe-Pd. Fe-PNIPAm-PMMA-PVDF membrane and run without any membrane served as control groups. Laminar flow reactor model was used for experimental data fitting. Effective surface area: 14 cm^2. $[PCB-1]_0 =$ 25 µM, 2 mg Fe per membrane, $[Pd] = 2.8$ wt % as Fe, pH = 6.5.
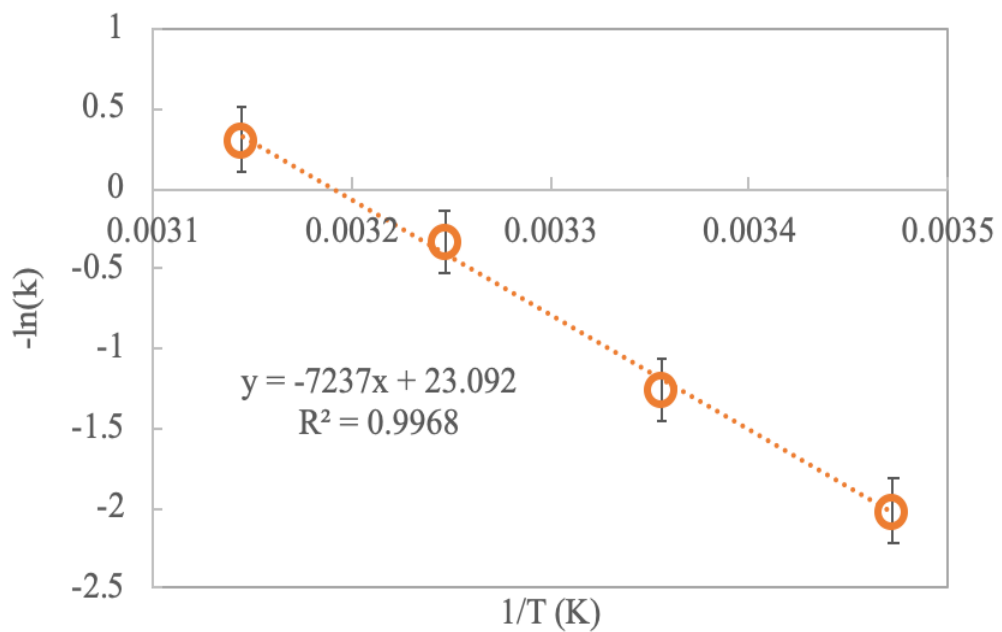
Figure 6.10: Arrhenius plot of the natural log of the surface area-normalized rate constant values derived from PCB-1 degradation experiment versus the reciprocal of temperature to determine activation energy for PCB-1 degradation by Fe-Pd-PNIPAm-PMMA-PVDF membrane (2 mg Fe per membrane, [Pd] = 2.8 wt % as Fe, pH = 6.5).
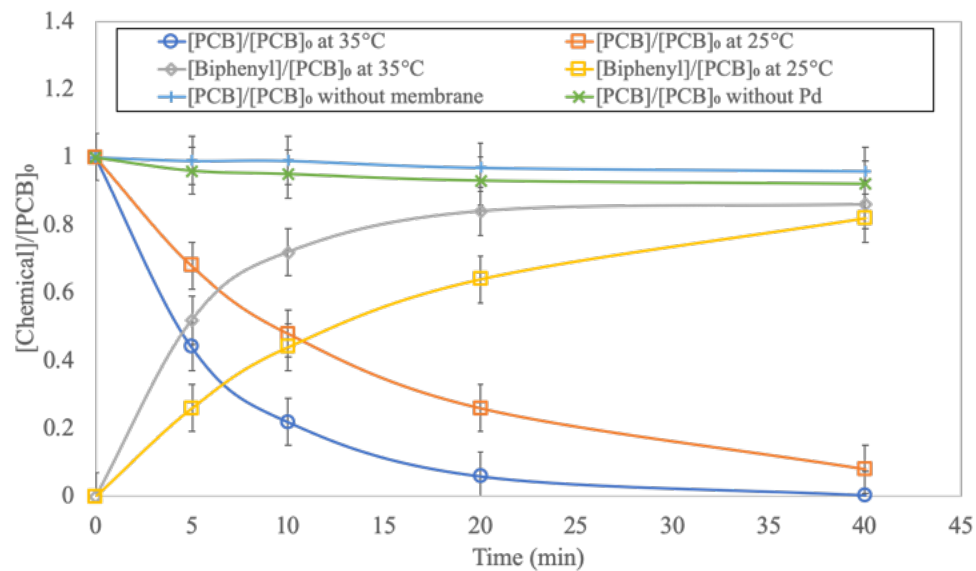
Figure 6.11: Batch study of PCB-1 degradation by PNIPAm-PMMA functionalized PVDF 400 membranes with Fe-Pd. Fe-PNIPAm-PMMA-PVDF membrane and run without any membrane served as control groups. Effective surface area: 14 cm^2. [PCB-1]$_0$ = 25 µM, 2 mg Fe per membrane, [Pd] = 2.8 wt % as Fe, pH = 6.5.
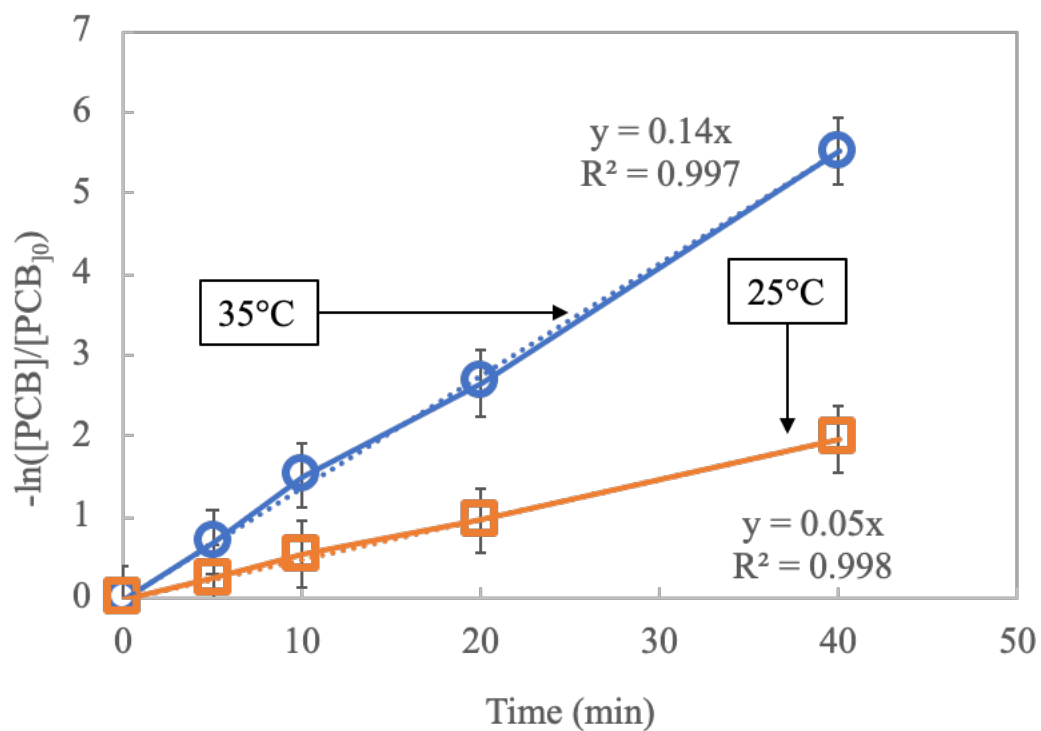
Figure 6.12: Plot of natural log of the ratio of PCB-1 present to the initial PCB-1 concentration versus time to determine observed rate constant coefficients for batch phase degradation of PCB-1 by Fe-Pd-PNIPAm-PMMA-PVDF membrane (2 mg Fe per membrane, [Pd] = 2.8 wt % as Fe, pH = 6.5).

CHAPTER 7: CONCLUSION

7.1 Overview

This dissertation explored the incorporation of PNIPAm into adsorptive and reactive membrane systems for the remediation of PFCs and PCBs through reversible adsorption and degradation via the reductive pathway, respectively. While commercial adsorbents exist with high adsorptive capacity for PFC adsorption from water, regeneration and reuse issues were tackled using the thermo-responsive hydrophobicity switch of PNIPAm. Interaction parameters of component functional groups were used to explain relative adsorption of PFOA versus PFOS, and shed light onto the types of contaminants that can be reversible adsorbed and desorbed. For PCB degradation via the reductive pathway, PNIPAm's thermo-responsiveness was leveraged to increase PCB adsorption and diffusion into the reactive membrane domain by manipulating temperature, in order to increase degradation efficiency in situations where mass transfer plays a role.

7.2 Chapter-specific accomplishments

CHAPTER 4: SYNTHESIS OF TEMPERATURE RESPONSIVE HYDROGELS AND MEMBRANES AND BIMETALLIC NANOPARTICLES

- PNIPAm was successfully polymerized in PVDF membrane pores, confirmed by FTIR, resulting an approximately 20% weight gain. PMMA was also successfully polymerized in PVDF membrane pores with PNIPAm for pH-responsive functionality and for the immobilization of Fe nanoparticles via ion exchange.

- The average swelling capacity was observed to be 10.3 for the hydrogels formed with 3 mol% crosslinker and 3.4 for the hydrogels formed with 10 mol%

crosslinker, indicating that the swelling capacity of PNIPAm hydrogels is inversely related to crosslinking density. The average swelling capacity was found to be 5.3 for PNIPAm-PMMA functionalized PVDF membrane. By controlling crosslinking density and PNIPAm content, effective membrane pore sizes can effectively be controlled with gating functionality.

- Hagen Poiseuille equation was applied to transmembrane permeance data in to determine relative pore sizes at various temperatures. The recorded water permeance values increased with temperature, displaying a sharper increase of over 2-fold from between 28 ºC and 34 ºC, shown in Figure 4. The estimated relative effective pore diameters over the temperature range are also shown, demonstrating an increase of about 3.5-fold.

- At lower pH values, when the PMMA is in its protonated collapsed state, the PNIPAm chain collapse is less restricted and therefore exhibits a much larger change in transmembrane permeance (about 4-fold at pH=2.5). However, at high pH, when PMMA is in its deprotonated swollen state, PNIPAm chain collapse is more restricted resulting in a smaller change in transmembrane permeance (about 2-fold at pH=10).

- Fe and Pd nanoparticles were immobilized within the membrane pores through the ion exchange method. The mean particle diameter was found to be 16 nm with a standard deviation of 7.5 nm. Assuming a normal distribution, the 95% confidence interval is 14.5 nm to 17.5 nm.

CHAPTER 5: THERMO-RESPONSIVE ADSORPTION-DESORPTION OF PFOA FROM WATER

- Equilibrium adsorption Freundlich distribution coefficients (K_d) of PFOA onto PNIPAm hydrogels were determined to be values of 0.073 L/g at 35 °C, 0.026 L/g at 22 °C, and 0.007 L/g at 4 °C.

- Adsorption kinetics of PFOA onto PNIPAm hydrogels were examined, determining initial adsorption rate of 28 mg/g/h and an initial desorption rate of 41 mg/g/h, with determined equilibrium adsorption values of 48 mg/g at 35 °C and 11 mg/g at 20 °C. The initial PFOA adsorption rate of 28 mg/g/h onto PNIPAm hydrogels is comparable to published PFOA adsorption rates using other adsorbents such as GAC (16.2 mg/g/h).

- Interaction parameters of component functional groups were used to explain relative adsorption onto PNIPAm in its different conformational states. PFOS partitioned less into the PNIPAm hydrogels than PFOA at 35 ºC because of the stronger hydrogen bonding interaction between its sulfonate head group and the surrounding aqueous environment. The ratio of K_d values for PFOS adsorption at 35 ºC versus 20 ºC is only 1.1, compared to a much larger ratio of 2.8 for PFOA. While equilibrium adsorption of PFOS by PNIPAm is higher than adsorption of PFOA below the LCST, much like PFOS adsorption onto GAC and other adsorbents, it is much lower above the LCST due to the presence of the sulfonate group, since sulfonic groups' affinity to form hydrogen bonds with OH groups has been shown to increase the interaction of compounds with polar solvents upon sulfonation.

- PVDF membranes were successfully functionalized with PNIPAm for PFOA adsorption and desorption. Functionalized membrane adsorptive capacity of PFOA was around the same value estimated from hydrogel adsorption data, based on the relative amount of PNIPAm in the membrane. Desorption by water permeation through the membrane led to 80% desorption of adsorbed PFOA. Initial adsorption and desorption rates were found to be 0.14 mg/L and 0.17 mg/L, respectively.

- Temperature swing adsorption was conducted over 5 cycles. As temperature was raised and aqueous PFOA was permeated, quantity adsorbed was constant for each 80 mL cycle. As temperature was then lowered below PNIPAm's LCST and water was permeated, 50-60% of adsorbed PFOA was desorbed consistently for each cycle, indicating promise for the use of PNIPAm-functionalized membranes for temperature swing adsorption.

CHAPTER 6: NANOPARTICLE INTEGRATED CATALYTIC DEGRADATION OF PCB

- Fe-Pd nanoparticles were immobilized through ion exchange with PMMA, resulting in a mean nanoparticle diameter of 16 nm within PVDF membrane pores.

- As temperature was raised above PNIPAm's LCST of 32 °C, diffusion coefficient for PCB-1 through the membrane increased from 6.6×10^{-11} m^2/s to 8.7×10^{-11} m^2/s at 25 °C and 35 °C, respectively. Adsorption of PCB-1 onto PNIPAm-PMMA hydrogels increased from 40% to 70% over the same temperature range, while PCB-1 adsorption onto PNIPAm-PMMA functionalized membranes

increased from 6% to 10%, indicating increased diffusion through the membrane and adsorption into the polymeric domain above PNIPAm's LCST.

- Using PNIPAm-PMMA hydrogels, temperature is varied from 35 ºC to 25 ºC and repeated over 5 adsorption/desorption cycles, demonstrating the reversible nature of thermo-responsive adsorption using PNIPAm, as has been demonstrated with PFOA. Adsorption of PCB-1 is constant at approximately 70% (0.07 mg PCB-1 / g hydrogel), while desorption releases approximately 40% of the adsorbed 70% over each cycle

- Convective flow degradation of PCB-1 using the PNIPAm-PMMA-functionalized PVDF membranes with immobilized Fe-Pd nanoparticles yielded first-order k_{SA} values of 0.13 L/m^2/g, 0.28 L/m^2/g, 0.72 L/m^2/g, and 1.36 L/m^2/g at 15 ºC, 25 ºC, 35 ºC, and 45 ºC, respectively, with an activation energy of 60 kJ/mol. Here, mass transfer resistance is negligible and PNIPAm's incorporation into the reactive membrane domain does not enhance reactivity.

- The effect of temperature on transmembrane flux and relative pore diameter was incorporated into the laminar flow first-order reaction model to effectively model PCB degradation in convective flow mode.

- Batch degradation of PCB-1 resulted in first-order k_{SA} values of 0.12 L/m^2/h and 0.35 L/m^2/h at 25 °C and 35 °C, respectively, with Thiele moduli of 2.7 and 3.6. As temperature was raised above PNIPAm's LCST, k_{SA} increased due to not only energetic effects according to the Arrhenius equation, but also due to increased diffusion and adsorption of PCB-1 into the reactive membrane domain attributed to PNIPAm's hydrophobicity switch.

7.3 Key science and engineering advancements

- Temperature and pH responsive polymers, as well as controlled nanostructured materials, were synthesized in membrane pores to create advanced stimuli responsive catalytic membranes with selective control over pore size and permeability for selective size-based rejection.

- Thermo-responsive membranes were developed and used for reversible temperature swing adsorption-desorption of emerging water pollutants (perfluoro-organics) with initial adsorption rates comparable to commercial adsorbents, but with the additional ability to readily desorb by temperature variations.

- Solubility parameters were calculated for the responsive polymer, in its different conformational states, and for the model compounds to develop an understanding of the interaction between the polymer domain and halo-pollutant domain in order to conduct reversible temperature swing adsorption.

- Fe-Pd bimetallic nanoparticles were in-situ immobilized in membrane pores to form catalytic stimuli-responsive (pH and temperature) polymeric membranes for enhanced halo-organic remediation with advanced properties.

- Advanced nanoparticle characterization in membrane pores combined with thermo-responsive permeability data and PCB degradation results enabled reaction modeling and evaluation of the effect of temperature variations on catalytic ability.

7.4 Implications of this work:

The development of stimuli-responsive polymeric membranes that are also catalytic has exciting implications. It has been shown that the addition of a stimuli-responsive polymer into a membrane support can enable antifouling, gating, and selective filtration characteristics. Leveraging the conformational change of the responsive polymers in order to enhance degradation is an attractive means by which to improve existing catalytic membrane processes. It has been shown that membrane-based degradation of chloro-organics can be enhanced through increasing contaminant adsorption and diffusion into the reactive membrane domain. It is important to note that the incorporation of stimuli-responsive polymers into catalytic membranes can also present antifouling properties. When using catalytic membranes in real water, conformational changes can be leveraged to de-foul the membrane. Polymers that exhibit conformational changes to readily desorb reaction products can be chosen based on interaction parameter analysis. For practical applications, post functionalization of membrane modules for in-situ synthesis of catalytic nanoparticles will further provide organic degradation flexibility.

CHAPTER 8: FUTURE WORK

This research sets the foundation for using stimuli responsive polymers to conduct reversible responsive adsorption/desorption of contaminants from water and for leveraging the conformational change of stimuli-responsive polymers in catalytic membrane to enhance halo-organic degradation. These developed stimuli-responsive catalytic membranes provide an exciting opportunity for improvements to current technologies. As this research continues, there are several avenues through which these stimuli responsive catalytic membranes can be further examined and improved. Following is a list of possible ways to further this research:

- The reversible adsorption of hydrophobic contaminants from water using thermo-responsive PNIPAm was shown. While PNIPAm has shown a large volume phase transition at its LCST, other responsive polymers that react to other stimuli can be examined for the reversible adsorption of contaminants from water, based on the interaction parameters of its functional groups.

- The adsorption of hydrophobic contaminants onto PNIPAm can be further examined to quantify the adsorption sites present, and whether adsorption is a single or multi-layer phenomenon.

- Real water samples will evidently contain many more contaminants and compounds, and the examination of how multi-component mixtures preferentially adsorb onto different stimuli-responsive polymers based on solubility parameter interactions would be useful to test viability for treatment of real contaminated water and for scale-up.

- Methods to increase adsorption capacity could be explored through various means, such as incorporating additional functional groups or increasing polymer surface area within membrane pores.

- For the catalytic degradation of halo-organics, adsorption of other natural organics that would be present in real water samples could be investigated to determine interference with the reaction.

- Adsorption/desorption of products from stimuli-responsive membrane-based catalytic reactions could be determined, because increased reaction product adsorption could hinder the reaction. Stimuli-responsive catalytic membranes provide an avenue by which to desorb reaction product compounds through stimuli-responsive conformational changes.

REFERENCES

[1] J.R. Werber, C.O. Osuji, M. Elimelech, Materials for next-generation desalination and water purification membranes, Nature Reviews Materials, 1 (2016) 16018.

[2] A. Asad, D. Sameoto, M. Sadrzadeh, Chapter 1 - Overview of membrane technology, in: M. Sadrzadeh, T. Mohammadi (Eds.) Nanocomposite Membranes for Water and Gas Separation, Elsevier, 2020, pp. 1-28.

[3] N. Pichel, M. Vivar, M. Fuentes, The problem of drinking water access: A review of disinfection technologies with an emphasis on solar treatment methods, Chemosphere, 218 (2019) 1014-1030.

[4] D.M. Warsinger, S. Chakraborty, E.W. Tow, M.H. Plumlee, C. Bellona, S. Loutatidou, L. Karimi, A.M. Mikelonis, A. Achilli, A. Ghassemi, L.P. Padhye, S.A. Snyder, S. Curcio, C.D. Vecitis, H.A. Arafat, J.H. Lienhard, A review of polymeric membranes and processes for potable water reuse, Progress in Polymer Science, 81 (2018) 209-237.

[5] P. Krzeminski, M.C. Tomei, P. Karaolia, A. Langenhoff, C.M.R. Almeida, E. Felis, F. Gritten, H.R. Andersen, T. Fernandes, C.M. Manaia, L. Rizzo, D. Fatta-Kassinos, Performance of secondary wastewater treatment methods for the removal of contaminants of emerging concern implicated in crop uptake and antibiotic resistance spread: A review, Science of The Total Environment, 648 (2019) 1052-1081.

[6] S.P. Nunes, P.Z. Culfaz-Emecen, G.Z. Ramon, T. Visser, G.H. Koops, W. Jin, M. Ulbricht, Thinking the future of membranes: Perspectives for advanced and new membrane materials and manufacturing processes, Journal of Membrane Science, 598 (2020) 117761.

[7] T.C. Merkel, B.D. Freeman, R.J. Spontak, Z. He, I. Pinnau, P. Meakin, A.J. Hill, Ultrapermeable, reverse-selective nanocomposite membranes, Science, 296 (2002) 519-522.

[8] Y.K. Vijay, V. Kulshrestha, K. Awasthi, N.K. Acharya, A. Jain, M. Singh, S.N. Dolia, S.A. Khan, D.K. Avasthi, Characterization of nanocomposite polymeric membrane, J Polym Res, 13 (2006) 357-360.

[9] M.M. Pendergast, E.M.V. Hoek, A review of water treatment membrane nanotechnologies, Energ Environ Sci, 4 (2011) 1946-1971.

[10] M. Sharma, A. Sharma, Polymer Nanocomposite Membranes for Water Treatment, in: S. Choudhury, R. Mishra, R.G. Mishra, A. Kumar (Eds.) Intelligent Communication, Control and Devices, Springer Singapore, Singapore, 2020, pp. 865-874.

[11] B. Saini, D. Vaghani, S. Khuntia, M.K. Sinha, A. Patel, R. Pindoria, A novel stimuli-responsive and fouling resistant PVDF ultrafiltration membrane prepared by using amphiphilic copolymer of poly(vinylidene fluoride) and Poly(2-N-morpholino)ethyl methacrylate, Journal of Membrane Science, 603 (2020) 118047.

[12] R. Wei, J. Guo, L. Jin, C. He, Y. Xie, X. Zhang, W. Zhao, C. Zhao, Vapor induced phase separation towards anion-/near-infrared-responsive pore channels for switchable anti-fouling membranes, Journal of Materials Chemistry A, 8 (2020) 8934-8948.

[13] Y. Shi, D. Wan, J. Huang, Y. Liu, J. Li, Stable LBL self-assembly coating porous membrane with 3D heterostructure for enhanced water treatment under visible light irradiation, Chemosphere, 252 (2020) 126581.

[14] F. oulad, S. Zinadini, A.A. Zinatizadeh, A.A. Derakhshan, Novel (4,4-diaminodiphenyl sulfone coupling modified PES/PES) mixed matrix nanofiltration membranes with high permeability and anti-fouling property, Separation and Purification Technology, 236 (2020) 116292.

[15] W. Chow, Z.M. Ishak, Smart polymer nanocomposites: A review, Express Polymer Letters, 14 (2020) 416-435.

[16] M.S. Islam, S. Hernández, H. Wan, L. Ormsbee, D. Bhattacharyya, Role of membrane pore polymerization conditions for pH responsive behavior, catalytic metal nanoparticle synthesis, and PCB degradation, Journal of Membrane Science, 555 (2018) 348-361.

[17] M. El-Shahat, A.E. Abdelhamid, R.M. Abdelhameed, Capture of iodide from wastewater by effective adsorptive membrane synthesized from MIL-125-NH2 and cross-linked chitosan, Carbohydrate Polymers, 231 (2020) 115742.

[18] J. Jang, I. Park, S.-S. Chee, J.-H. Song, Y. Kang, C. Lee, W. Lee, M.-H. Ham, I.S. Kim, Graphene oxide nanocomposite membrane cooperatively cross-linked by monomer and polymer overcoming the trade-off between flux and rejection in forward osmosis, Journal of Membrane Science, 598 (2020) 117684.

[19] C.Y. Lai, A. Groth, S. Gray, M. Duke, Nanocomposites for Improved Physical Durability of Porous PVDF Membranes, Membranes (Basel), 4 (2014) 55-78.

[20] Y. Zhao, J. Wen, H. Sun, D. Pan, Y. Huang, Y. Bai, L. Shao, Thermo-responsive separation membrane with smart anti-fouling and self-cleaning properties, Chemical Engineering Research and Design, 156 (2020) 333-342.

[21] Z. Yaghoubi, J. Basiri-Parsa, Modification of ultrafiltration membrane by thermo-responsive Bentonite-poly(N-isopropylacrylamide) nanocomposite to improve its antifouling properties, Journal of Water Process Engineering, 34 (2020) 101067.

[22] D. Zhi, J. Wang, Y. Zhou, Z. Luo, Y. Sun, Z. Wan, L. Luo, D.C.W. Tsang, D.D. Dionysiou, Development of ozonation and reactive electrochemical membrane coupled process: Enhanced tetracycline mineralization and toxicity reduction, Chemical Engineering Journal, 383 (2020) 123149.

[23] S.-C. Low, Q.-H. Ng, Chapter 4 - Progress of stimuli responsive membranes in water treatment, in: W.-J. Lau, A.F. Ismail, A. Isloor, A. Al-Ahmed (Eds.) Advanced Nanomaterials for Membrane Synthesis and its Applications, Elsevier, 2019, pp. 69-99.

[24] S.M. Husson, Synthesis Aspects in the Design of Responsive Membranes, in: Responsive Membranes and Materials, John Wiley & Sons, Ltd., 2012, pp. 73-96.

[25] K. Tauer, D. Gau, S. Schulze, A. Volkel, R. Dimova, Thermal property changes of poly(N-isopropylacrylamide) microgel particles and block copolymers, Colloid Polym Sci, 287 (2009) 299-312.

[26] H. Yim, M.S. Kent, S. Mendez, S.S. Balamurugan, S. Balamurugan, G.P. Lopez, S. Satija, Temperature-dependent conformational change of PNIPAM grafted chains at high surface density in water, Macromolecules, 37 (2004) 1994-1997.

[27] M. Rackaitis, K. Strawhecker, E. Manias, Water-soluble polymers with tunable temperature sensitivity: Solution behavior, J Polym Sci Pol Phys, 40 (2002) 2339-2342.

[28] Y. Kotsuchibashi, Recent advances in multi-temperature-responsive polymeric materials, Polymer Journal, (2020).

[29] N. Adrus, M. Ulbricht, Novel hydrogel pore-filled composite membranes with tunable and temperature-responsive size-selectivity, J Mater Chem, 22 (2012) 3088-3098.

[30] L. Wu, E. Sancaktar, Effect of PET support membrane thickness on water permeation behavior of thermally responsive PNIPAM-g-PET membranes, Journal of Membrane Science, (2020) 118304.

[31] L. Xiao, A. Isner, K. Waldrop, A. Saad, D. Takigawa, D. Bhattacharyya, Development of Bench and Full-Scale Temperature and pH Responsive Functionalized PVDF Membranes with Tunable Properties, J Memb Sci, 457 (2014) 39-49.

[32] H. Du, R. Wickramasinghe, X. Qian, Effects of salt on the lower critical solution temperature of poly (N-isopropylacrylamide), J Phys Chem B, 114 (2010) 16594-16604.

[33] H.B. Du, X.H. Qian, Molecular Dynamics Simulations of PNIPAM-co-PEGMA Copolymer Hydrophilic to Hydrophobic Transition in NaCl Solution, J Polym Sci Pol Phys, 49 (2011) 1112-1122.

[34] P.M. Reddy, P. Venkatesu, Ionic liquid modifies the lower critical solution temperature (LCST) of poly(N-isopropylacrylamide) in aqueous solution, J Phys Chem B, 115 (2011) 4752-4757.

[35] R. Xie, Y. Li, L.Y. Chu, Preparation of thermo-responsive gating membranes with controllable response temperature, J Membrane Sci, 289 (2007) 76-85.

[36] S. Frost, M. Ulbricht, Thermoresponsive ultrafiltration membranes for the switchable permeation and fractionation of nanoparticles, J Membrane Sci, 448 (2013) 1-11.

[37] C. Bombonnel, C. Vancaeyzeele, G. Guérin, F. Vidal, Fabrication of bicontinuous double networks as thermal and pH stimuli responsive drug carriers for on-demand release, Materials Science and Engineering: C, 109 (2020) 110495.

[38] H. Liu, J. Zhu, L. Hao, Y. Jiang, B. van der Bruggen, A. Sotto, C. Gao, J. Shen, Thermo- and pH-responsive graphene oxide membranes with tunable nanochannels for water gating and permeability of small molecules, Journal of Membrane Science, 587 (2019) 117163.

[39] D. Wandera, H.H. Himstedt, M. Marroquin, S.R. Wickramasinghe, S.M. Husson, Modification of ultrafiltration membranes with block copolymer nanolayers for produced water treatment: The roles of polymer chain density and polymerization time on performance, J Membrane Sci, 403 (2012) 250-260.

[40] Z. Liu, W. Wang, R. Xie, X.-J. Ju, L.-Y. Chu, Stimuli-responsive smart gating membranes, Chemical Society Reviews, 45 (2016) 460-475.

[41] P. Varanasi, A. Fullana, S. Sidhu, Remediation of PCB contaminated soils using iron nano-particles, Chemosphere, 66 (2007) 1031-1038.

[42] V. Smuleac, R. Varma, S. Sikdar, D. Bhattacharyya, Green Synthesis of Fe and Fe/Pd Bimetallic Nanoparticles in Membranes for Reductive Degradation of Chlorinated Organics, J Memb Sci, 379 (2011) 131-137.

[43] L. Xiao, A.B. Isner, J.Z. Hilt, D. Bhattacharyya, Temperature responsive hydrogel with reactive nanoparticles, J Appl Polym Sci, 128 (2013) 1804-1814.

[44] C.R. Wilke, P. Chang, Correlation of Diffusion Coefficients in Dilute Solutions, Aiche J, 1 (1955) 264-270.

[45] J.J. Chen, A.L. Ahmad, B.S. Ooi, Thermo-responsive properties of poly(N-isopropylacrylamide-co-acrylic acid) hydrogel and its effect on copper ion removal and fouling of polymer-enhanced ultrafiltration, J Membrane Sci, 469 (2014) 73-79.

[46] H. Yang, S. Fang, H.-M. Song, L.-J. Zhu, Z.-X. Zeng, pH-responsive poly(vinylidene fluoride)/poly(acrylic acid) porous membranes prepared via an vapor

induced phase separation technique for removing copper ions from water, Materials Letters, 260 (2020) 126957.

[47] S.P. Sun, A.T. Lemley, p-Nitrophenol degradation by a heterogeneous Fenton-like reaction on nano-magnetite: Process optimization, kinetics, and degradation pathways, J Mol Catal a-Chem, 349 (2011) 71-79.

[48] G.E. Morris, B. Vincent, M.J. Snowden, The interaction of thermosensitive, anionic microgels with metal ion solution species, in: J.B. Rosenholm, B. Lindman, P. Stenius (Eds.) Trends in Colloid and Interface Science XI, Steinkopff, 1997, pp. 16-22.

[49] F. Liu, M.W. Urban, Recent advances and challenges in designing stimuli-responsive polymers, Prog Polym Sci, 35 (2010) 3-23.

[50] Q. Zhang, F. Xia, T. Sun, W. Song, T. Zhao, M. Liu, L. Jiang, Wettability switching between high hydrophilicity at low pH and high hydrophobicity at high pH on surface based on pH-responsive polymer, Chem Commun (Camb), (2008) 1199-1201.

[51] P. B.K, V. B, Karaya gum-graft-poly(N,N'-dimethylacrylamide) gel: A pH responsive potential adsorbent for sequestration of cationic dyes, Journal of Environmental Chemical Engineering, 8 (2020) 103608.

[52] I. Katime, J.L. Velada, R. Novoa, E.D. deApodaca, J. Puig, E. Mendizabal, Swelling kinetics of poly(acrylamide)/poly(mono-n-alkyl itaconates) hydrogels, Polym Int, 40 (1996) 281-286.

[53] N.A. Peppas, S.L. Wright, Solute diffusion in poly(vinyl alcohol) poly(acrylic acid) interpenetrating networks, Macromolecules, 29 (1996) 8798-8804.

[54] A. Thakur, R.K. Wanchoo, P. Singh, Structural Parameters and Swelling Behavior of pH Sensitive Poly(acrylamide-co-acrylic acid) Hydrogels, Chem Biochem Eng Q, 25 (2011) 181-194.

[55] S. Hernandez, J.K. Papp, D. Bhattacharyya, Iron-Based Redox Polymerization of Acrylic Acid for Direct Synthesis of Hydrogel/Membranes, and Metal Nanoparticles for Water Treatment, Ind Eng Chem Res, 53 (2014) 1130-1142.

[56] P. Mondal, N.S. Samanta, A. Kumar, M.K. Purkait, Recovery of H2SO4 from wastewater in the presence of NaCl and KHCO3 through pH responsive polysulfone membrane: Optimization approach, Polymer Testing, 86 (2020) 106463.

[57] A.C. Sagle, E.M. Van Wagner, H. Ju, B.D. McCloskey, B.D. Freeman, M.M. Sharma, PEG-coated reverse osmosis membranes: Desalination properties and fouling resistance, J Membrane Sci, 340 (2009) 92-108.

[58] Y.F. Li, Y.L. Su, X.T. Zhao, R.N. Zhang, J.J. Zhao, X.C. Fan, Z.Y. Jiang, Surface fluorination of polyamide nanofiltration membrane for enhanced antifouling property, J Membrane Sci, 455 (2014) 15-23.

[59] M. Gui, L.E. Ormsbee, D. Bhattacharyya, Reactive Functionalized Membranes for Polychlorinated Biphenyl Degradation, Ind Eng Chem Res, 52 (2013) 10430-10440.

[60] V. Smuleac, L. Bachas, D. Bhattacharyya, Aqueous - Phase Synthesis of PAA in PVDF Membrane Pores for Nanoparticle Synthesis and Dichlorobiphenyl Degradation, J Memb Sci, 346 (2010) 310-317.

[61] J. Xu, D. Bhattacharyya, Fe/Pd nanoparticle immobilization in microfiltration membrane pores: Synthesis, characterization, and application in the dechlorination of polychlorinated biphenyls, Ind Eng Chem Res, 46 (2007) 2348-2359.

[62] M. Gui, J.K. Papp, A.S. Colburn, N.D. Meeks, B. Weaver, I. Wilf, D. Bhattacharyya, Engineered Iron/Iron Oxide Functionalized Membranes for Selenium and

Other Toxic Metal Removal from Power Plant Scrubber Water, J Memb Sci, 488 (2015) 79-91.

[63] M.H. Gui, V. Smuleac, L.E. Ormsbee, D.L. Sedlak, D. Bhattacharyya, Iron oxide nanoparticle synthesis in aqueous and membrane systems for oxidative degradation of trichloroethylene from water, J Nanopart Res, 14 (2012) 1-16.

[64] B. Seteni, J.C. Ngila, K. Sikhwivhilu, R.M. Moutloali, B. Mamba, Dechlorination of 3,3′,4,4′-tetrachlorobiphenyl (PCB77) in water, by nickel/iron nanoparticles immobilized on L-lysine/PAA/PVDF membrane, Physics and Chemistry of the Earth, Parts A/B/C, 66 (2013) 60-67.

[65] J.J. Li, Y.N. Zhou, Z.H. Luo, Smart Fiber Membrane for pH-Induced Oil/Water Separation, ACS Appl Mater Interfaces, 7 (2015) 19643-19650.

[66] L. Tang, G. Wang, Z. Zeng, L. Shen, L. Zhu, Y. Zhang, Q. Xue, Three-dimensional adsorbent with pH induced superhydrophobic and superhydrophilic transformation for oil recycle and adsorbent regeneration, Journal of Colloid and Interface Science, 575 (2020) 231-244.

[67] Q. Yang, H.H. Himstedt, M. Ulbricht, X.H. Qian, S.R. Wickramasinghe, Designing magnetic field responsive nanofiltration membranes, J Membrane Sci, 430 (2013) 70-78.

[68] Y. Xiao, J. Du, Superparamagnetic nanoparticles for biomedical applications, Journal of Materials Chemistry B, 8 (2020) 354-367.

[69] H.H. Himstedt, Q. Yang, X.H. Qian, S.R. Wickramasinghe, M. Ulbricht, Toward remote-controlled valve functions via magnetically responsive capillary pore membranes, J Membrane Sci, 423 (2012) 257-266.

[70] F. Schacher, T. Rudolph, F. Wieberger, M. Ulbricht, A.H. Muller, Double stimuli-responsive ultrafiltration membranes from polystyrene-block-poly(N,N-dimethylaminoethyl methacrylate) diblock copolymers, ACS Appl Mater Interfaces, 1 (2009) 1492-1503.

[71] N. Lundquist, M.J. Sweetman, K. Scroggie, M. Worthington, L. Esdaile, S. Alboaiji, S.E. Plush, J.D. Hayball, J.M. Chalker, Polymer supported carbon for safe and effective remediation of PFOA-and PFOS-contaminated water, ACS Sustainable Chemistry & Engineering, (2019).

[72] C. Cooper, Destruction of Perfluorinated Compounds (PFCs), in, United States, 2020.

[73] Q. Zhou, S. Deng, Q. Zhang, Q. Fan, J. Huang, G. Yu, Sorption of perfluorooctane sulfonate and perfluorooctanoate on activated sludge, Chemosphere, 81 (2010) 453-458.

[74] Z. Du, S. Deng, S. Zhang, B. Wang, J. Huang, Y. Wang, G. Yu, B. Xing, Selective and High Sorption of Perfluorooctanesulfonate and Perfluorooctanoate by Fluorinated Alkyl Chain Modified Montmorillonite, The Journal of Physical Chemistry C, 120 (2016) 16782-16790.

[75] Y. Yao, K. Volchek, C.E. Brown, A. Robinson, T. Obal, Comparative study on adsorption of perfluorooctane sulfonate (PFOS) and perfluorooctanoate (PFOA) by different adsorbents in water, Water Science and Technology, 70 (2014) 1983-1991.

[76] M.M. Schultz, D.F. Barofsky, J.A. Field, Quantitative Determination of Fluorotelomer Sulfonates in Groundwater by LC MS/MS, Environmental Science & Technology, 38 (2004) 1828-1835.

[77] M. Murakami, H. Shinohara, H. Takada, Evaluation of wastewater and street runoff as sources of perfluorinated surfactants (PFSs), Chemosphere, 74 (2009) 487-493.

[78] C.Y. Tang, Q.S. Fu, A.P. Robertson, C.S. Criddle, J.O. Leckie, Use of Reverse Osmosis Membranes to Remove Perfluorooctane Sulfonate (PFOS) from Semiconductor Wastewater, Environmental Science & Technology, 40 (2006) 7343-7349.

[79] C.D. Vecitis, H. Park, J. Cheng, B.T. Mader, M.R. Hoffmann, Treatment technologies for aqueous perfluorooctanesulfonate (PFOS) and perfluorooctanoate (PFOA), Frontiers of Environmental Science & Engineering in China, 3 (2009) 129-151.

[80] J.S.C. Liou, B. Szostek, C.M. DeRito, E.L. Madsen, Investigating the biodegradability of perfluorooctanoic acid, Chemosphere, 80 (2010) 176-183.

[81] L.-h. Zhang, J.-h. Cheng, X. You, X.-y. Liang, Y.-y. Hu, Photochemical defluorination of aqueous perfluorooctanoic acid (PFOA) by Fe 0/GAC micro-electrolysis and VUV-Fenton photolysis, Environmental Science and Pollution Research, 23 (2016) 13531-13542.

[82] S. Yang, J. Cheng, J. Sun, Y. Hu, X. Liang, Defluorination of Aqueous Perfluorooctanesulfonate by Activated Persulfate Oxidation, PLoS ONE, 8 (2013) 1-10.

[83] Y.-C. Lee, Y.-f. Li, M.-J. Chen, Y.-C. Chen, J. Kuo, S.-L. Lo, Efficient decomposition of perfluorooctanic acid by persulfate with iron-modified activated carbon, Water Research, 174 (2020) 115618.

[84] H. Park, C.D. Vecitis, J. Cheng, W. Choi, B.T. Mader, M.R. Hoffmann, Reductive Defluorination of Aqueous Perfluorinated Alkyl Surfactants: Effects of Ionic Headgroup and Chain Length, The Journal of Physical Chemistry A, 113 (2009) 690-696.

[85] C. Boo, Y. Wang, I. Zucker, Y. Choo, C.O. Osuji, M. Elimelech, High Performance Nanofiltration Membrane for Effective Removal of Perfluoroalkyl Substances at High Water Recovery, Environmental Science & Technology, 52 (2018) 7279-7288.

[86] S.T.M.L.D. Senevirathna, S. Tanaka, S. Fujii, C. Kunacheva, H. Harada, B.R. Shivakoti, R. Okamoto, A comparative study of adsorption of perfluorooctane sulfonate (PFOS) onto granular activated carbon, ion-exchange polymers and non-ion-exchange polymers, Chemosphere, 80 (2010) 647-651.

[87] Z. Du, S. Deng, Y. Bei, Q. Huang, B. Wang, J. Huang, G. Yu, Adsorption behavior and mechanism of perfluorinated compounds on various adsorbents—A review, Journal of Hazardous Materials, 274 (2014) 443-454.

[88] S.T.M.L.D. Senevirathna, S. Tanaka, S. Fujii, C. Kunacheva, H. Harada, B.H.A.K.T. Ariyadasa, B.R. Shivakoti, Adsorption of perfluorooctane sulfonate (n-PFOS) onto non ion-exchange polymers and granular activated carbon: Batch and column test, Desalination, 260 (2010) 29-33.

[89] X. Chen, X. Xia, X. Wang, J. Qiao, H. Chen, A comparative study on sorption of perfluorooctane sulfonate (PFOS) by chars, ash and carbon nanotubes, Chemosphere, 83 (2011) 1313-1319.

[90] X. Li, S. Chen, X. Quan, Y. Zhang, Enhanced Adsorption of PFOA and PFOS on Multiwalled Carbon Nanotubes under Electrochemical Assistance, Environmental Science & Technology, 45 (2011) 8498-8505.

[91] C. Patterson, J. Burkhardt, D. Schupp, E.R. Krishnan, S. Dyment, S. Merritt, L. Zintek, D. Kleinmaier, Effectiveness of point-of-use/point-of-entry systems to remove per- and polyfluoroalkyl substances from drinking water, AWWA Water Science, 1 (2019) e1131.

[92] T.-Y. Wu, A.B. Zrimsek, S.V. Bykov, R.S. Jakubek, S.A. Asher, Hydrophobic Collapse Initiates the Poly(N-isopropylacrylamide) Volume Phase Transition Reaction Coordinate, The Journal of Physical Chemistry B, 122 (2018) 3008-3014.

[93] H. Lai, P. Wu, A infrared spectroscopic study on the mechanism of temperature-induced phase transition of concentrated aqueous solutions of poly (N-isopropylacrylamide) and N-isopropylpropionamide, Polymer, 51 (2010) 1404-1412.

[94] O. Ramon, E. Kesselman, R. Berkovici, Y. Cohen, Y. Paz, Attenuated total reflectance/fourier transform infrared studies on the phase-separation process of aqueous solutions of poly (n-isopropylacrylamide), Journal of Polymer Science Part B: Polymer Physics, 39 (2001) 1665-1677.

[95] S. Sun, J. Hu, H. Tang, P. Wu, Chain collapse and revival thermodynamics of poly (N-isopropylacrylamide) hydrogel, The Journal of Physical Chemistry B, 114 (2010) 9761-9770.

[96] B. Sun, Y. Lin, P. Wu, H.W. Siesler, A FTIR and 2D-IR spectroscopic study on the microdynamics phase separation mechanism of the poly (N-isopropylacrylamide) aqueous solution, Macromolecules, 41 (2008) 1512-1520.

[97] M. Kanduč, W.K. Kim, R. Roa, J. Dzubiella, Transfer Free Energies and Partitioning of Small Molecules in Collapsed PNIPAM Polymers, The Journal of Physical Chemistry B, (2018).

[98] L. Xiao, D.M. Davenport, L. Ormsbee, D. Bhattacharyya, Polymerization and Functionalization of Membrane Pores for Water Related Applications, Ind Eng Chem Res, 54 (2015) 4174-4182.

[99] M. Gui, L.E. Ormsbee, D. Bhattacharyya, Reactive functionalized membranes for polychlorinated biphenyl degradation, Industrial & engineering chemistry research, 52 (2013) 10430-10440.

[100] V. Smuleac, L. Bachas, D. Bhattacharyya, Aqueous-phase synthesis of PAA in PVDF membrane pores for nanoparticle synthesis and dichlorobiphenyl degradation, J Membrane Sci, 346 (2010) 310-317.

[101] S.R. Lewis, S. Datta, M. Gui, E.L. Coker, F.E. Huggins, S. Daunert, L. Bachas, D. Bhattacharyya, Reactive nanostructured membranes for water purification, Proceedings of the National Academy of Sciences, 108 (2011) 8577-8582.

[102] J. Xu, D. Bhattacharyya, Fe/Pd Nanoparticle Immobilization in Microfiltration Membrane Pores: Synthesis, Characterization, and Application in the Dechlorination of Polychlorinated Biphenyls, Industrial & Engineering Chemistry Research, 46 (2007) 2348-2359.

[103] A. Bera, C.U. Kumar, P. Parui, S.K. Jewrajka, Stimuli responsive and low fouling ultrafiltration membranes from blends of polyvinylidene fluoride and designed library of amphiphilic poly(methyl methacrylate) containing copolymers, Journal of Membrane Science, 481 (2015) 137-147.

[104] A.P.H. Association, Resolution 9304: Recognizing and addressing the environmental and occupational health problems posed by chlorinated organic chemicals, Am J Public Health, 84 (1994) 514-515.

[105] R. Rodrigues, S. Betelu, S. Colombano, T. Tzedakis, G. Masselot, I. Ignatiadis, In Situ Chemical Reduction of Chlorinated Organic Compounds, in: E.D. van Hullebusch, D. Huguenot, Y. Pechaud, M.-O. Simonnot, S. Colombano (Eds.) Environmental Soil

Remediation and Rehabilitation: Existing and Innovative Solutions, Springer International Publishing, Cham, 2020, pp. 283-398.

[106] J. Jiang, L. Zhu, L. Zhu, B. Zhu, Y. Xu, Surface characteristics of a self-polymerized dopamine coating deposited on hydrophobic polymer films, Langmuir, 27 (2011) 14180-14187.

[107] N. Luo, M.J. Stewart, D.E. Hirt, S.M. Husson, D.W. Schwark, Surface modification of ethylene-co-acrylic acid copolymer films: Addition of amide groups by covalently bonded amino acid intermediates, Journal of applied polymer science, 92 (2004) 1688-1694.

[108] L. Setiawan, R. Wang, K. Li, A.G. Fane, Fabrication of novel poly (amide–imide) forward osmosis hollow fiber membranes with a positively charged nanofiltration-like selective layer, Journal of Membrane Science, 369 (2011) 196-205.

[109] M.A. Shannon, P.W. Bohn, M. Elimelech, J.G. Georgiadis, B.J. Marinas, A.M. Mayes, Science and technology for water purification in the coming decades, Nature, 452 (2008) 301-310.

[110] H. Wan, N.J. Briot, A. Saad, L. Ormsbee, D. Bhattacharyya, Pore functionalized PVDF membranes with in-situ synthesized metal nanoparticles: Material characterization, and toxic organic degradation, Journal of Membrane Science, 530 (2017) 147-157.

[111] X. Shen, T. Xie, J. Wang, P. Liu, F. Wang, An anti-fouling poly(vinylidene fluoride) hybrid membrane blended with functionalized ZrO2 nanoparticles for efficient oil/water separation, Rsc Adv, 7 (2017) 5262-5271.

[112] Y.-F. Guan, B.-C. Huang, C. Qian, L.-F. Wang, H.-Q. Yu, Improved PVDF membrane performance by doping extracellular polymeric substances of activated sludge, Water Research, 113 (2017) 89-96.

[113] S. Ayyaru, Y.-H. Ahn, Application of sulfonic acid group functionalized graphene oxide to improve hydrophilicity, permeability, and antifouling of PVDF nanocomposite ultrafiltration membranes, J Membrane Sci, 525 (2017) 210-219.

[114] M. Gui, J.K. Papp, A.S. Colburn, N.D. Meeks, B. Weaver, I. Wilf, D. Bhattacharyya, Engineered iron/iron oxide functionalized membranes for selenium and other toxic metal removal from power plant scrubber water, J Membrane Sci, 488 (2015) 79-91.

[115] J. Karppi, S. Åkerman, K. Åkerman, A. Sundell, I. Penttilä, Adsorption of metal cations from aqueous solutions onto the pH responsive poly(vinylidene fluoride grafted poly(acrylic acid) (PVDF-PAA) membrane, J Polym Res, 17 (2010) 71-76.

[116] C.O. M'Bareck, Q.T. Nguyen, S. Alexandre, I. Zimmerlin, Fabrication of ion-exchange ultrafiltration membranes for water treatment: I. Semi-interpenetrating polymer networks of polysulfone and poly(acrylic acid), J Membrane Sci, 278 (2006) 10-18.

[117] J. Xu, D. Bhattacharyya, Modeling of Fe/Pd nanoparticle-based functionalized membrane reactor for PCB dechlorination at room temperature, Journal of Physical Chemistry C, 112 (2008) 9133-9144.

[118] T. Phenrat, P. Skácelová, E. Petala, A. Velosa, J. Filip, Nanoscale Zero-Valent Iron Particles for Water Treatment: From Basic Principles to Field-Scale Applications, in: J. Filip, T. Cajthaml, P. Najmanová, M. Černík, R. Zbořil (Eds.) Advanced Nano-Bio Technologies for Water and Soil Treatment, Springer International Publishing, Cham, 2020, pp. 19-52.

[119] C.D. Powell, Development of Non-conventional Iron-based Nanomaterials for Water Treatment, in, Rice University, 2020.

[120] H.-L. Lien, W.-X. Zhang, Nanoscale Pd/Fe bimetallic particles: Catalytic effects of palladium on hydrodechlorination, Applied Catalysis B: Environmental, 77 (2007) 110-116.

[121] F. He, D. Zhao, Hydrodechlorination of trichloroethene using stabilized Fe-Pd nanoparticles: Reaction mechanism and effects of stabilizers, catalysts and reaction conditions, Applied Catalysis B: Environmental, 84 (2008) 533-540.

[122] Y.H. Tee, L. Bachas, D. Bhattacharyya, Degradation of Trichloroethylene and Dichlorobiphenyls by Iron-Based Bimetallic Nanoparticles, J Phys Chem C Nanomater Interfaces, 113 (2009) 9454-9464.

[123] G.V. Lowry, K.M. Johnson, Congener-Specific Dechlorination of Dissolved PCBs by Microscale and Nanoscale Zerovalent Iron in a Water/Methanol Solution, Environmental Science & Technology, 38 (2004) 5208-5216.

[124] Y. Liu, G.V. Lowry, Effect of particle age (Fe0 content) and solution pH on NZVI reactivity: H2 evolution and TCE dechlorination, Environ Sci Technol, 40 (2006) 6085-6090.

[125] Y. Liu, S.A. Majetich, R.D. Tilton, D.S. Sholl, G.V. Lowry, TCE dechlorination rates, pathways, and efficiency of nanoscale iron particles with different properties, Environ Sci Technol, 39 (2005) 1338-1345.

[126] J.M. Thompson, B.J. Chisholm, A.N. Bezbaruah, Reductive Dechlorination of Chloroacetanilide Herbicide (Alachlor) Using Zero-Valent Iron Nanoparticles, Environ Eng Sci, 27 (2010) 227-232.

[127] C.C. Huang, S.L. Lo, H.L. Lien, Zero-valent copper nanoparticles for effective dechlorination of dichloromethane using sodium borohydride as a reductant, Chem Eng J, 203 (2012) 95-100.

[128] R.A. Crane, T.B. Scott, Nanoscale zero-valent iron: future prospects for an emerging water treatment technology, J Hazard Mater, 211-212 (2012) 112-125.

[129] H. Liu, Q. Wang, C. Wang, X.Z. Li, Electron efficiency of zero-valent iron for groundwater remediation and wastewater treatment, Chem Eng J, 215 (2013) 90-95.

[130] F. He, D. Zhao, C. Paul, Field assessment of carboxymethyl cellulose stabilized iron nanoparticles for in situ destruction of chlorinated solvents in source zones, Water Res, 44 (2010) 2360-2370.

[131] S.R. Lewis, V. Smuleac, L. Xiao, D. Bhattacharyya, Tunable Separations, Reactions, and Nanoparticle Synthesis in Functionalized Membranes, in: Responsive Membranes and Materials, John Wiley & Sons, Ltd., 2012, pp. 97-142.

[132] S. Xiao, S. Wu, M. Shen, R. Guo, Q. Huang, S. Wang, X. Shi, Polyelectrolyte multilayer-assisted immobilization of zero-valent iron nanoparticles onto polymer nanofibers for potential environmental applications, ACS Appl Mater Interfaces, 1 (2009) 2848-2855.

[133] F. He, D. Zhao, Manipulating the size and dispersibility of zerovalent iron nanoparticles by use of carboxymethyl cellulose stabilizers, Environmental Science & Technology, 41 (2007) 6216-6221.

[134] R. Hudson, G. Hamasaka, T. Osako, Y.M. Yamada, C.J. Li, Y. Uozumi, A. Moores, Highly efficient iron (0) nanoparticle-catalyzed hydrogenation in water in flow, Green Chemistry, 15 (2013) 2141-2148.

[135] Y.P. Sun, X.Q. Li, W.X. Zhang, H.P. Wang, A method for the preparation of stable dispersion of zero-valent iron nanoparticles, Colloids and Surfaces A: Physicochemical and Engineering Aspects, 308 (2007) 60-66.

[136] C.G. Hadjipanayis, M.J. Bonder, S. Balakrishnan, X. Wang, H. Mao, G.C. Hadjipanayis, Metallic iron nanoparticles for MRI contrast enhancement and local hyperthermia, Small, 4 (2008) 1925-1929.

[137] L.F. Greenlee, N.S. Rentz, ATMP-stabilized iron nanoparticles: chelator-controlled nanoparticle synthesis, Journal of Nanoparticle Research, 16 (2014) 1-16.

[138] B. Schrick, J.L. Blough, A.D. Jones, T.E. Mallouk, Hydrodechlorination of trichloroethylene to hydrocarbons using bimetallic nickel− iron nanoparticles, Chemistry of Materials, 14 (2002) 5140-5147.

[139] Y. Wang, H. Zhao, G. Zhao, Iron-copper bimetallic nanoparticles embedded within ordered mesoporous carbon as effective and stable heterogeneous Fenton catalyst for the degradation of organic contaminants, Applied Catalysis B: Environmental, 164 (2015) 396-406.

[140] D. O'Carroll, B. Sleep, M. Krol, H. Boparai, C. Kocur, Nanoscale zero valent iron and bimetallic particles for contaminated site remediation, Advances in Water Resources, 51 (2013) 104-122.

[141] C.L. Chun, D.R. Baer, D.W. Matson, J.E. Amonette, R.L. Penn, Characterization and reactivity of iron nanoparticles prepared with added Cu, Pd, and Ni, Environ Sci Technol, 44 (2010) 5079-5085.

[142] N. Zhu, H. Luan, S. Yuan, J. Chen, X. Wu, L. Wang, Effective dechlorination of HCB by nanoscale Cu/Fe particles, J Hazard Mater, 176 (2010) 1101-1105.

[143] G.K. Parshetti, R.A. Doong, Dechlorination of trichloroethylene by Ni/Fe nanoparticles immobilized in PEG/PVDF and PEG/nylon 66 membranes, Water Res, 43 (2009) 3086-3094.

[144] H.L. Lien, W.X. Zhang, Nanoscale Pd/Fe bimetallic particles: Catalytic effects of palladium on hydrodechlorination, Appl Catal B-Environ, 77 (2007) 110-116.

[145] V. Nagpal, A.D. Bokare, R.C. Chikate, C.V. Rode, K.M. Paknikar, Reductive dechlorination of gamma-hexachlorocyclohexane using Fe-Pd bimetallic nanoparticles, J Hazard Mater, 175 (2010) 680-687.

[146] W. Yan, A.A. Herzing, X.Q. Li, C.J. Kiely, W.X. Zhang, Structural evolution of Pd-doped nanoscale zero-valent iron (nZVI) in aqueous media and implications for particle aging and reactivity, Environ Sci Technol, 44 (2010) 4288-4294.

[147] M. Zhang, F. He, D. Zhao, X. Hao, Degradation of soil-sorbed trichloroethylene by stabilized zero valent iron nanoparticles: effects of sorption, surfactants, and natural organic matter, Water Res, 45 (2011) 2401-2414.

[148] B.W. Zhu, T.T. Lim, Catalytic reduction of chlorobenzenes with Pd/Fe nanoparticles: reactive sites, catalyst stability, particle aging, and regeneration, Environ Sci Technol, 41 (2007) 7523-7529.

[149] X. Wang, C. Chen, H. Liu, J. Ma, Preparation and characterization of PAA/PVDF membrane-immobilized Pd/Fe nanoparticles for dechlorination of trichloroacetic acid, Water Res, 42 (2008) 4656-4664.

[150] H. Choi, S.R. Al Abed, S. Agarwal, D.D. Dionysiou, Synthesis of reactive nano-Fe/Pd bimetallic system-impregnated activated carbon for the simultaneous adsorption and dechlorination of PCBs, Chemistry of Materials, 20 (2008) 3649-3655.

[151] J.G. Doyle, T. Miles, E. Parker, I.F. Cheng, Quantification of total polychlorinated biphenyl by dechlorination to biphenyl by Pd/Fe and Pd/Mg bimetallic particles, Microchemical Journal, 60 (1998) 290-295.

[152] H. Choi, S.R. Al Abed, Effect of reaction environments on the reactivity of PCB (2-chlorobiphenyl) over activated carbon impregnated with palladized iron, Journal of hazardous materials, 179 (2010) 869-874.

[153] F. He, D. Zhao, C. Paul, Field assessment of carboxymethyl cellulose stabilized iron nanoparticles for in situ destruction of chlorinated solvents in source zones, Water Research, 44 (2010) 2360-2370.

[154] F. He, D. Zhao, Hydrodechlorination of trichloroethene using stabilized Fe-Pd nanoparticles: Reaction mechanism and effects of stabilizers, catalysts and reaction conditions, Applied Catalysis B: Environmental, 84 (2008) 533-540.

[155] A. Saad, R. Mills, H. Wan, M.A. Mottaleb, L. Ormsbee, D. Bhattacharyya, Thermo-responsive adsorption-desorption of perfluoroorganics from water using PNIPAm hydrogels and pore functionalized membranes, Journal of Membrane Science, 599 (2020) 117821.

[156] Z. Du, S. Deng, S. Zhang, W. Wang, B. Wang, J. Huang, Y. Wang, G. Yu, B. Xing, Selective and Fast Adsorption of Perfluorooctanesulfonate from Wastewater by Magnetic Fluorinated Vermiculite, Environmental Science & Technology, 51 (2017) 8027-8035.

[157] H. Wan, M.S. Islam, N.J. Briot, M. Schnobrich, L. Pacholik, L. Ormsbee, D. Bhattacharyya, Pd/Fe nanoparticle integrated PMAA-PVDF membranes for chloro-organic remediation from synthetic and site groundwater, Journal of Membrane Science, 594 (2020) 117454.

[158] S. Hernandez, A. Saad, L. Ormsbee, D. Bhattacharyya, Nanocomposite and responsive membranes for water treatment, Emerging Membrane Technology For Sustainable Water Treatment; Hankins, NP, Singh, R., Eds, (2016) 389-431.

[159] L. Ying, W.H. Yu, E.T. Kang, K.G. Neoh, Functional and Surface-Active Membranes from Poly(vinylidene fluoride)-graft-Poly(acrylic acid) Prepared via RAFT-Mediated Graft Copolymerization, Langmuir, 20 (2004) 6032-6040.

[160] Y. Li, L.-Y. Chu, J.-H. Zhu, H.-D. Wang, S.-L. Xia, W.-M. Chen, Thermoresponsive Gating Characteristics of Poly(N-isopropylacrylamide)-Grafted Porous Poly(vinylidene fluoride) Membranes, Industrial & Engineering Chemistry Research, 43 (2004) 2643-2649.

[161] J.-Z. Yu, L.-P. Zhu, B.-K. Zhu, Y.-Y. Xu, Poly(N-isopropylacrylamide) grafted poly(vinylidene fluoride) copolymers for temperature-sensitive membranes, Journal of Membrane Science, 366 (2011) 176-183.

[162] L. Ying, E.T. Kang, K.G. Neoh, Synthesis and Characterization of Poly(N-isopropylacrylamide)-graft-Poly(vinylidene fluoride) Copolymers and Temperature-Sensitive Membranes, Langmuir, 18 (2002) 6416-6423.

[163] N. Boon, P. Schurtenberger, Swelling of micro-hydrogels with a crosslinker gradient, Physical Chemistry Chemical Physics, 19 (2017) 23740-23746.

[164] C. Wu, S. Zhou, S.C.F. Au-yeung, S. Jiang, Volume phase transition of spherical microgel particles, Die Angewandte Makromolekulare Chemie, 240 (1996) 123-136.

[165] T. Tanaka, D.J. Fillmore, Kinetics of swelling of gels, The Journal of Chemical Physics, 70 (1979) 1214-1218.

[166] R. Acciaro, T. Gilányi, I. Varga, Preparation of Monodisperse Poly(N-isopropylacrylamide) Microgel Particles with Homogenous Cross-Link Density Distribution, Langmuir, 27 (2011) 7917-7925.

[167] W. Su, K. Zhao, J. Wei, T. Ngai, Dielectric relaxations of poly(N-isopropylacrylamide) microgels near the volume phase transition temperature: impact of cross-linking density distribution on the volume phase transition, Soft Matter, 10 (2014) 8711-8723.

[168] S.J. Lue, C.-H. Chen, C.-M. Shih, M.-C. Tsai, C.-Y. Kuo, J.-Y. Lai, Grafting of poly(N-isopropylacrylamide-co-acrylic acid) on micro-porous polycarbonate films: Regulating lower critical solution temperatures for drug controlled release, Journal of Membrane Science, 379 (2011) 330-340.

[169] T.E. de Oliveira, C.M. Marques, P.A. Netz, Molecular dynamics study of the LCST transition in aqueous poly(N-n-propylacrylamide), Physical Chemistry Chemical Physics, 20 (2018) 10100-10107.

[170] X.-L. Wang, J. Huang, X.-Z. Chen, X.-H. Yu, Graft polymerization of N-isopropylacrylamide into a microporous polyethylene membrane by the plasma method: technique and morphology, Desalination, 146 (2002) 337-343.

[171] M.H. Futscher, M. Philipp, P. Müller-Buschbaum, A. Schulte, The role of backbone hydration of poly (N-isopropyl acrylamide) across the volume phase transition compared to its monomer, Scientific reports, 7 (2017) 17012.

[172] H. Du, X. Qian, Molecular dynamics simulations of PNIPAM-co-PEGMA copolymer hydrophilic to hydrophobic transition in NaCl solution, Journal of Polymer Science Part B: Polymer Physics, 49 (2011) 1112-1122.

[173] Y.S. Ho, G. McKay, Pseudo-second order model for sorption processes, Process Biochemistry, 34 (1999) 451-465.

[174] A.F.M. Barton, Handbook of Solubility Parameters and Other Cohesion Parameters 2nd Edition ed., CRC Press, Inc., Boca Raton, Florida, 1991.

[175] W.H. Ferrell, D.I. Kushner, M.A. Hickner, Investigation of polymer–solvent interactions in poly(styrene sulfonate) thin films, Journal of Polymer Science Part B: Polymer Physics, 55 (2017) 1365-1372.

[176] C.M. Hansen, Hansen Solubility Parameters: A User's Handbook, CRC Press, 2002.

[177] C. Gong, R. Guan, Y.-C. Shu, F.-S. Chuang, W.-C. Tsen, Effect of sulfonic group on solubility parameters and solubility behavior of poly(2,6-dimethyl-1,4-phenylene oxide), Polymers for Advanced Technologies, 18 (2007) 44-49.

[178] C. Yang, E.E. Nuxoll, E. Cussler, Reactive barrier films, AIChE journal, 47 (2001) 295-302.

[179] Y. Liu, K. Sakurai, Thickness Changes in Temperature-Responsive Poly(N-isopropylacrylamide) Ultrathin Films under Ambient Conditions, in: ACS Omega, 2019, pp. 12194-12203.

[180] X. Fang, J. Li, B. Ren, Y. Huang, D. Wang, Z. Liao, Q. Li, L. Wang, D.D. Dionysiou, Polymeric ultrafiltration membrane with in situ formed nano-silver within the inner pores for simultaneous separation and catalysis, Journal of Membrane Science, 579 (2019) 190-198.

Anthony Saad was born and raised in Dubai and graduated from high school at the American School of Dubai in 2010. He then went to MIT and completed his Bachelor's in Chemical Engineering, graduating with minors in both Economics and Energy studies in 2014. Looking to apply his chemical engineering knowledge in a practical research-based manner, Anthony began his doctoral program at the University of Kentucky in chemical engineering in the fall of 2014, with a focus on water treatment membranes under the guidance of Dr. Dibakar Bhattacharyya and the support of NIH-NIEHS-SRP grant.

EDUCATION and CREDENTIALS

DOCTOR OF PHILOSOPHY (PH.D.) IN CHEMICAL ENGINEERING | University of Kentucky
September 2014 to June 2020
Lexington, KY, United States
With a focus on responsive water treatment membranes, performed original research on the functionalization of polymeric membranes with reactive nanoparticles for water decontamination and degradation of toxic organic compounds.

BACHELOR OF SCIENCE (B.SC.) IN CHEMICAL ENGINEERING | Massachusetts Institute of Technology
September 2010 to June 2014
Cambridge, MA, United States
Minor in Economics, Minor in Energy
GPA: 4.4/5; SAT: 770M, 760V, 800W; SAT II: 800 Math II, 770 Chemistry
Member of the golf club and soccer team, Tao Beta Pi Engineering Honor Society

SUMMER SCHOOL | Harvard University
2011 and 2012
Cambridge, MA, United States
Coursework in Organic Chemistry, Managerial Finance, Capital Markets and Investments

HIGH SCHOOL DIPLOMA | American School of Dubai
September 2006 to June 2010
Dubai, United Arab Emirates
GPA: 4.2/4.3
Member of the National Honor Society
Captain of the varsity soccer team

PROFESSIONAL EXPERIENCE

UNIVERSITY OF KENTUCKY | Lexington, KY
September 2014 to Present
PhD RESEARCHER (advisor: Dr. Dibakar Bhattacharyya)

- Performed advanced research in chemical engineering, specifically water treatment membranes with novel polymeric designs with immobilized reactive nanoparticles.
- Collaborated with different department for NIEHS grant proposals
- Co-authored four peer-reviewed publications.
- Trained and supervised research assistants in the field of polymeric and reactive membranes for water treatment.
- Collaborated with US specialized membrane companies to implement their novel membranes in the UAE.

SHELL OIL CO | Ras Laffan, Qatar
June – August 2013
TECHNOLOGY INTERN

- Orchestrated a study on optimizing ammonia injection in DENOX units for various furnaces on site in the world's largest gas-to-liquid plant that generated 140,000 barrels of oil per day.
- Coordinated logistics for a third-party contractor to perform testing on site and organized site visits with various departments.
- Directed supplementary studies on the feasibility of changing current in-line analyzers on site.

PUBLICATIONS

A. Saad, R. Mills, H. Wan, L. Ormsbee, D. Bhattacharyya, Thermo-responsive PNIPAm-PMMA functionalized PVDF membranes with reactive Fe-Pd nanoparticles for enhanced PCB degradation (to be submitted 06/2020).

A. Saad, R. Mills, H. Wan, A. Mottaleb, L. Ormsbee, D. Bhattacharyya, Thermo-responsive adsorption-desorption of perfluoroorganics from water using PNIPAm hydrogels and pore functionalized membranes, J Membrane Sci, 599 (2020).

H. Wan, N.J. Briot, A. Saad, L. Ormsbee, D. Bhattacharyya, Pore functionalized PVDF membranes with insitu synthesized metal nanoparticles: Material characterization, and toxic organic degradation, J Membrane Sci, 530 (2017) 147-157.

S. Hernández, A. Saad, L. Ormsbee, D. Bhattacharyya, Chapter 16 - Nanocomposite and Responsive Membranes for Water Treatment A2 - Hankins, Nicholas P, in: R. Singh (Ed.)

Emerging Membrane Technology for Sustainable Water Treatment, Elsevier, Boston, 2016, pp. 389-431.

L. Xiao, A. Isner, K. Waldrop, A. Saad, D. Takigawa, D. Bhattacharyya, Development of Bench and Full Scale Temperature and pH Responsive Functionalized PVDF Membranes with Tunable Properties, J Memb Sci, 457 (2014) 39-49.

CONFERENCE PRESENTATIONS

A. Saad, M. Gui, L. Xiao, D. Bhattacharyya: PNIPAm Functionalized Membranes: Tunability and Pollutant Partitioning / Degradation. 2015 NAMS Annual Meeting, Boston, MA (June 2015).

A. Saad, H. Wan, D. Bhattacharyya: Temperature Responsive Membranes and Pollutant Degradation. 2016 NAMS Annual Meeting, Bellevue, WA (May 2016).

A. Saad, H. Wan, D. Bhattacharyya: Degradation of Chlorinated Organics by Temperature Responsive PNIPAMco-PAA Functionalized MF Membranes with Reactive Nanoparticles. 2016 NIEHS EHS Fest, Durham, NC (December 2016).

A. Saad, H. Wan, D. Bhattacharyya: Temperature Responsive Membranes and Pollutant Degradation. 2017 Imagine Membrane Conference, Horta, Portugal (September 2017). **Received Outstanding Poster presentation award.**

A. Saad, H. Wan, and D. Bhattacharyya: Temperature Responsive Membranes and Pollutant Degradation. North American Membrane Society 2018 Annual Meeting, Lexington, KY (June 2018)

A. Saad, H. Wan, D. Bhattacharyya: PNIPAm functionalized temperature responsive membranes and pollutant adsorption. 2018 AICHE Annual Meeting, Pittsburgh, PA (November 2018)

A. Saad, H. Wan, A. Aher, D. Bhattacharyya: PNIPAm functionalized temperature responsive membranes for PFOA adsorption. 2019 ACS Annual Meeting, Orlando, FL (April 2019)